CANADIAN THESES

THÈSES CANADIENNES

NOTICE

The quality of this microfiche is heavily dependent upon the quality of the original thesis submitted for microfilming. Every effort has been made to ensure the highest quality of reproduction possible.

If pages are missing, contact the university which granted the degree.

Some pages may have indistinct print especially if the original pages were typed with a poor typewriter ribbon or if the university sent us an inferior photocopy.

Previously copyrighted materials (journal articles, published tests, etc.) are not filmed.

Reproduction in full or in part of this film is governed by the Canadian Copyright Act, R.S.C. 1970, c. C-30. Please read the authorization forms which accompany this thesis.

AVIS

La qualité de cette microfiche dépend grandement de la qualité de la thèse soumise au microfilmage. Nous avons tout fait pour assurer une qualité supérieure de reproduction.

S'il manque des pages, veuillez communiquer avec l'université qui a conféré le grade.

La qualité d'impression de certaines pages peut laisser à désirer, surtout si les pages originales ont été dactylographiées à l'aide d'un ruban usé ou si l'université nous a fait parvenir une photocopie de qualité inférieure.

Les documents qui font déjà l'objet d'un droit d'auteur (articles de revue, examens publiés, etc.) ne sont pas microfilmés.

La reproduction, même partielle, de ce microfilm est soumise à la Loi canadienne sur le droit d'auteur, SRC 1970, c. C-30. Veuillez prendre connaissance des formules d'autorisation qui accompagnent cette thèse.

THIS DISSERTATION HAS BEEN MICROFILMED EXACTLY AS RECEIVED

LA THÈSE A ÉTÉ MICROFILMÉE TELLE QUE NOUS L'AVONS REÇUE

FRACTURE ENERGY OF FIBRE HYBRID COMPOSITES

by

Zalman C. P. Lai

A thesis
presented to the University of Ottawa
in partial fulfillment of the
requirements for the degree of
Master of Applied Science in Mechanical Engineering
in
the Department of Mechanical Engineering

OTTAWA, Ontario, 1983

I hereby declare that I am the sole author of this thesis.

I authorize the University of Ottawa to lend this thesis to other institutions or individuals for the purpose of scholarly research.

Zalman C. P. Lai

I further authorize the University of Ottawa to reproduce this thesis by photocopying or by other means, in total or in part, at the request of other institutions or individuals for the purpose of scholarly research.

Zalman C. P. Lai

ABSTRACT

The fracture energy of a model carbon fibre/glass fibre/epoxy resin hybrid composite system has been evaluated as a function of the carbon fibre/glass fibre ratio at different temperatures. Three models of fracture mechanisms, namely, the fibre pull-out, the fibre debond, and the post-debond sliding, were considered to account for the fracture energy of the hybrid composite. The said models of microscopic fracture behaviour were successful in quantitatively describing the observed fracture behaviour of the hybrid fibrous composites for most of the temperatures tested. For carbon fibres, fibre pull-out mechanism was the chief contributor to the fracture energy of the composite for all temperatures tested. This is in agreement with all other previous studies. The post-debond friction energy was found to provide a major contribution to the fracture energy of the glass fibres. This trend was found at all temperatures tested.

The temperature study had given more insight into one of the parameters in post-debond friction energy, $\Delta\varepsilon$, the differential failure strain between the glass fibre and the matrix. It was found that $\Delta\varepsilon$ increased with temperature and was related to the specimen geometry. A new approach to

evaluate $\Delta\varepsilon$ analytically, rather than estimating as was done in other studies, was introduced. The differential strain, $\Delta\varepsilon$, was evaluated for each specimen tested. It was found that this approach gave very good agreement between the work of fracture and theoretical fracture energy except for high glass fibre contents specimens tested at high temperatures.

ACKNOWLEDGEMENTS

The author would like to express his sincere gratitude to Dr. Munro who has patiently devoted his time to encourage and to give numerous helpful discussions and technical advices during this work.

Dr. A. Miyase, who has given many constructive suggestions and criticisms, is deeply appreciated. Lastly, the author would like to thank the technical staff in the Mechanical Engineering Machine Shop at the University of Ottawa for the assistance he had received.

NOMENCLATURE

A	-	cross-sectional area of fibre
A_c	-	area under the load deflection curve
A_{eq}	-	equivalent area transformed by the ratio of elastic modulus
b	-	width of a specimen
c	-	distance from the neutral axis (N.A.)
d	-	fibre diameter
E_f , E_m	-	elastic modulus of fibre or matrix
$f(x)$	-	probability function of existence
G_{11}	-	energy required to create a unit area of new surface
I	-	moment of inertia
L	-	span of a specimen
ℓ	-	average pull-out length of fibre
ℓ_c	-	critical transfer length of fibre
ℓ_{max}	-	maximum fibre pull-out length (as measured)
M	-	maximum bending moment
N	-	total number of fibres
N_o	-	number of fibres per unit area
P	-	applied load
r	-	fibre radius
U	-	toughness, or total fracture energy
V_f , V_m	-	volume fraction of fibre or matrix
W'	-	work done by one fibre

W_d - work done by fibre debond

W_{pdf} - work done by relative sliding of fibre and matrix after debond

W_{po} - work done by extracting fibres out of the matrix

W_r - work done by stress relaxation between fibre and matrix

x - displacement between fibre and matrix

y - debond length of the fibre

γ_d - debond energy

γ_{pdf} - post-debond sliding energy

γ_{po} - pull-out energy

γ_r - stress redistribution energy

δ - deflection under applied load

$\Delta\varepsilon$ - differential failure strain between fibre and matrix

ϵ - strain

σ - stress on the fibre

σ_f - ultimate tensile stress of fibre

τ - interlaminar shear stress

Subscripts and Superscripts:

f - fibre

m - matrix

g - glass fibre

c - carbon fibre

CONTENTS

LIST OF FIGURES

LIST OF TABLES

Chapter I

INTRODUCTION

There is a constant search for ideal materials: ones which are strong, tough and light. It is the availability of strong materials that secures engineering achievements and even the very existence of human beings.

Over the past few decades, emphasis has been given to the development of space programs, oceanography, and supersonic flight endeavours. The demands on materials in these applications are so diverse and severe that the naturally occurring materials are gradually falling short. A great deal of time and money has been spent in studying the physical and mechanical properties of metallic materials with the hope of improving their strengths by means of cold working, substitutional and precipitation hardening and alloying. In fact, developments in alloying techniques have greatly improved the physical properties of engineering materials. Yet, this does not seem to be the final solution to the problem. Consequently, the concept of combining several materials (in a high strength fibrous form) into a matrix to produce a composite system has gained added significance as a means of meeting these requirements. Nowadays, composites, along with alloys and ceramics, are at

the forefront of research and development in the field of material science.

1.1 COMPOSITES

1.1.1 What are Composites?

Composites, in the strictest sense, consist of any type of multiphase materials. They include such common materials as wood, concrete and steel. However, the term 'composite' usually refers to a combination of at least two chemically distinct materials in which the minor or dispersed phase is introduced deliberately by man rather than being allowed to develop fortuitously subject to the forces of nature. Such systems of materials yield performance potentials often unattainable by the components acting individually.

One distinct characteristic of composite materials is that there exists a distinct interface between the constituent materials which serves as the medium for load transfer in the composite. In some composites the dispersed phase is in the form of fibres, and such structures are known as fibre-reinforced materials. Fibre-reinforced composites are the subject of this thesis.

1.1.2 Historical Background of Composites

The idea of composite materials is not new. In ancient times, the Egyptians had learned to include chopped straw as reinforcing fibres, in mud for building bricks to prevent

the brick from cracking. The Eskimos incorporated moss (which contains fragments of cellulose) into ice to prevent the propagation of cracks in ice. There were also early civilizations which used laminated bows for extra strength. These examples are typically referred to as some of the first users of composite materials [1]. Yet, it is even more interesting to know that composites exist in nature itself, of which bone and wood are bona fides examples. Bone contains hydroxyapatite crystals incorporated into a matrix of collagen fibres. Wood is an organic substance composed primarily of cellulose chains embedded in lignin matrix.

In spite of the long history in the use and development of composites, the modern science of fibre composite materials began relatively recently. Many materials, when produced in fibrous form, are much stronger and stiffer than in the bulk state. In addition, many fibres have a low density. Metals have the merits of stiffness, strength and toughness but are not light; while plastics, invented earlier this century, are light but lack strength, stiffness and toughness. Therefore, researchers combined materials with complementary properties together hoping to get the combined advantages of their constituents, i.e. light weight, strong, stiff and tough materials. Thus was launched the development of modern fibre composite materials.

1.1.3 Why Composite Materials?

There are many reasons which lead to the development of composite materials. The following are five major advantages:

1. Composite materials provide a balance of stiffness, strength and toughness - the strong and stiff reinforcing materials (eg. fibres) are responsible for carrying the load; while the tough (especially metallic matrix) but less strong matrix contributes to the ductility or toughness of the material.
2. Composites are versatile. There is a wide choice of constituent materials available for making composites. Composites also offer the additional advantage of design flexibility. In contrast to monolithic materials, the properties of these multiphase systems could be adjusted (through control of orientation and composition) to give a combination of desired properties that cannot be achieved in conventional materials.
3. Weight Saving: In conventional isotropic materials, the material strength is identical in all directions. However, in composite materials, the reinforcement(s) could be aligned in the direction(s) of loading. As a result, the weight of structures using composite materials is greatly reduced. Also the high Specific Modulus (modulus per unit weight) and the high

Specific Strength (strength per unit weight) of the reinforcing fibre make the structure constructed by these reinforcing materials strong and yet light in weight (Figure 1).

4. Composite parts could usually be molded to final stage. This feature greatly reduces the wastage of material. In addition, the need of precise machining of the products (especially in making air foils or fan blades), which is very costly, is eliminated. This would eventually lead to a reduced manufacturing cost.
5. Manufacturing cost for composites is competitive to metals due to lower material costs and new manufacturing techniques.

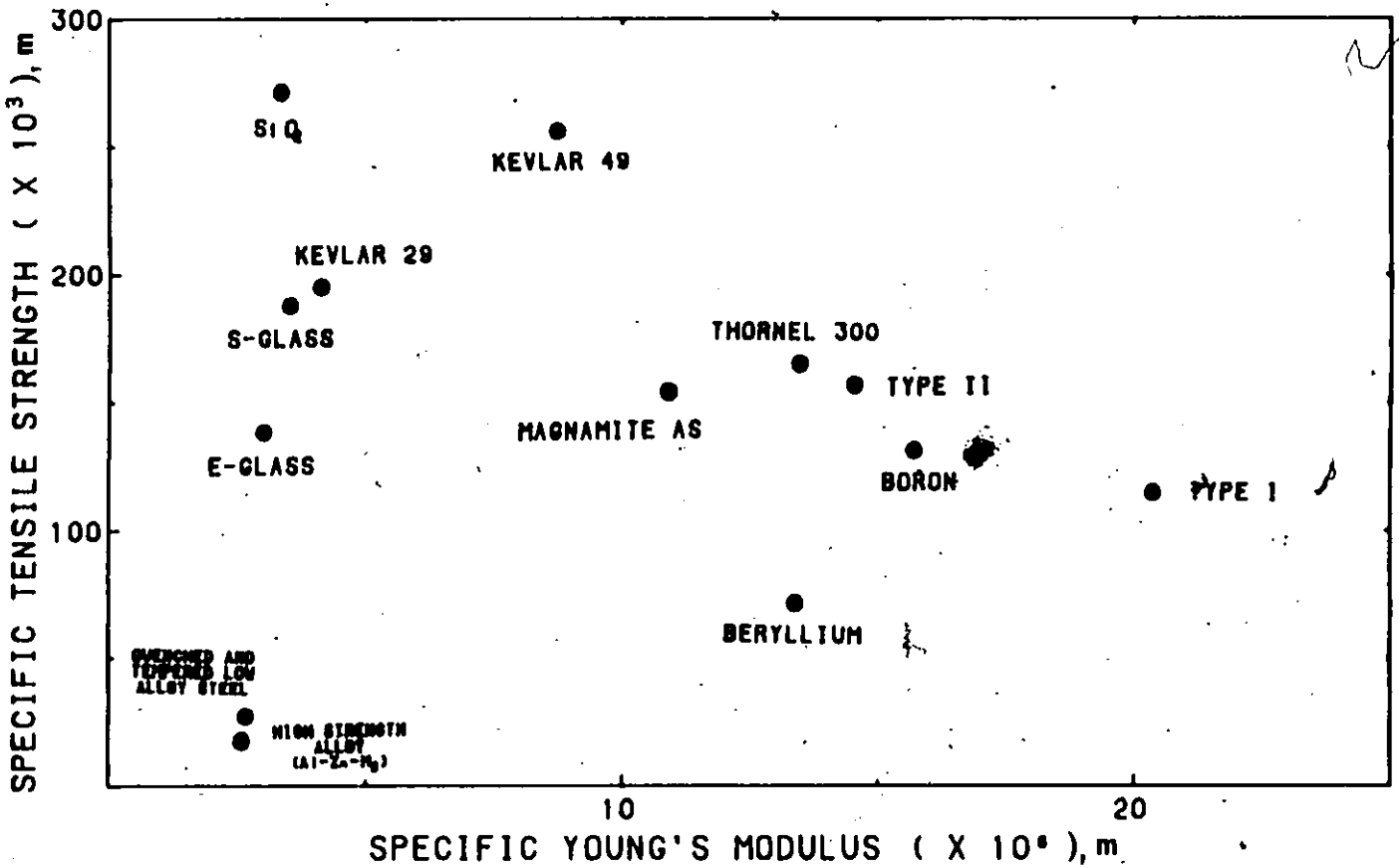

Figure 1: Specific properties of reinforcing fibres

1.1.4 Reinforcing Materials

There are different types of fibres being used today; the more common ones are described below.

1.1.4.1 Glass

The use of glass fibres could be dated to the Ancient Egyptian times [1]. However, the modern glass fibre technology was first introduced by the Owens-Corning Fiberglas Corporation in the late 1930's following successful development of a new manufacturing technique to produce glass fibres. In 1938, the Owens-Corning Fiberglas Corporation started to market glass fibres and their products. Glass fibre is produced by melting in a high temperature refractory furnace such ingredients as sand, limestone and boric acid, at a temperature of about 1260 degrees Celsius. The molten glass flows directly into the fibre drawing furnace where it is drawn into continuous fibres. Figure 2 illustrates the manufacturing process.

Among all the commercially available glass fibres, E-glass is the most commonly used one because it has good strength, stiffness and is cheap. S-glass is more expensive than E-glass but it has a higher Young's Modulus and is more temperature resistant.

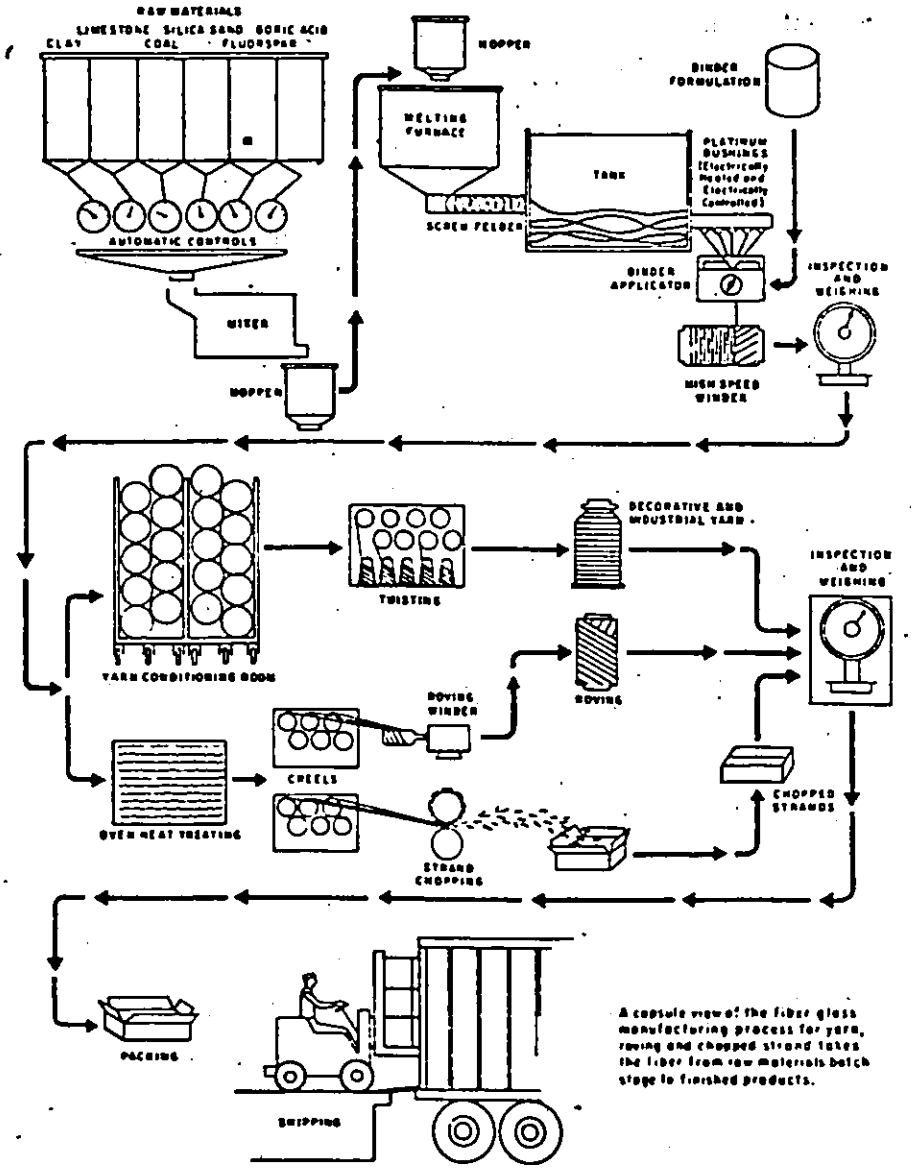

Figure 2: Manufacturing process of glass fibre [7]

1.1.4.2 Whiskers

In 1952, Herring and Galt [2,3] discovered the high stiffness and strength of single crystal filaments of materials, called whiskers. They bent some tin whiskers and noticed that the whiskers could be bent to a strain of about 2% and still recover elastically. Yet, the corresponding stress required was extremely high - higher than had ever been observed before in tin and perhaps in any other metal. This discovery may well be considered to mark the beginning of interest in high strength fibre-reinforced composites.

Further research on whiskers had revealed that the strongest whiskers in terms of stiffness and ultimate tensile strength per unit weight are found in the covalently bonded materials. For example, silicon carbide, silicon nitride, graphite, alumina and boron are materials of high strength and stiffness - close to that of the theoretical strength (about E/10) as proposed by Griffith [4]. However, the high cost of production of whiskers discouraged their being used extensively in engineering applications.

1.1.4.3 Carbon

Almost a century ago, Thomas A. Edison [5] had successfully produced carbon fibres. Nevertheless, the fibres thus produced were mainly for the use of electrical lamps and had quite low strength and stiffness. The development of modern strong carbon fibre was initiated by

Akio Shindo of Industrial Research Institute of Osaka in Japan in the early 1960's. He showed that carbon filaments having a tensile modulus up to 165 GPa could be produced from a polyacrylonitrile precursor. In 1966, W. Watt, L. N. Phillips, and W. Johnson [6] of Royal Aircraft Establishment at Farnborough, continuing on from original work by Shindo, developed a technique for the manufacturing of strong carbon fibres. This was the first development in carbon fibre technology in Great Britain. Subsequently, commercial carbon fibres were produced in Britain and the United States.

Carbon fibres could be manufactured from a variety of precursors (starting material fibres). The basic process in manufacturing graphite fibres is to utilize an organic base precursor with a high percentage of carbon atoms and, through heat and tension, drive off all volatile fractions leaving only the carbon atoms.

In early 60's, the rayon-based carbon fibres were produced commercially in the United States under the brand names Thornel 40 by Union Carbide. Typically, the rayon-base fibres are manufactured from heat-treating the rayon filaments to high temperatures (2700 - 2800 degrees Celsius) and stretching the fibre to cause the strong C-C covalent bonds to align along the fibre axis.

Polyacrylonitrile (PAN) was the most widely used precursor for producing carbon fibres today. The

commercially available carbon fibre Thornel 300 by Union Carbide is an example of PAN-based carbon fibres. Its manufacturing method was developed by Watt et al, [6] and was first produced commercially in mid 1960's in England. PAN-based carbon fibres are made from a long chain linear polymer consisting of a carbon chain with attached carbonitrile groups. The polymer is first oxidized at 200 - 250 degrees Celsius for up to 24 hours. Then the resulting fibre is heat-treated in an inert atmosphere to temperatures from 1400 to 3000 degrees Celsius. This final processing temperature significantly influences the modulus and ultimate tensile strength of the carbon fibres (Figure 3).

The newest carbon fibre processing technique used today was introduced by Otani and his colleagues in Japan. This technique involves melt spinning of molten pitch to above 350 degrees Celsius and spinning the pitch through a small orifice into filament form (Figure 4). The filaments were then oxidized to make it infusible and then they were carbonized at temperature around 2000 degrees Celsius. The advantages of this technique are that it is cheap and it could produce carbon fibres at a much faster rate. Table 1 shows the mechanical properties of carbon fibre manufactured from different precursors.

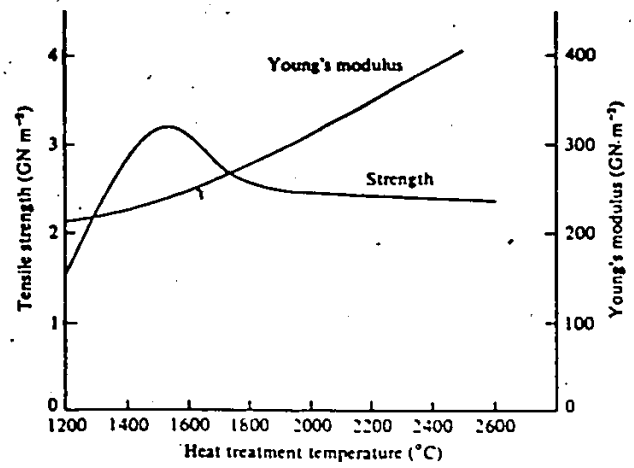

Figure 3: Heat-treatment temperature effect on PAN-based carbon fibre [10]

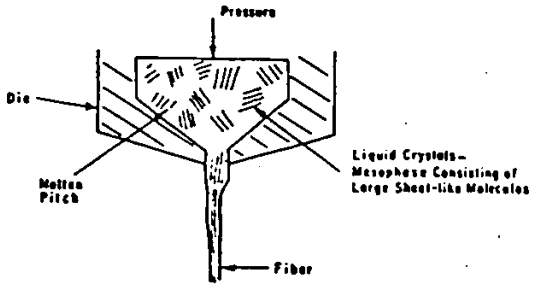

Figure 4: Manufacturing carbon fibre from pitch [7]

TABLE 1

Properties of Different Types of Carbon Fibres [7,8]

Property	Pitch-Based	Rayon-Based	PAN-Based
Tensile strength (GPa)	1.72	2.1 - 2.8	2.5 - 3.1
Young's Modulus (GPa)	380	410 - 550	200 - 345
Specific Gravity	2.02	1.7	1.8
Elongation (%)	0.5	...	1.2 - 0.6
Fibre Diameter (μm)	11	6.5	7.5

1.1.4.4 Boron

The emergence of boron fibres gave birth to a new generation of composites in the early 1960's. The composites that employed high modulus continuous filaments like boron and graphite are referred to as advanced composites from the standpoint of modulus.

Boron fibre is synthesized by chemical vapor deposition (CVD) from the reduction of Boron Trichloride (BCl_3) with Hydrogen on a Tungsten or carbon monofilament substrate. The substrate is resistively heated to a temperature of about 1260 degrees Celsius and continuously pulled through the reactor to obtain the desired Boron coating thickness.

1.1.4.5 Aramid Fibres

Nylon and other types of polymer fibres have been developed and in use for many years as reinforcements in automobile tires, large balloons and dirigibles, parachutes, fuel tanks, body armor etc.

Among the aramid type fibre, Kevlar, which was developed by DuPont in the 1960's, is of prime importance. Kevlar possesses very high specific strength (strength/density) and good specific modulus (or stiffness) because of its low density. These properties made Kevlar very attractive to designers. The Kevlar type materials are available under the names Kevlar 29 and Kevlar 49. They are formed through the spinning of the polymer poly-p Benzamide at temperatures above 260 degrees Celsius; but the detailed manufacturing method still remains an industrial secret. These two Kevlar type materials have a small difference in modulus so as to better suit different needs. Kevlar 29 has a high strength and intermediate modulus. Kevlar 49 has a higher modulus but approximately the same strength as Kevlar 29 and is mostly used for high performance composite materials.

1.1.5 Matrix Resins

In this discussion, emphasis would be directed to a synthetic resin system, Epoxy (Epoxide) Resin. There are other type of matrices, for example, metal matrix and carbon matrix; but they are beyond the scope of this thesis.

The research on epoxy resin technology was conducted in the U.S. and Europe just before World War II. The first resin - the reaction products of Epichlorohydrin and Bisphenol A - were produced commercially in 1947. Within ten years, a production volume of some 30 million pounds had been achieved. This was further tripled six years later. By 1965, approximately 110 million pounds of epoxy resin were sold, and the growth rate appeared to increase at a stable rate of about 10% per year [9].

A variety of matrix resins are used for fabricating graphite, boron, glass fibre, and aramid fibre-reinforced composite forms and structures. Thermoset resins are the generic class that is most commonly used for resin matrix composites. Two of the most commonly used resins are discussed as follows:

1. Epoxy Resins are mainly used to produce high performance composites. They are compatible with all types of fibres. They can have low glass transition temperatures, therefore, they are generally used for service at temperatures less than 120 degrees Celsius.
2. Polyester Resins are usually room temperature curable ones. They are used mainly for commercial glass fibre applications. One disadvantage of this resin is that it shrinks considerably during curing. It is not used for advanced composites.

The physical properties of epoxy and polyester resins are listed in Table 2. Epoxy resins are very heavily used in today's industry. They are used in casting, potting and in the encapsulation of electrical/electronic parts. In chemical industry, the non-corrosive character of the epoxy resins leads to their application in making protective coating for containers, pipes, and tanks for chemicals. However, their most important application is in being the matrix of fibre-reinforced materials. This is discussed in the next section.

TABLE 2

Comparison of Epoxy and Polyester Resins [10]

Property	Epoxy Resins	Polyester Resins
Tensile Strength (MPa)	35 - 100	40 - 90
Compressive Strength (MPa)	100 - 200	90 - 250
Young's Modulus (GPa)	3 - 6	2 - 4.5
Specific Gravity	1.1 - 1.4	1.2 - 1.5
Elongation (%)	1 - 6	2
Glass Transition Temperature (deg. C.)	50 - 300	50 - 110
Shrinkage on Curing (%)	1 - 2	4 - 8

1.1.6 Hybrid Composites

Hybridization is the incorporation of two or more kinds of fibres into a single matrix. The resulting material is generally referred to as a 'Hybrid' or 'Hybrid Composite'. It is, in fact, a breakthrough in the development of composite materials.

A variety of reinforcing fibres and matrices are used to form hybrids, among them, the most common one is the carbon/glass hybrid reinforced plastics (CGHRP). Carbon fibres are strong and stiff and have a low density but they are relatively expensive. On the other hand, glass fibres are relatively cheap. They have higher failure strain than carbon fibre and good fracture stress but are not stiff. By combining the two fibres within the same resin matrix, it is possible to achieve a balance between the properties of all carbon fibre reinforced plastics (CFRP) and all glass fibre reinforced plastics (GFRP) at a fraction of the total individual costs.

Some other fibres which are also used to produce hybrids are boron/carbon hybrids and Kevlar/carbon hybrids. Applications of these will be discussed in later sections.

1.2 APPLICATIONS OF COMPOSITES

In view of their unique properties (fatigue characteristics, low density, high modulus, high strength and so on), fibre composite materials are being utilized in a very broad range of applications: Aeronautic and aerospace industries, automotive industry, defence (especially weapons), and in recreation activities. These applications would probably evolve initially on a part and material substitution basis rather than by the design of a completely new system.

Reinforced plastics were first applied to aircraft propellers and blades around 1950: this year also marked the beginning of an era of rapid development in the application of fibre-reinforced composites in the aeronautical industry. The superior structural performance advantages of composites (where applicable), their potential and real energy saving, practical weight savings (up to 30%) and design flexibility are the principal factors which provide the impetus for the expanded use of composites in various applications.

The following discussions present the various generic applications of fibre-reinforced composites with emphasis on carbon/glass hybrids.

1.2.1 Fibreglass Reinforced Composites

Glass fibre was first employed to reinforce plastics in 1940. The first successful application was found in its use in nose radar domes, known as radomes, used to protect aircraft antennas [11]. Since then, fibre glass reinforced composites have become widely used in various engineering applications where a high strength-to-weight ratio is required. Even nowadays, fibre glass is still the most common of all reinforcing fibres for resin matrix composite structures. The most commonly used glass fibres for structural composites are E- and various S-glasses. Their unique properties plus the variety of plastic materials available today give rise to a broad spectrum of glass-resin combinations. This enables the designers to choose a composite to best suit their specific end-product requirements such as: high strength, light weight, corrosion and weather resistance and complex shapes.

In the automotive industries, fibre glass is very outstanding in its applications in making auto bodies (eg. Corvette) and trailers. Some automotive parts, for example, cooling system components, subway and bus seatings are also fabricated using fibre glass materials. The glass fibre reinforced composites are also heavily used in the aerospace industry and military market to produce advanced composite parts. Those structural components include aircraft parts, radomes, heat shields, high pressure tanks and missile

shells and rocket motor cases are also made with or reinforced by glass fibres.

Major advantages for glass fibre are low cost, increased durability and increased resistance to degradation by water. Further applications in other areas are being explored. In domestic markets, fibre glass is used to make patio roofing, paneling, siding and curtain wall materials, luxury office seating, school and auditorium furnitures, consumer appliance components, dishwasher lids, laundry tubs, air-conditioner components and a lot of other household appliances.

Fibreglass, with a corrosion resistant resin, finds its applications in piping, fuel and chemical storage tanks and chemical processing equipment. In the field of recreation, glass fibre is also indispensible. Boats, canoes, surf boards, tennis racquets, skis, hockey sticks, vaulting poles, protective helmets (racing and baseball) and swimming pools made by fibreglass materials are just a few examples. A more recent application of glass fibres in constructing radomes can be seen in the 107 m long glass-polyester radome atop Toronto's 550 m CN Tower [12].

1.2.2 Carbon Fibre Reinforced Composites

Carbon fibre was introduced to the industry at the turn of the Twentieth Century. Its main application then was on electrical lamps [5]. Nowadays, applications of carbon

fibre composites are primarily oriented to helicopter and aircraft structures. For example, several helicopter companies in the United States, including Boeing, Sikorsky and Bell, have developed helicopter drive shaft using all-carbon or combinations of carbon and other fibres in resin matrix systems [13]. By using these composite structures, a significant weight reduction is realized. In addition to weight reduction, design simplification which leads to a reduced operational maintenance cost is also an advantage for using these materials.

In aircraft structures, carbon fibre composites are often used to construct some secondary structures. The access panels, cargo-doors, wing-tips, fairings and luggage-racks are some of the examples [14].

Besides the application to helicopter and aircraft structures, carbon fibre reinforced composites are also highly utilized in space flight applications. Currently, they are being used in all types of space vehicles: communication satellites [15], the Viking Space-craft and the Space Shuttle. The Remote Manipulator System (RMS) of the NASA Space Shuttle [16] consists of two adjoining arm booms which are made of graphite/epoxy composite. This composite provides a very high stiffness which is critical for the stability of the system. Carbon fibre reinforced composites are attractive to aerospace designers because they have very high specific Young's Modulus values, good

tensile strength values, and low coefficients of thermal expansion which are crucial to orbital spacecraft.

In the automotive industry, graphite/epoxy composite is also being studied for the applications in leaf springs and automobile drive shafts. A weight saving of 70% and 68% respectively were reported [17].

Owing to its unique properties (lightweight, superior vibrational damping and high stiffness), carbon fibre reinforced composites are also successfully applied in fishing rods, golf clubs, tennis rackets, and other sporting goods.

1.2.3 Boron Fibre Reinforced Composites

Boron fibres have a very high stiffness and strength. They have very important applications in the field of aerospace. The General Dynamics Fighter F-111 horizontal stabilizer [18,19] and the Grumman F-14 horizontal stabilizer [20] were among the earliest applications of the boron fibre reinforced epoxy composites in aircraft. With the mentioned structures installed in these aircraft, 27%, and 19% weight reductions were realized respectively. Consequently, more and more aircraft have boron fibre composite structures installed in order to realize weight savings. The McDonnell Douglas F-15 [21] and the subsonic attack aircraft A-70 [22] contained boron fibre composite structures which lead to a substantial weight saving. The

Boeing 707 has its wing foreflap made of boron fibre composites [23] and this is only one of the applications of boron composites in commercial aeroplanes.

Besides military aircraft and commercial aircraft, boron fibre composites are used in spacecraft structures also. The boron epoxy truss which was made for the Space Shuttle engine thrust structure weighed 30% less than the equivalent truss made by titanium [24].

Boron composites also have significant applications in sporting goods such as fishing rods, golf shafts, and tennis rackets. They have been used in the construction of a number of different tennis rackets, both in the United States and in Europe. In addition, boron prepreg is applied to the tip of masts on sailboats to prevent deflection under high loads.

Currently, these composites are being evaluated in their possible application in ski poles, cross-country skis and bicycle racing frames with the objective to reduce weight without loss of stiffness and increase efficiency of performance.

In the medical field, several boron reinforced containers have been designed and built for ultra-high speed centrifuges. Some preliminary work has been conducted on light weight wheelchairs for use in marathon and sprint races [7].

In the automotive industries, several companies are evaluating boron/epoxy composite push rods in automotive racing engines recently [7]. They weigh only one third of their steel counterparts; but the bending stiffness is approximately doubled. Boron composites have also been employed to stiffen the rear fork of a motorcycle in order to prevent excessive deflection of the rear fork [7].

There are still a lot of other applications where boron fibre composites are used. However, most of these applications are in the form of hybrid composite reinforcement (that is, incorporated with more than one kind of fibre in the same matrix, eg. Kevlar/boron hybrid) in order to reduce the cost (boron fibre is very expensive). These applications are discussed in Section 1.2.5.

1.2.4 Aramid Fibre Reinforced Composites

Due to technological advances, the properties of the Aramid types have been improved, and this allows them to be applied in high performance structures for aircraft and space systems, automobiles, marine craft, solid rocket missile cases and sporting goods. The principal polymer fibre reinforcements that are of current interest include nylon and the Aramid class of fibres. Yet, in this discussion, emphasis would be devoted primarily to Kevlar 49 due to the great interest in fibre composite industry.

Like most other reinforcing fibres, Kevlar 49 has found its applications in aerospace, aircraft, marine and sports equipments. They have been used to substitute glass fibres in many fairing structures in order to realize the weight saving from the lower fibre density of Kevlar. Now Kevlar fairings are in commercial service on the Lockheed L-1011 aircraft [25]. Because of its light weight, high strength and modulus and good fatigue and creep characteristics, Kevlar 49 is used in filament wound pressure vessels and solid rocket motor cases. The space shuttle contains spherical pressure vessels which are reinforced with Kevlar 49 in an epoxy. The escape slide/life raft systems on the Boeing 747 SP are activated by metal-lined pressure vessels overwarped with Kevlar 49 in an epoxy resin matrix. Kevlar 49 was selected to be the filament winding material to construct the Trident I missile motor chamber because of its high specific strength and acceptable stiffness properties [26].

In secondary structures of aircraft, applications for Kevlar 49 composites include overhead storage bins, lavatories, seats and ceiling panels in the cabin of aircraft.

In sports equipment, composites of Kevlar 49 are used to reinforce hulls, decks and bulkheads of many types of boats, including both large and small racing sailboats and power race boats where the light weight increases speed,

provides optimum weight distribution, and facilitates portability [27].

In the automotive industries, Kevlar 49 could also find its potential. They are now being evaluated for a number of automotive parts: leaf springs, transmission supports, drive shafts, body parts, clutch faces and brake linings.

1.2.5 Hybrid Composites

The motivations for using hybrids in structures are the improved stiffness and weight savings. The lower cost of using hybrids compared to that of the alternative materials is another factor attractive to designers, manufactures and buyers. Only a limited amount of cost information is correctly available. Yet, a potential cost saving over those of alternative materials is evident [20,28].

Applications of hybrid composites have been made in various areas. Current or anticipated commercial and defence-related applications include: recreational products, prosthetic devices, autobody frames, automotive reciprocating devices, turbine blades, aircraft and spacecraft components, and so on.

One of the earliest reports on the use of both carbon and glass fibres in the same matrix was for the Ford GT 40 racing car body in 1968 [29]. In it the use of 1.4 Kg of a carbon fibre web allowed a great reduction of weight (almost 40%) yet simultaneously increased the stiffness and so

maintained to aerodynamic shape at high speed, eliminated roof vibration and increased the life of the car body [29,30].

The selective use of carbon fibres, in conjunction with other composite materials, has been specified for production applications in some recent helicopter designs [31,32,33]. The potential uses for hybrid composites in fan blades of gas turbine engines [28,34,35] and helicopter rotor blades [36,37,38] are being studied and published.

The BO-105 helicopter, produced in West Germany by Messerschmitt-Bolkow-Blohm, has main rotors composed of glass fibres and is in commercial production. At Bolkow, experimental work is being conducted on the utilization of combinations of glass and graphite in both main and tail rotor blades [13]. The Kevlar/carbon hybrid is also used, along with fibre glass, in the structures of Boeing's new 757 and 767 aircraft. They encompass about 3% of the structural weight of these aircraft [39].

Besides the applications to aerospace products, hybrid design concepts have been introduced to the public for their use. Current commercial applications rely heavily on the construction of sports equipment including sail boat hulls [37,38,40], archery bows [28], golf club shafts [41,42] and bicycle frames [43]. Carbon/glass hybrid reinforced composites are now considered to be used in automotive industry for autobody and parts to reduce the weight of

automobiles [44]. Boron fibre is used to incorporate with carbon epoxy in making fishing rods to strengthen the rods without resorting to an increased tip diameter. Also, some golf club manufacturers use boron to strengthen the golf shafts made by carbon reinforced composites. Kevlar is also being used together with carbon fibres. In making sports equipment, Kevlar contributes excellent vibration damping and damage resistance, while carbon provides the needed stiffness. Boron, graphite, and epoxy were used together in constructing the spinnaker pole of the 1970 US America's Cup Defender 'Intrepid' [20,38].

Chapter II

FRACTURE MECHANISMS IN COMPOSITES

2.1 INTRODUCTION

In Chapter 1, it was mentioned that the applications of fibre-epoxy composites in the commercial and military area are gaining more and more attention. Yet, they are not being used extensively in these fields. One of the reasons is that although they possess many other good qualities such as light weight, high strength and corrosion resistance, the fibre composites are very brittle in comparison to metallic materials. Typical value of fracture energy for composites and metals are listed in Table 3.

TABLE 3

Typical Toughness Values for Composites and Metals [45]

Material	Work of Fracture (J/m^2)
Duraluminum (Al-Cu-Mg)	140,000
Maraging Steel	50,000
60% E-glass/epoxy resin	10,000
40% Carbon(Type I)/epoxy resin	2,500
Epoxy resin	200
Glass	6

For many properties (tensile strength, tensile modulus, density, thermal conductivity etc.), a Rule of Mixtures relationship (eqn. 2.1) can be used to predict composite values using component properties:

$$\begin{Bmatrix}\text{Composite}\\ \text{Property}\end{Bmatrix} = \begin{Bmatrix}\text{Property of}\\ \text{Component}\\ \text{Number 1}\end{Bmatrix}\begin{Bmatrix}\text{Volume Fraction}\\ \text{of Component}\\ \text{Number 1}\end{Bmatrix} + \ldots . \qquad (2.1)$$

Yet, this rule is inadequate when it is used to explain the fracture energy of fibre composite materials. Outwater and Murphy [46,47] had pointed out that the fracture energy of glass is less than 6 J/m^2. For polyester resin, the fracture energy is about 100 J/m^2. For a typical epoxy resin, the fracture energy is around 200 J/m^2. Yet for a glass fibre reinforced plastic, the fracture energy can be as large as 100 KJ/m^2. Clearly, there must be some interactions between the two components (the fibre and matrix) which are responsible for this great difference in fracture energy. A lot of research had been done in this area and as a result, different theories concerning the fracture energy were published. In this chapter, emphasis will be made on the different mechanisms proposed by various researchers to describe the fracture process. The various parameters which contribute to the fracture energy of the composites will also be reviewed.

2.2 TOUGHNESS - FRACTURE MECHANISMS RELATIONSHIP

Researchers who wanted to improve the fracture energy of composite materials had used various approaches to toughen fibre composites. Generally, these are all essentially varying parameters and monitoring the gross resultant change in toughness. Many researchers have investigated fracture mechanisms in order to better understand what are the effects of varying these parameters. In particular, changing one parameter might affect a number of mechanisms while only the gross result is recorded.

As a result of different composite models chosen and different testing, measuring and analysing methods used, different results were obtained by various researchers. This had led to a wide range of explanations of the fracture mechanisms of fibre-reinforced composites. There was evidence that carbon fibre reinforced epoxy resin composites (CFRP) derived their fracture energy mainly from the frictional work done to extract broken fibres out of the fractured matrix [48]. Gershon and Marom [49] reported that this Fibre Pull-Out model was also the major contribution to the fracture energy of glass fibre reinforced epoxy resin composites (GFRP). However, the energy dissipated during the debonding of fibre and matrix [46,47] as well as the frictional sliding between fibre and matrix after debonding [50] were also proposed mechanisms that were put forward by other researchers to be large contributors to the fracture

energy of GFRP. Each of the various energy terms for the various mechanisms used at least one experimentally measured length parameter (fibre debond length, fibre pull-out length). These lengths were difficult to determine and the measurements were quite subjective. This perhaps explains why different mechanisms were said by different authors to account for the same experimental fracture energy.

Kirk, Munro and Beaumont had studied these mechanisms and assumed that a composite which combined carbon fibres and glass fibres in the same matrix would have some of the microfracture characteristics of the two individual composite systems [51]. They examined this hybrid composite with a three-point slow bend test while Munro had also investigated the same hybrid using a Charpy impact tester [52]. From the results, he concluded that the Fibre Pull-Out mechanism was the main fracture mechanism for CFRP. As for GFRP, fracture energy is contributed through the Fibre Pull-Out, Fibre Debond and Post-Debond Sliding mechanisms (Figure 5).

In the following sections, some of the more important processes which are related to the energy absorbing mechanisms when the composites fail will be discussed. Emphasis will be on the micromechanisms of the fracture process and the relevance of the theory to the study of fracture energy in this thesis.

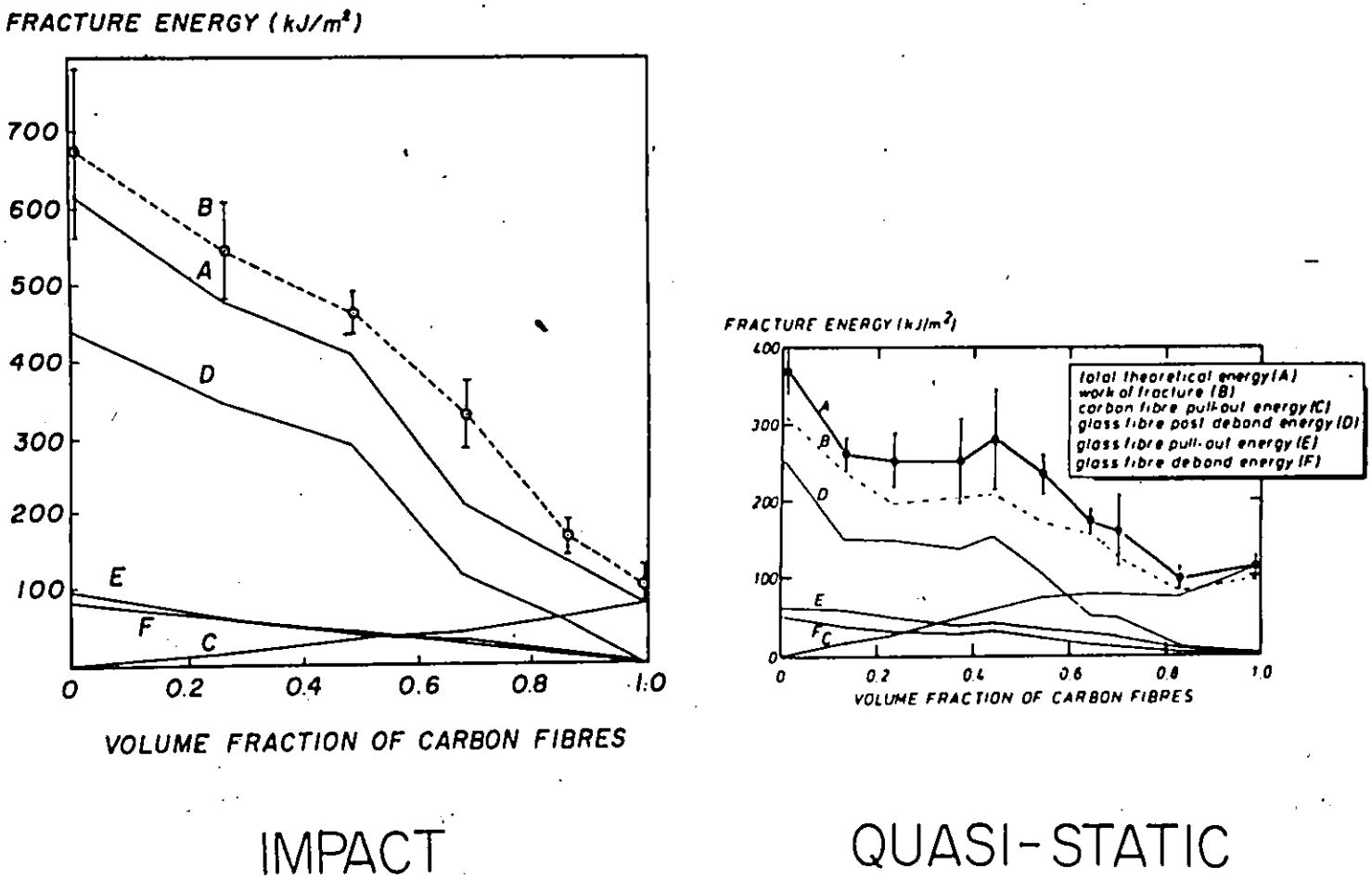

Figure 5: Comparison of fracture energy of hybrid composites [51,52]

2.3 FIBRE PULL-OUT

It had been recognized, from the early days of interest in composite materials, that when a composite was fractured, fibres broke and were withdrawn from the matrix through the fracture surface. A considerable amount of work was done through this mechanism. Kelly [53,54] and Cottrell [55] explained this phenomenon with a mechanism which was called the Fibre Pull-Out, and the energy absorbed through this process the Pull-Out Energy.

The Pull-Out Energy is the work done to extract the broken fibres from their 'sockets' in the matrix when the composites were fractured. This energy is dissipated through the frictional work over a distance 'x' against a shear stress, τ, which exists at the interface between the fibre and the matrix.

The work done to extract a broken fibre of length 'x' from the matrix is given by:

$$W'_{po} = \pi r^2 \int_0^x \sigma \, dx \qquad (2.2)$$

If the frictional shear stress, τ, is constant throughout the length 'x', the fibre stress would increase with distance from the ends as:

$$\sigma = 2\tau \left\{\frac{x}{r}\right\} \qquad (2.3)$$

Therefore, the work done to pull out one fibre of length 'x' from the matrix becomes:

$$W'_{po} = \pi r^2 \int_0^x \left(\frac{2\tau}{r}\right) x \, dx = \pi r \tau x^2 \qquad (2.4)$$

The study of the Fibre Pull-Out mechanism lead to the concept of critical length, ℓ_c. It is the maximum length of fibre that could be extracted out of the matrix without breaking. If the fibre has an ultimate strength σ_f, then from Equation (2.3),

$$\ell_c = \frac{\sigma_f r}{\tau} \tag{2.3a}$$

The total work done to pull out all the broken fibres from the matrix is then:

$$W_{po} = N \int_0^{\ell_c/2} \pi r \tau x^2 f(x) dx \tag{2.5}$$

where: N is the total number of fibres

f(x) is the probability of existence of pull-out length of each fibre. If the pull-out length is uniformly distributed, f(x) is defined as:

$$f(x) = 2/\ell_c$$

After integration, the total work done becomes:

$$W_{po} = \frac{N\pi r\tau}{12} \ell_c^2 \tag{2.6}$$

Therefore,

$$\gamma_{po} = \frac{W_{po}}{2A} = \frac{V_f \sigma_f \ell_c}{24} \tag{2.7}$$

where: V_f = volume fraction of fibre in composite

σ_f = ultimate tensile strength of fibre

ℓ_c = critical transfer length of fibre

It could be seen from Equation (2.7) that ℓ_c is a dominating parameter of this energy absorption mechanism.

Cottrell pointed out that to maximize the work of fracture (ie. to improve toughness of composite), the fibre length should be kept closely equal to the critical stress transfer length, ℓ_c , and ℓ_c should be made as large as possible. This could be obtained from a weak matrix or a weak interface. Cooper [56] has found out that for discontinuous fibre reinforcement, the toughness is greatest when the length of the fibre is equal to the critical stress transfer length. This claim was also proved experimentally by Harris et al, [57] who studied the fracture of carbon fibre/polyester composites and found that improvement of fibre/resin bond would lead to the increase of brittleness of composites. This is because of increased difficulty in pulling fibres out of the matrix, as a result, fibres break in the crack plane. Philips [58] also observed the pull-out effects in the carbon fibres/glass matrix composites.

Besides discontinuous fibre-reinforced composites, pull-out effects had also been observed in continuous fibre-reinforced composites [57,58,59]. Harris et al, [57] suggested that pull-out of broken fibre was preceded by the debond of fibre-matrix interface and the fibre would break somewhere within the debonded length. The average pull-out length was equal to a quarter of the critical stress transfer length ($\ell_c/4$). For brittle fibres, the pull-out length would be even less. Therefore, the pull-out work could be considered as an upperbound for brittle fibre-reinforced composites.

Piggott [60] explained the effect of fibre pull-out in continuous fibre-reinforced composites in another way. He looked at the deformation accompanying the stress concentration around the crack tip. For sharp cracks under enough stress (as due to stress concentration), a plastic zone would result. If the plastic zone in the fibre direction is sufficiently extensive, brittle fibres could break up into lengths of between $\ell_c/2$ and ℓ_c. The effect is thus controlled by this plastic deformation at the crack tip. However, Piggott based his discussion mainly on ductile matrices and therefore it is believed to be not applicable to the brittle matrices such as epoxy resins, which allow little plastic deformation.

2.4 FIBRE DEBONDING

Fibre Debonding is another often quoted mechanism being put forward to explain the origins of toughness in brittle fibre/brittle matrix composites. This mechanism is normally associated with the Pull-Out mechanism; but it is different from Fibre Pull-Out. Fibre debond occurs when the fibre-matrix interface fails. Energy is dissipated when a debonded fibre snaps. The stored elastic strain energy in the fibre at failure is released as kinetic, acoustic and thermal energies. This results in the retraction of fibre ends in their sockets. This dissipation of energy is not recoverable and is considered lost to the environment.

The Debond mechanism was first published by Outwater and Murphy [46,47]. They had studied the toughness of glass fibre/resin composites and found out that the work of fracture of the composite was about one or two orders greater than the fracture surface energy of the individual component of the composite. They proposed that this high fracture energy came from the debonding of fibre and matrix before the failure of the composite.

To obtain an expression for the energy involved in this mechanism, Outwater and Murphy first considered the energy required to debond a fibre a length dx to be:

$$\therefore W_d' = G_{11}\pi d\, dx \qquad (2.8)$$

where: G_{11} is the work done/unit area to create new surface in the interface by debonding

d is the fibre diameter

Then they equated the elastic energy release rate of the fibre after debonding to the energy of debonding the fibre a distance dx, and get:

$$G_{11}\pi d\, dx = \frac{\pi d^2}{8E}\left(\sigma - \frac{4\tau x}{d}\right)^2 dy \qquad (2.9)$$

The total work of debonding a fibre of diameter 'd' over a length 'x' on both side of the crack is then:

$$\int_0^x G_{11}\pi d\, dx = \frac{\pi d^2}{8E}\int_0^x \left(\sigma - \frac{4\tau x}{d}\right)^2 dy \qquad (2.10)$$

If W' is the total debond energy for 1 fibre,

$$W_d' = G_{11}\pi d\, x = \frac{\pi d^2}{8E}\left(\sigma^2 x - \frac{16\tau\sigma}{d}x^2 + \frac{64}{3}\frac{\tau^2}{d^2}x^3\right) \qquad (2.11)$$

Outwater and Murphy further suggested that the interlaminer shear stress, τ, falls to zero after debonding. Therefore, the Debond Equation becomes:

$$W_d' = \frac{\pi d^2}{8E} \sigma^2 x \qquad (2.12)$$

The maximum value for debonding occurs if the stress on the fibre, σ, reaches its ultimate strength. Thus:

$$W_d' = \frac{\pi d^2}{8E} \sigma_f^2 y \qquad (2.13)$$

If N fibres break,

$$W_d = \frac{N\pi d^2}{8E} \sigma_f^2 y \qquad (2.14)$$

The volume fraction of composite is defined as:

$$V_f = N \frac{\pi d^2}{4A}$$

$$W_d = \frac{1}{2} \frac{V_f \sigma_f^2}{E_f} A \qquad (2.15)$$

Therefore,

$$\gamma_d = \frac{W_d}{2A} = \frac{1}{4} \frac{\sigma_f^2 V_f}{E_f} y \qquad (2.16)$$

where A = cross-sectional area of fibre

Kelly [61] had considered the fracture energy of the fibre matrix interface, G_{11}:

$$G_{11} = \frac{\sigma_f^2 d}{8E_f}$$

He pointed out that if $G_{11} \geq \frac{\sigma_f^2 d}{8E_f}$, then the fibres would not

be able to debond from the matrix and the fibre would break at the fracture surface. Therefore, the maximum work of debonding increases with fibre diameter as does the maximum work of pull-out.

One of the most important parameters for the Debond Energy is the debond length. It is defined by the debond area. The debond area is that area on the composite which turns translucent after the bonds between the fibre and matrix fail. It is very visible especially in resin matrices with glass fibres. Therefore, the debond length is usually measured experimentally. Marston et al, [62] suggested that the debond length must be of the order of the critical transfer length since the debond length on either side of a broken fibre has to be at least half as long as the critical transfer length in order for the fibre to reach its ultimate tensile strength.

Cook and Gordon [63] envisaged a form of debonding where a tensile component perpendicular to the fibres in the stress field ahead of a running crack causes interfacial fracture before the crack reaches the fibre - this requires the fracture strain of the matrix to be bigger than that of the fibre. Yet, the assumption Outwater and Murphy made was that the fibre started to debond only when a crack in the matrix passes through it. This assumption required the failure strain of the fibre to be bigger than that of the matrix (which is the case in glass fibre and resin matrix).

Therefore, the Outwater/Murphy approach is not applicable to the model envisaged by Cook and Gordon.

In the Outwater/Murphy model of fibre debond, the interfacial shear stress was assumed to be zero after the debond of fibre and matrix took place. Harris et al, [50] pointed out that the interfacial shear stress, in fact, does not fall to zero after debonding. Thus, this model must be an overestimate of the actual energy dissipated. Therefore, the Debond Energy calculated by the Outwater/Murphy model is an upperbound value of the actual work done.

2.5 STRESS RELAXATION AND REDISTRIBUTION

Piggott [64] had introduced another form of energy absorption mechanism in unidirectional fibre-reinforced composites. He stated that when a crack in the matrix passed through the fibres, the fibres would tend to be stressed and would bridge the crack in order to stop the crack from extending. During this bridging, the stress distribution on the fibre would become maximum in the crack surface. Those fibre ends with lengths less than the critical transfer length will be pulled out of the matrix. Those fibre ends with lengths greater than the critical transfer length and have uniform strength along the fibre would be expected to fail at the crack surface of the matrix. For a ductile matrix, the fracture of the strong brittle fibres would contribute to the work of fracture of

the composite. This is by virtue of plastic flow in the matrix at the fibre surface before they fractured, as well as further plastic deformation in the matrix as the fibres relax after the fracture.

At the instant of fracture, the total stored elastic energy in a fibre neglecting that arising from elastic stress transfer, is:

$$W_f' = \frac{\pi d^3 \sigma_f^3}{48 \tau E_f} \qquad (2.17)$$

When there are N fibres per unit area of matrix:

$$\gamma_r = \frac{V_f \sigma_f^3 d}{6 E_f \tau} \qquad (2.18)$$

where σ_f = ultimate tensile strength of fibre

τ = yield strength of matrix

d = fibre diameter

E_f = Young's Modulus of fibre

The strain energy gained by the matrix is neglected since it is small when compared to that of the fibre. This theory is applicable to those cases when polymers are reinforced by fibre bundles where the fibre usually breaks in the plane of the crack.

Piggott based this theory on the assumption that the matrix is visco-elastic. This assumption does not allow the debond between fibre and matrix. Thus, the mechanism of Stress Redistribution will be inadequate to explain the fracture process of the brittle matrices, where debond

between the fibres and matrix is very common and the matrix has very little plastic deformation.

If the expression describing Debond mechanism and the expression describing Stress Redistribution are compared, it could be seen that the Redistribution Energy is a direct multiple of the Debond Energy [62]:

$$\frac{\gamma_r}{\gamma_d} = \frac{V_f \sigma_f^2 \ell_c}{6E_f} \frac{4E_f}{V_f \sigma_f^2 y} = \frac{2}{3} \frac{\ell_c}{y}$$

$$\gamma_d = \frac{3y}{2\ell_c} \gamma_r \qquad (2.19)$$

Therefore, it could be concluded that the Debond Energy term is always bigger than the Redistribution Energy term because the debond length is at least equal to (if not bigger than) the critical transfer length.

2.6 POST-DEBOND SLIDING

When the bonds between the fibres and matrix fail, there would be a sliding of the fibre relative to the matrix. This relative sliding would contribute a considerable amount of energy to the fracture energy of the composite. This energy is in the form of frictional work between the fibre and the matrix. According to Kelly [61], a considerable contribution to the energy required to break the bond between the fibre and matrix will be made by the work done by the interfacial frictional forces between fibre

and matrix moving over a distance relative to each other. This distance is equal to the difference in displacement between fibre and matrix as soon as the bond between them fails. From Harris et al, [50], this distance is roughly equal to the product of the debond length and the differential fracture strain. For a constant shear stress between matrix and fibre, the friction force over the debond length would be given by:

$$F_f' = \tau \pi d \frac{y}{2}$$

This force would act in each direction from the crack face over a distance taken as:

$$d_f' = \Delta\varepsilon \frac{y}{2}$$

Then the work done for each fibre would be:

$$W_{pdf} = 2\ F_f'\ d_f'$$

$$= 2\tau\pi d\frac{y}{2}\Delta\varepsilon\frac{y}{2} \qquad (2.20)$$

Thus for a composite with volume fracton:

$$V_f = N\frac{\pi d^2}{4A}$$

$$\gamma_{pdf} = \frac{V_f \tau y^2}{d}\Delta\varepsilon \qquad (2.21)$$

Kirk et al, [51] had studied the fracture energy of hybrid carbon and glass fibre composites. They found that the work done by Post-Debond Sliding mechanism was the major energy absorption mechanism to the fracture energy of the

glass fibres. The studies according to Munro and Beaumont [66] also indicated that the work done by Post-Debond Sliding mechanism was the dominant energy absorbing mechanism. In fact, in their study, the Theoretical Fracture Energy contributed by the Post-Debond Sliding mechanism constituted more than half of the Theoretical Energy to fracture the composite with debond length the dominating parameter.

2.7 OTHER ENERGY ABSORPTION MECHANISMS

Besides the mechanisms mentioned above, there are also other mechanisms proposed by different scholars. Cook and Gordon [63] had calculated the stress distribution close to the tip of a crack. They showed that there exist tensile stresses parallel to the plane of the crack and ahead of the crack tip. If flaws exist in the interface, these stresses would split the matrix parallel to the fibres and produce a secondary crack which made crack propagation more difficult and thus increases the strength and toughness of the material. Yet little work had been done with this mechanism for fibre composites, therefore, this mechanism would not be considered here.

Hing and Groves [67] observed that the pull-out fibres were often bent and the matrix is always fragmented during fibre pull-out. They proposed a shearing effect which must have been engendered when misaligned ductile wires were

pulled out from the crack. This effect is accountable for part of the energy required to fracture the composite. However, the application of this effect is only restricted to those ductile fibres which could be plastically deformed when being pulled out and is therefore not adequate for the elastic fibres (eg. Glass or Carbon).

Cooper and Kelly [68] had considered the contribution of the matrix to the work of fracture in composites. They suggested that as the crack started to grow, the matrix would deform plastically and by this plastic flow of the matrix, the composite would have high toughness. This mechanism, however, is valid only for ductile matrices (such as metal matrix) which permit extensive plastic deformation. Brittle matrices do not deform plastically. the contributions of matrix to the fracture energy, therefore, becomes very insignificant. Helfet and Harris [69] even ignored the contribution of fracture energy from the matrix resin since it is so insignificantly small in comparision to the other toughness contributions.

2.8 PROBLEM DEFINITION

Munro, in collaboration with other researchers [48,50,51,66] has studied the effects of testing rate (quasi-static and impact) and hybridization in fibre reinforced epoxy resin composites. He has consistently found that the Fibre Pull-Out Energy is the main contributor

to the fracture energy of CFRP; while for GFRP, the value of fracture energy dissipated during fibre pull-out is quite similar to that of the fibre debond. The fracture energy dissipated through the Post-Debond Sliding mechanism is significantly greater than that of the fibre pull-out and debond.

Wells & Beaumont [70] in their recent study proposed that the pull-out lengths of brittle fibre composites were directly related to the flaw distribution in the material and presented analytical expressions which utilized the Weibull Distribution Theory to predict the pull-out and debond lengths of the composites.

Similar work had been published earlier by Beaumont and Anstice [71]. They compared the debond and pull-out lengths calculated by the expressions they derived from the Weibull Distribution Function, with the debond and pull-out lengths calculated by the arithmetic mean method from Kirk et al, [51]. The average difference of these two methods, according to their results, were about 5% for debond length and about 7% for pull-out length. This is not a very significant improvement to the accuracy of the debond and pull-out lengths. Their effects to the Debond and Pull-Out Energies were also not too significant. Therefore, the simple method used by Kirk et al, to estimate the average debond and pull-out lengths was still considered to be accurate enough and was thus used in this thesis to estimate the average debond and pull-out lengths.

As mentioned earlier, the Post-Debond Sliding mechanism was the most significant contributor to the work to fracture glass fibres in epoxy resin. The main effort of this thesis would, therefore, concentrate on this mechanism and would try to investigate more on this important mechanism so as to better understand it.

A closer look at the expression for Post-Debond Sliding work (Equation 2.19) had found that the debond length is an important parameter because its effect is squared (y^2). In all of the above mechanisms studied, most of the parameters were either material constants or measurable experimentally. However, there was a parameter $\Delta\varepsilon$ (the difference in failure strain between the fibre and matrix) which could not be measured, and had to be estimated. This term was not well understood in the past studies. Its value was thus estimated since it could not be measured. In his past studies, Munro estimated this parameter to be a constant of value in the order of 0.01.

From Lubin [72], the failure strain of epoxy resin increased with temperature (Figure 6). It is also known that the tensile strength of glass fibre is relatively constant up to 150 deg. C. [73,74]; while the changes in Young's Modulus of glass with temperature is less than 2% from 0 to 100 deg. C. [75]. The change of failure strain for glass fibre with temperature from 0 to 100 deg. C., therefore, becomes negligible. Thus, a study concerning the

effect of temperature on the fracture energy of the hybrid composites would provide additional information on estimating the $\Delta\varepsilon$ term.

This thesis is an extension of the series of fracture energy experiments for carbon/glass hybrid composites in order (i) to investigate temperature effects on the Fracture Mechanisms of carbon/glass fibre reinforced hybrid composites and (ii) to obtain a better understanding of the $\Delta\varepsilon$ term.

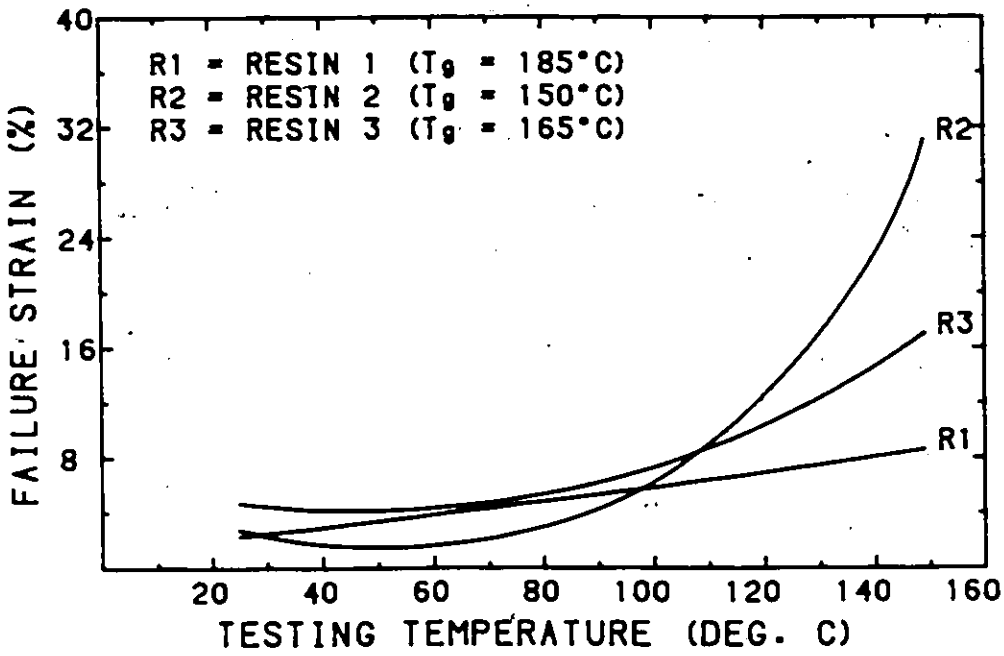

Figure 6: The change of failure strain of resin with temperature [72]

Chapter III

WORK OF FRACTURE OF HYBRID SPECIMENS

3.1 SELECTION OF MATERIALS

3.1.1 Reinforcing Fibres

The reinforcing fibres chosen for this study were the carbon fibre Type II and Glass Fibre Type E (E-glass) as mentioned previously. The reasons for this choice are as follows:

1. In terms of material costs, glass fibres are inexpensive and the cost of carbon fibres, due to advances in production techniques, is decreasing. This made it comparable to other commercially available fibres, eg. boron and Kevlar. Thus, they were very important in today's (and tomorrow's) industry.
2. As hybrid composites, carbon/glass hybrid reinforced composites were the most commonly used ones. Their applications to industry were increasing.
3. Munro [51,66] had studied the same hybrid composites under various conditions. In order to relate his results and to compare them with those of this thesis, the same kind of fibres were used.

3.1.2 Matrix System

It was also mentioned previously that epoxy resin was chosen to be the matrix for the hybrid composites. It was used because it was the most common material used in making high performance fibre composite materials. The epoxy used was Epon 828, manufactured by Shell Chemical Company (Canada); while the hardener chosen was the Ancamine Epoxy Hardener - Anchor 1222. Advantages of this system were that it was nontoxic and was relatively simple to work with. Yet, the most important reason for choosing this matrix system was that it was not room temperature curable. Even if the epoxy and the hardener were mixed, the chemical reaction would not start unless it was heated up to temperatures above 150 degrees Celsius. It was a very desirable property because one of the difficulties in working with composites is the differences in microstructure from specimen to specimen. Part of this difference was contributed from the difference in composition of matrix in various specimens. By using this epoxy system, it would be possible to mix at one time a large quantity of resin, enough to cast all specimens needed. Then, all specimen casts would be cast from the epoxy with the same chemical composition. This was believed to reduce effects caused by non-consistent matrix properties.

3.2 SPECIMEN DESIGN AND TESTING METHOD

The specimen was essentially a rectangular epoxy resin beam reinforced with five (5) fibre tows or rovings which were embedded in the resin (Figure 7). The reinforcing fibres were carbon fibres and E-glass fibres. They were arranged in such a way that there were 6 different ratios of glass fibre to carbon fibre. The different arrangements were shown in Figure 8.

The specimens were tested in three-point bending in order to provide a more controlled failure mode than in tensile testing. The fibre bundles were offset towards the tensile face in order to simulate a tensile testing only mode. Another advantage of the model specimen used here was that it permits the accurate measurement of fibre-matrix debond and fibre pull-out length which were not possible in previous studies. Finally, the quality of specimen can be evaluated in terms of fibre alignment and fibre wetting. Details for the above comments were given in the following sections.

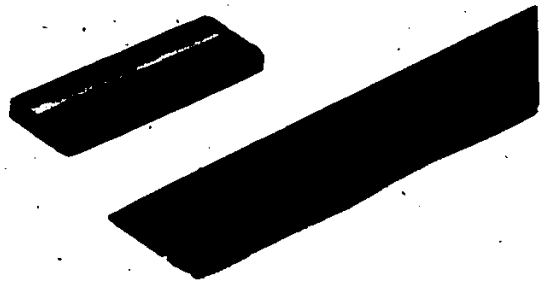

Figure 7: A typical hybrid composite spetimen

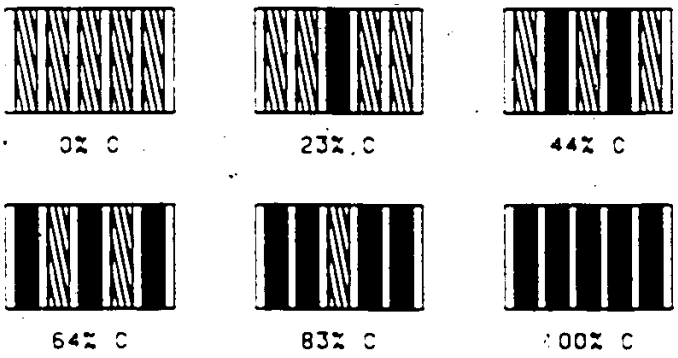

Figure 8: Arrangement of fibre tows for each specimen group

3.2.1 Specimen Size

The width of each specimen was 10 mm. This would allow all the fibres to be embedded in the matrix while leaving enough space between individual strands/tows so that they would not touch each other. As mentioned previously, the specimen was designed to ensure tensile failure of all the fibres. This was accomplished by putting the fibre tape layer in the tensile face of the specimen so that all the fibres would be in tension when it was loaded flexurally.

In the three-point bend test, valid results could be expected only if the crack in the specimen propagates quasi-statically. The size of the specimen was thus very important to ensure stable failure. Since the width of the specimen was practically fixed, a certain criterion was imposed on the thickness of the specimen. The thickness requirement of the specimen was such that the pure epoxy resin layer above the fibre layer had to be thick enough to ensure the neutral axis of the specimen to lie above the hybrid tape. Also, the pure epoxy resin layer should be as thin as possible to minimize unstable fracture. A notch was machined across the middle of the tensile face of the specimen to aid the initiation and propagation of the crack.

In his studies on the three-point bend test, Cooper [76] proposed that with fixed width and thickness, the span of the specimen was important for stable failure when tested flexurally. According to experiments performed on similar

specimens by Kirk et al, [51], it was found that with the size of the cross-section of the specimen, a span of 20 mm was optimal. This corresponds to the shortest length that could be used in the test without causing shear failure of the specimen (as in short beams).

With all the specifications imposed, the dimensions of the specimen were chosen to be 10mm x 3mm x 30mm (Figure 7).

3.2.2 Testing Method

The specimens were tested in a three-point slow bend test. As mentioned in the previous section, the advantage of the three-point slow bend test was that it is much easier to produce a controlled fracture. In addition, the specimen used in the test was relatively easy to fabricate as compared to tensile specimens. By putting the reinforcing fibre tape in the tension face of the specimen, a tensile failure mode of the fibre could be obtained [51]. Thus the experiment was essentially performed as a tensile test on the hybrid composite by using a simple three-point bend test machine (Figure 9).

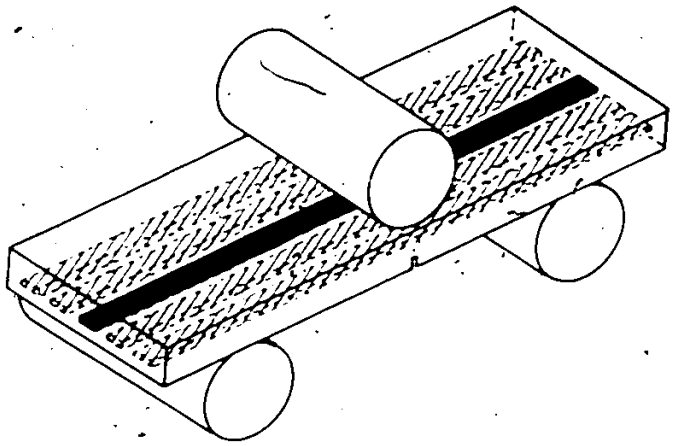

Figure 9: Three-point bending beam specimens [51].

3.3 FABRICATION OF SPECIMENS

3.3.1 Mould

Figure 10 shows the mould used to cast the hybrid specimen plates. This mould was an improved version of the similar mould used by Dr. Munro in his previous studies [51,66].

The brass mould was divided into four sections by three rows of slots across its surface. Each section was 30 mm long. There were 76 slots in each row. The purpose of the slots was to keep the bundles in place and parallel to, but without touching, one another.

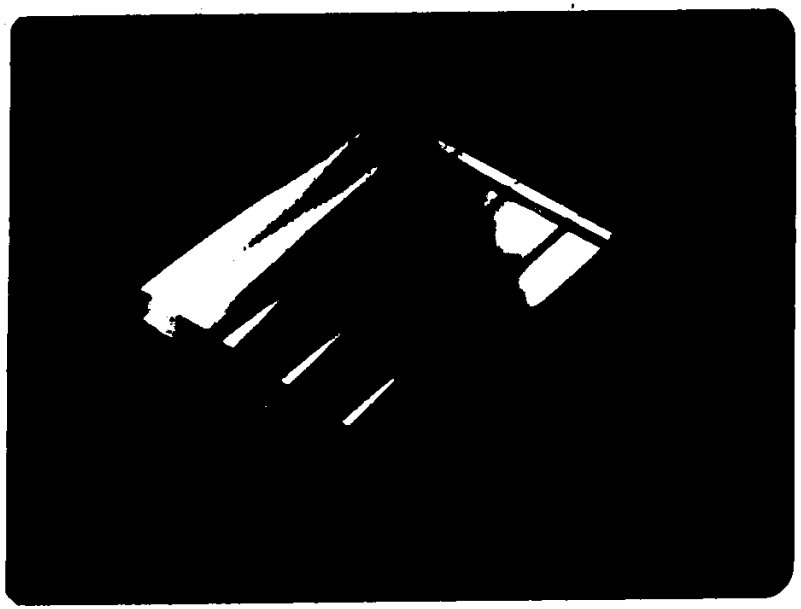

(a) original method

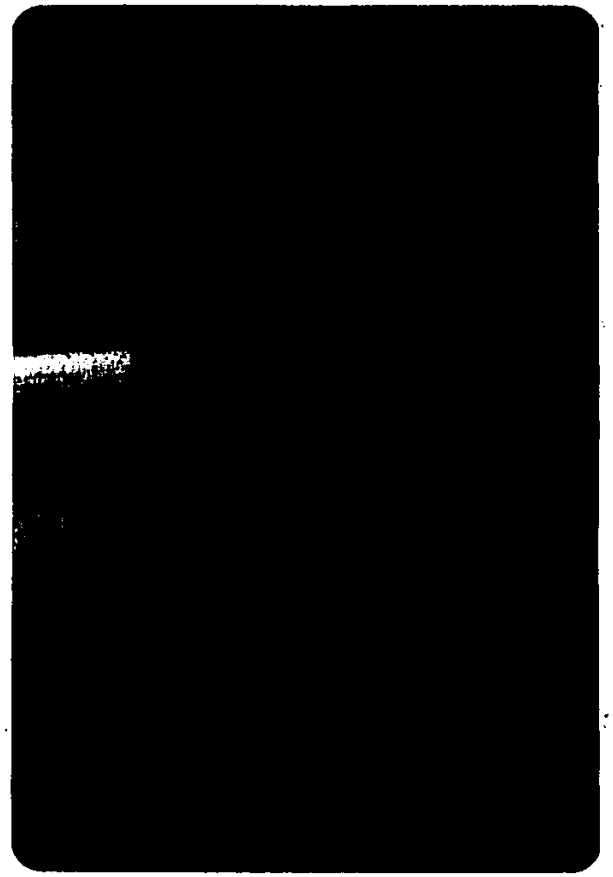

(b) improved method

Figure 10: The brass mould

3.3.2 Preparation of Mould

In order to prevent the resin from sticking to the brass mould, a mould release treatment, Dow Corning Compound No. 7, was applied to the mould. A thin layer of the compound was carefully applied to the surface of the mould including the spaces between the machined slots. It was then baked in an oven at 175 degrees Celsius for twelve hours. After the heat treatment, the excess release agent was wiped off by a piece of soft cloth. Caution was taken to make sure that the excess release agent stuck between the machined slots were also cleaned out. The brass mould was cleaned to the extent that no greasiness was felt (through touching).

3.3.3 Casting the Hybrid Plate

After the mould was cleaned, the fibre bundles were then placed in the mould. The fibre bundles (both glass and carbon) were cut into about 20 cm. long tapes. They were then laid by hand on the slots of the clean mould. Different ratios of glass to carbon tows were used to produce specimens of different carbon to glass volume fractions (Figure 8).

One end of the fibre tows was sealed with polyester resin in order to prevent the resin from leaking out from that end. The polyester resin also serves to fix the bundles to the mould (temporarily) and prevent the fibre

tows from sliding. A counter-weight (75 gm) was attached to the other end of the fibre bundle to provide some tension to the fibre so that the fibres could be kept straight and parallel to each other.

The well-mixed epoxy (EPON 828 and hardener ANCHOR 1222) which was preheated to 50 degrees Celsius was then poured on the surface of the mould (which was also preheated to 50 degrees Celsius). The mould, with the fibre and resin in it, was then transferred to the vacuum jar for 10 minutes. During this period, all the air bubbles which were trapped between the fibres would be released. This process of vacuuming would promote good wetting between the fibre and resin. After the vacuum treatment, the mould was removed to the oven to be cured. The heating cycle used was two hours at 150 degrees Celsius and two hours at 175 degrees Celsius. (The heating cycle was shown in Figure 11).

After this four-hour heating cycle, the resin would be cured and the mould, which was still hot, was removed from the oven and quickly disassembled. The cast plate was then carefully unloaded from the mould and was left to cool inside the oven under a weight to prevent it from warping when it was cooled. After the cast-plate cooled down to room temperature, it was cut into specimens. A maximum of forty-eight (48) specimens could be obtained from a well-cast plate.

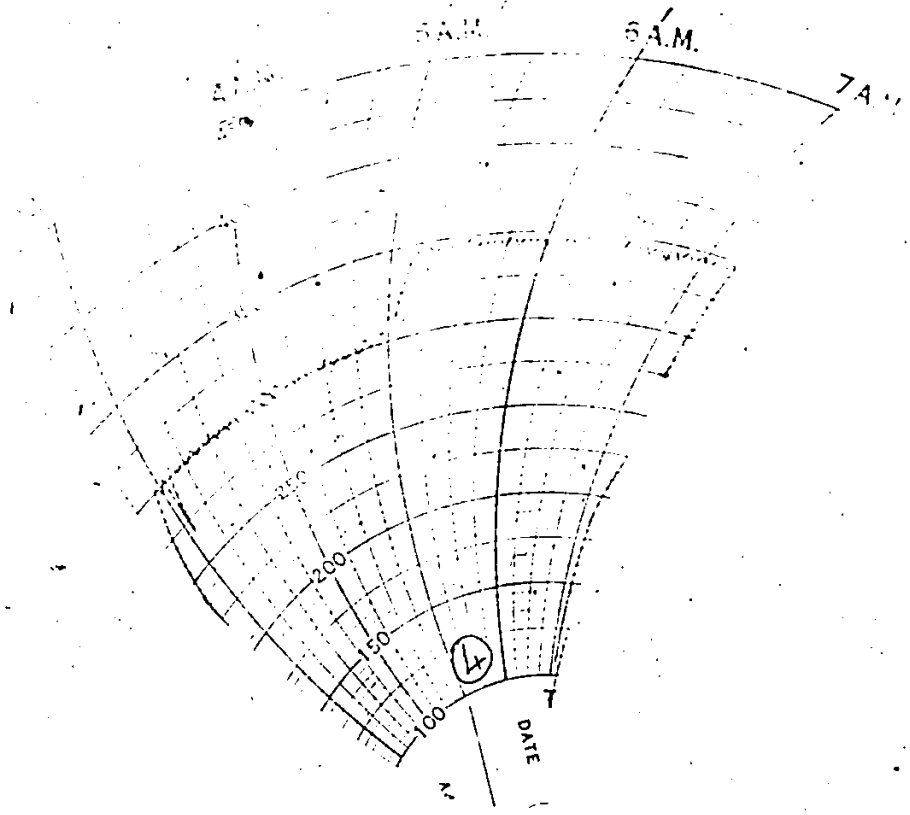

Figure 11: Heating cycle to cure the epoxy resin

3.3.4 Machining the Specimens

After fabrication, the hybrid plates were ready to be machined. First, each plate was cut into four 30 mm wide, 150 mm long strips along the existing slots on the plate with a fine tooth bandsaw. Each of these 30 mm x 150 mm strips was then mounted on a vacuum fixture (Figure 12).

The top surface of the composite was machined to a thickness of 3.0 ± 0.1 mm. On the bottom surface of the strip, a slot of 0.2 mm wide and approximately 0.3 mm was machined. The slot was cut at the middle and along the width of the strip. This slot was a crack initiator when the specimen was fractured. The strip was then cut into 10 mm wide specimens along the fibre direction. A total of 12 specimens could be obtained from each strip.

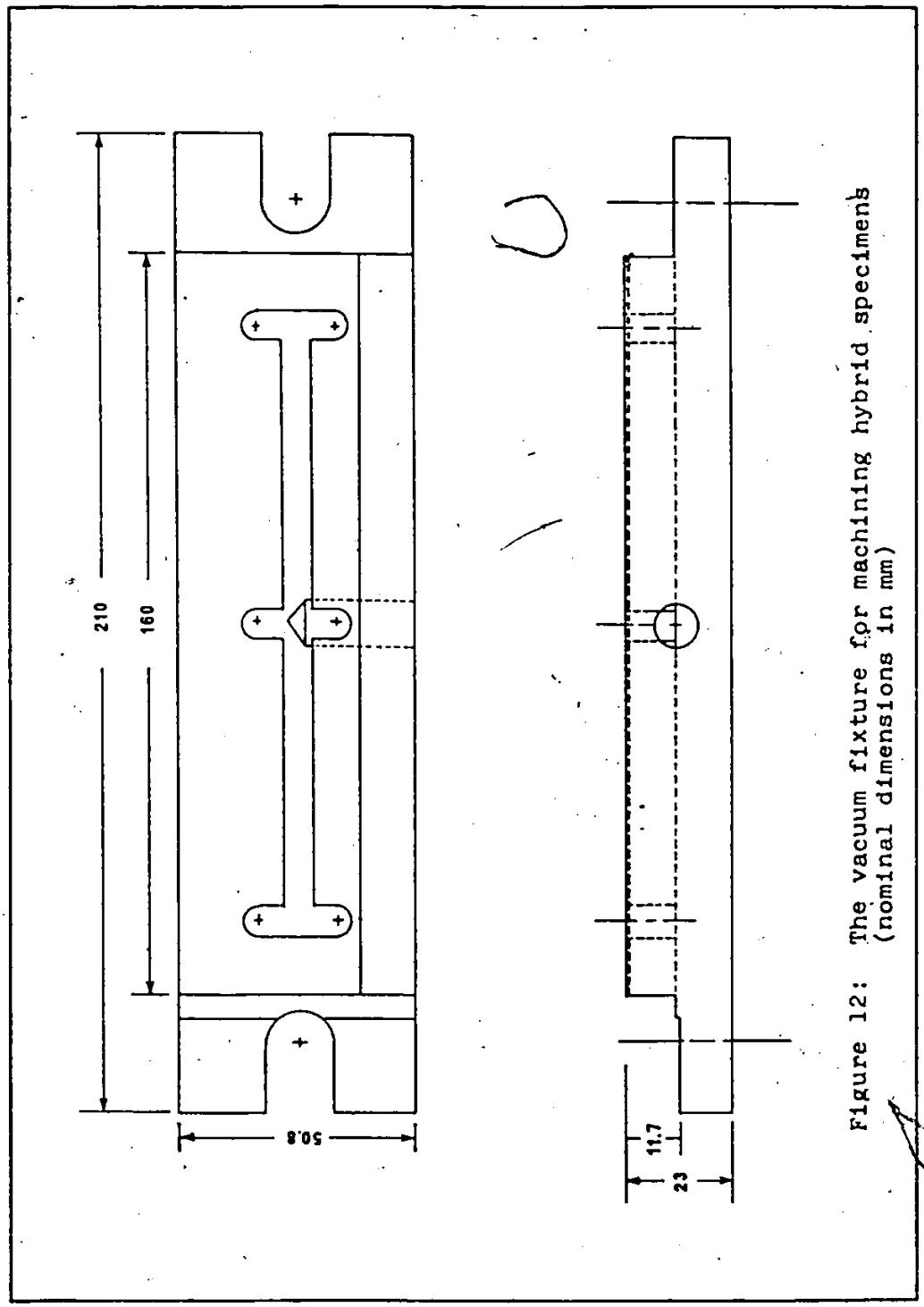

Figure 12: The vacuum fixture for machining hybrid specimens (nominal dimensions in mm)

3.3.5 Quality of Specimens

After the specimens were machined, each of them was carefully examined to choose the best quality ones for the final test. First, the alignment of the fibres was checked. It was stipulated that all the specimens used in the final test should not have the fibres misaligned for more than three (3) degrees from the y-direction as shown in Figure 13. Also, all the fibre tows in the specimen should not be damaged during the cutting and machining of the plate.

According to the criteria mentioned, all the specimens machined from the six cast hybrid plates were divided into four groups, ranging from the best quality ones, group 1, to the unacceptable ones, group 4. All the specimens in groups 1 and 2 would be tested while only some of the better quality ones in group 3 were tested. All the group 4 specimens, the worst quality ones, were rejected. A total 187 specimens were selected and tested. Among them, 65 of them were from group 1, 74 from group 2, and 48 from group 3. The specimens for each temperature test were selected to have equal number from groups 1, 2, and 3.

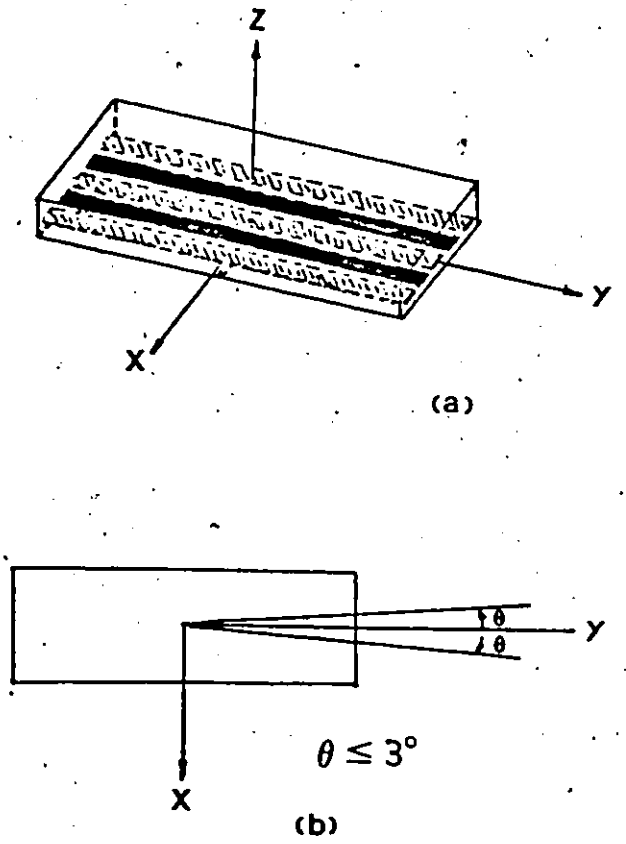

Figure 13: The fibre alignment requirement of the specimens

3.4 INSTRUMENTATION AND TESTING PROCEDURE

3.4.1 Instrumentation

The instrument used for the three-point bend test was the Instron Universal Tensile Testing Instrument Model #TTCM. The load during the test was monitored by a Instron 5000 N Reversible Load Cell. A corresponding load-deflection curve was plotted by the Instron Chart Recorder simultaneously for each specimen during the test. The Instron Environmental Chamber Model 3111, which had the capacity to control thermal environment over the temperature range from -75 degrees Celsius to +205 degrees Celsius, was used to provide the needed thermal environment for the experiment. A digital thermometer, the Digimite Digital Temperature Indicator - using the K-type (Chromel Alumel) thermocouple probe, was used to measure the correct temperature of the environmental chamber during the experiment. A small blower was used to circulate cool air to the extension rods and to the load cell to keep the load cell from being overheated by the heat conducted from the chamber.

3.4.2 Preparation of Specimens Prior to the Experiment

The surfaces of the specimens were first abraded with #240 and #600 grade silicon carbide paper. Then, the specimens were polished in the Struers DP-U Electric Disc Polisher with Grade A (0.3 micron) polishing Alumina powder.

The specimens were polished to ensure that the debond area between the fibre and the matrix could be seen clearly after they were fractured. This would make the precise measurement of the debond area possible. A razor blade was used to run along the machined notch of the specimen to create a sharp initial crack. This sharp crack would aid the failure of the specimen and to make a 'straight' failure surface. A 'straight' failure surface was desired because it would make the measurement of the pull-out length much more straightforward and simple.

3.4.3 Testing Procedure

The procedure of the experiment is summarized as follows:

1. The environmental chamber was first adjusted to desired temperature and batch of specimens were placed inside the oven.
2. The prepared specimen was then transferred to the chamber and rested on the supporting jig.
3. Alignment of the specimen and the indentor was checked - the machined notch of the specimen was adjusted so that it was aligned parallel to the indentor.
4. The specimen was then left inside the chamber for approximately twenty minutes to warm up to the prescribed testing temperature.

5. The temperature of the specimen was estimated by using a sample specimen with a hole drilled at the centre. Then a thermocouple probe was inserted into the hole. The temperature registered by the Digital Thermometer would indicate approximately the temperature of the specimen.
6. Once the specimen reached the prescribed testing temperature, it was then fractured by the indentor on the Instron testing machine at a crosshead speed of 2.8 cm per min.
7. The corresponding load-deflection curve was plotted during the experiment.

3.5 OBSERVATIONS

Certain observations were made during the experiment and they were summarized as follows:

1. Some specimens, especially at lower temperatures (room temperature), flew apart when they failed. But at higher temperatures (especially at about 80 degrees Celsius), the specimens tend to fail in a more controllable manner.
2. In spite of the ventilating blower which kept blowing cool air to the extension rod and to the load cell, high testing temperature (especially at 80 degrees Celsius) in the chamber did have some effect to the load cell. The overall effect of the temperature was

to shift the origin while the overall scale of the Chart Recorder was not affected. Therefore, the measurement made from the Recorder was still accurate.

3. When the specimens (tested at various temperatures) failed, there was emission of acoustic energy which could not be measured. Thus the acoustic energy was not included in calculation of the total Fracture Energy.

3.6 EXPERIMENTAL RESULTS

The total energy (**U**) required to fracture the specimen could be obtained from the load-deflection curve (Figure 14). The Experimental Fracture Energy, or Work of Fracture (WOF), of a specimen was measured by finding the area under the load-deflection curve which was plotted during the experiment for the specimen. A planimeter was used to measure the area. It had the dimension of kg/min. This area was converted into appropriate unit (i.e. Joules) by the method outlined in Appendix A. The Work of Fracture of the fibrous composite was given by:

$$\gamma_f = \frac{U}{2A} \qquad (4)$$

where A was the total cross-sectional area of the ends of the fibres in the composite. The assumption made was that

the resin in the specimens does not have any contribution to the total Fracture Energy. It only serves the purpose to bind the fibres together. The experimental results for the four temperatures are shown in Figure 15. The results are tabulated in Table 5 in Appendix E.

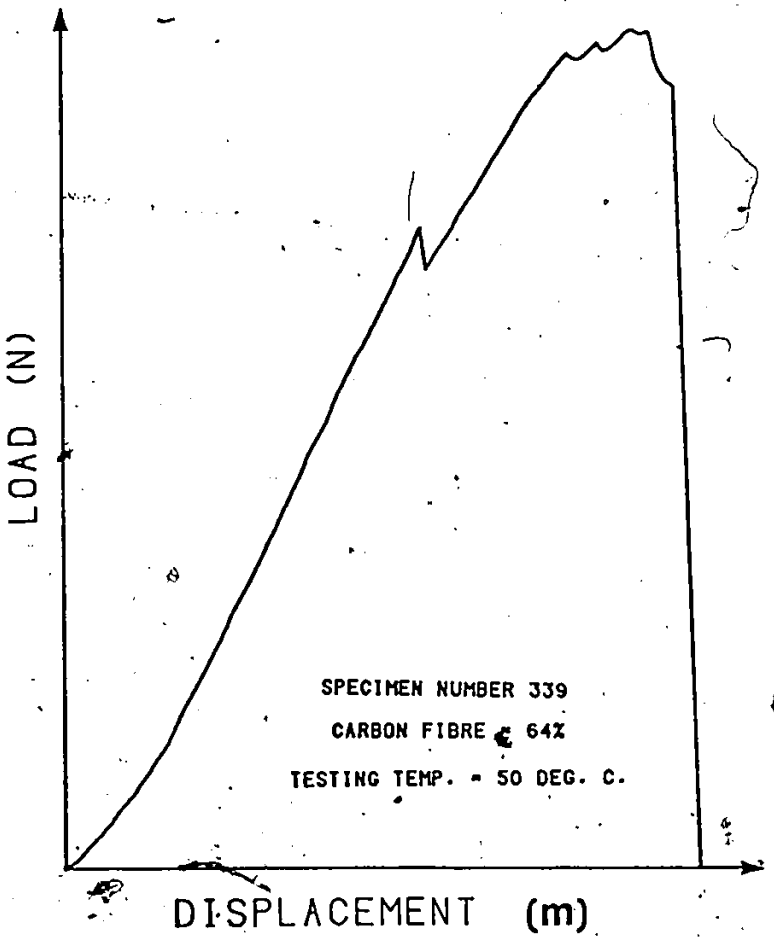

Figure 14: Load-deflection curve of a typical specimen

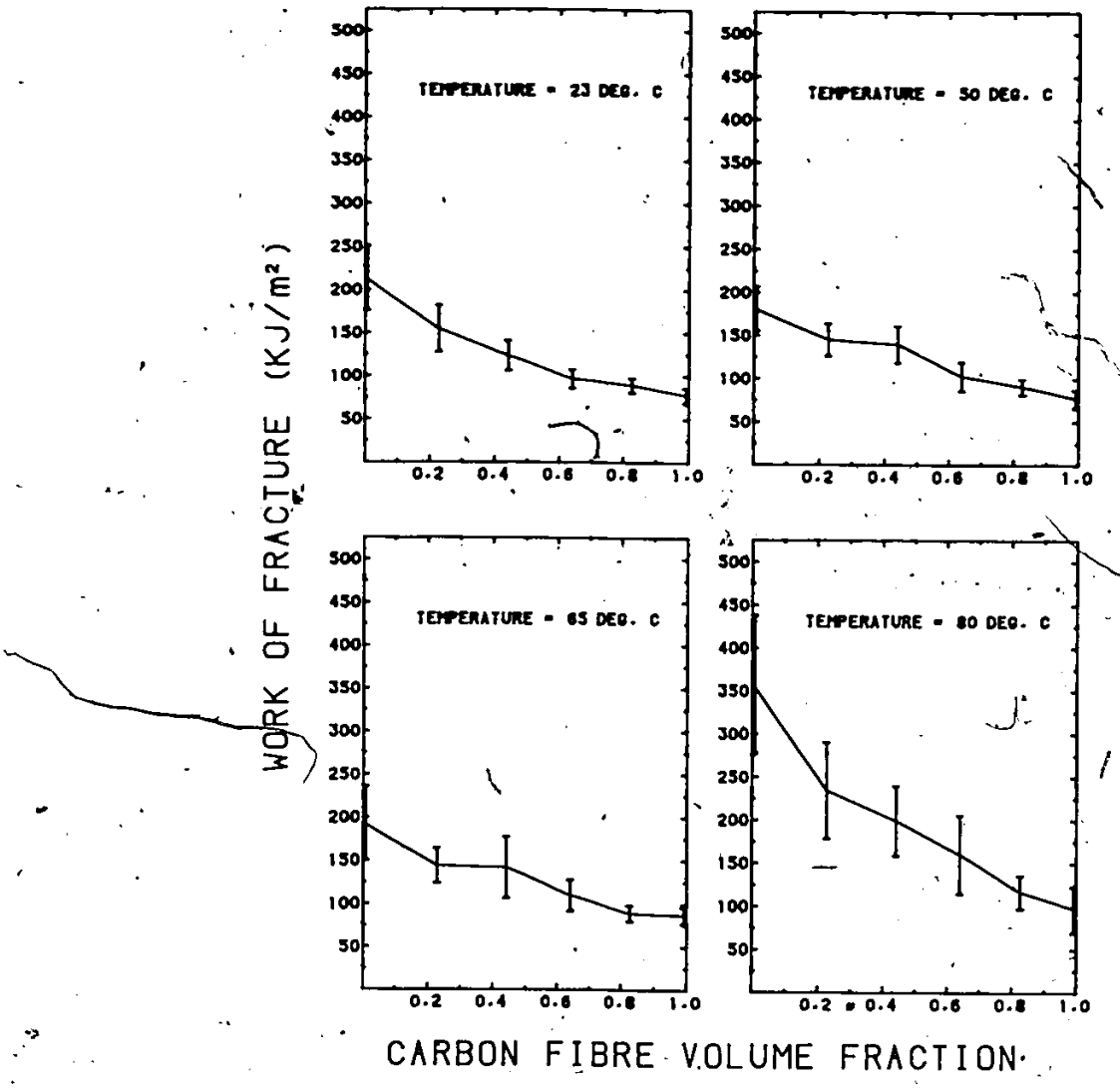

Figure 15: Work of fracture as a function of carbon fibre volume fraction (mean ±1 standard deviation)

Chapter IV

EXPERIMENTAL PARAMETERS

4.1 PULL-OUT AND DEBOND LENGTHS

4.1.1 Introduction

It was mentioned in Chapter 2 that fibre pull-out was the chief mechanism governing the fracture energy of CFRP; while fibre pull-out and debond together with the Post-Debond Sliding mechanism were the main contributors to the fracture energy of GFRP. In this thesis, the hybrid specimens similar to those used by Kirk et al, [51] and Munro [66] were used. Therefore, it is logical to assume that the same mechanisms applicable to those of Kirk and Munro's would also be suitable to predict the fracture mechanism of this work. The expressions for Pull-Out and Debond were listed as follows:

$$\gamma_{po} = \frac{V_f \sigma_f \ell_c}{24} \qquad (2.7)$$

$$\gamma_d = \frac{V_f \sigma_f^2}{4E_f} y \qquad (2.16)$$

For these two Equations, the ultimate tensile stress, σ_f, and elastic modulus, E_f, of the fibres were known material constants and the volume fraction of fibre, V_f, could be

calculated from the total number of fibres in the matrix and known fibre diameters. There were two parameters, ℓ_c and y, which were not known. However, they could be measured experimentally. The term ℓ_c, the critical transfer length, is, according to Harris et al, [50], equal to twice the pull-out length of the fibre. Thus, ℓ_c could be measured indirectly from the average pull-out length of the specimens.

The debond zone was the opaque area which developed after the interface bond was broken. It was verified, by observation of both faces of the specimen, that the extent of the debonded zones was constant throughout the thickness of each fibre tow. This implies that measuring the average length of fibres within the translucent area on the fractured specimens would give the debond length of the specimen. The detailed procedure in measurement and related evaluation of the pull-out length and debond length for each specimen tested are described in the following sections.

4.1.2 Pull-Out Lengths of the Hybrid Specimens

The pull-out length of a specimen is the average length of fibres protruding from the fracture surface of the specimen after it was broken into two parts (Figure 16). Since the fibre bundles of glass and carbon of the specimen did not mix together, it is possible to identify the pull-out length of glass fibre and of carbon fibre separately.

This allows the precise measurement of individual glass fibre and carbon fibre pull-out lengths respectively.

The protruding fibre tows could be seen clearly against a light background when it was projected on a screen using a profile projector. The profiles of the fibre tows were magnified 50 times. The silhouette of the bundle protruding from the fracture surface was then carefully traced. This trace was made for each fibre bundle in the specimen. Since the specimen was broken into two after the test, ten traces were made for each specimen - 5 bundles of fibre per specimen and 2 'halves' for each specimen. There were 187 specimens tested in this study, therefore, there were 1870 traces made for the pull-out lengths of the specimens. A typical trace of the pull-out fibre tow is shown in Figure 17.

The area of each trace was measured carefully by a planimeter. The maximum pull-out length of each fibre bundle could be obtained by dividing the pull-out area of the bundle by its width. The maximum average fibre pull-out length (ℓ_{max}) of a specimen is then calculated by averaging all maximum pull-out lengths of the same kind of fibre within that specimen. Thus, in the hybrid specimen, there are maximum average pull-out lengths for glass fibres and carbon fibres. The effect of temperature on the pull-out lengths of reinforcing fibres in the hybrid specimens is shown in Figures 18 and 19.

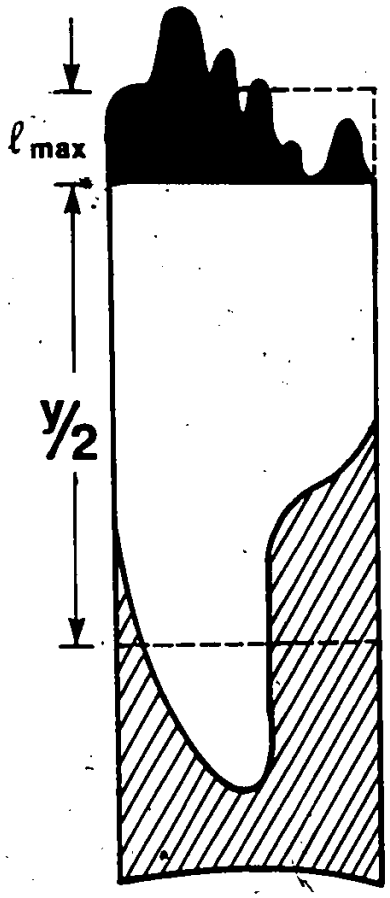

Figure 16: The pull-out and debond length of a specimen [51]

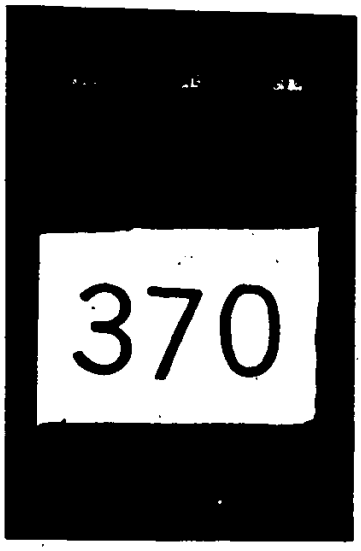

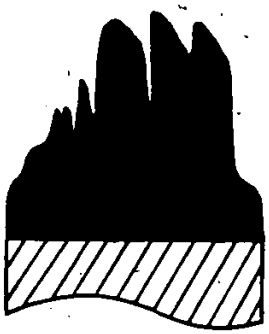

Trace of the glass fibre tow in the centre of specimen No. 370

Figure 17: Typical tracing of the maximum pull-out length of a fibre tow

4.1.3 Debond Lengths of the Hybrid Specimens

The debond area could be seen clearly when it was reflected under a light source. In the hybrid specimen, only the debond area of glass fibre was measured. The debond area of carbon fibre was considered to be negligible. This assumption could be verified by merely inspecting the debond area of the carbon specimens. Beaumont and Harris [48] had performed experiments on the carbon composites and found out that the fracture energy of carbon composites was dependent principally on the work done to pull the broken fibre out of the matrix. This further verified the assumption made here.

The Profile Projector was set to the reflected light mode. Light was then shone on the fractured specimen. The image of the specimen, which was projected on the screen of the projector, was magnified by ten times. A similar trace of the debond area was then made with respect to the crack surface. Only traces of the glass debond area were made. A total of 935 such traces were made for the debond area of glass fibre tows. A typical trace of the pull-out and debond area is shown in Figure 16. The same method used to find the maximum average pull-out length (ℓ_{max}) was repeated to find the average debond length (y) of the specimen. The debond length thus obtained is equal to half of the total debond length (y/2) of the fibre. The total debond length, y, of a fibre tow is the sum of the two

average debond length, measured from the fibre tow, obtained from the two fragments of the specimens. The results were shown in Figure 20.

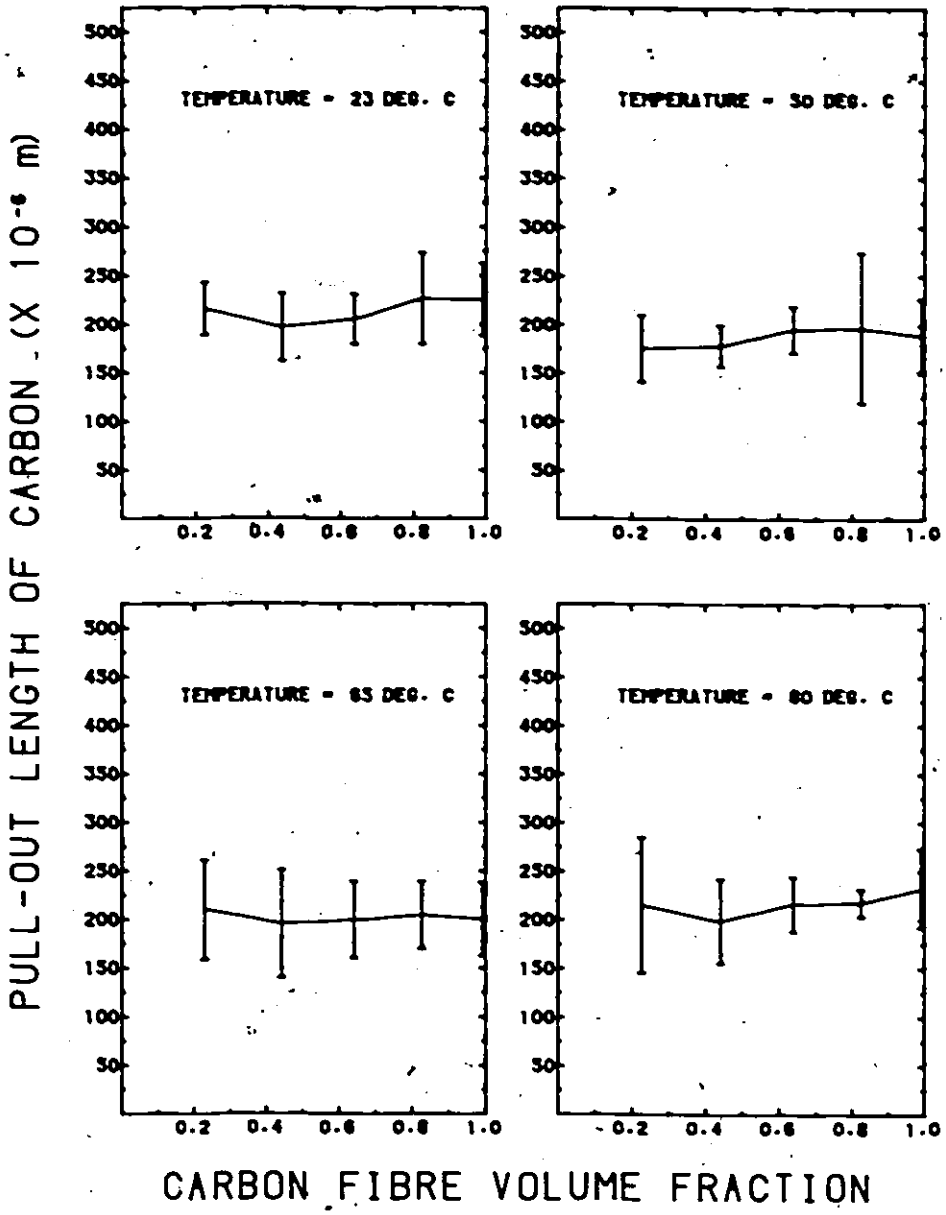

Figure 18: The effect of temperature on pull-out length of carbon fibre (mean ±1 standard deviation)

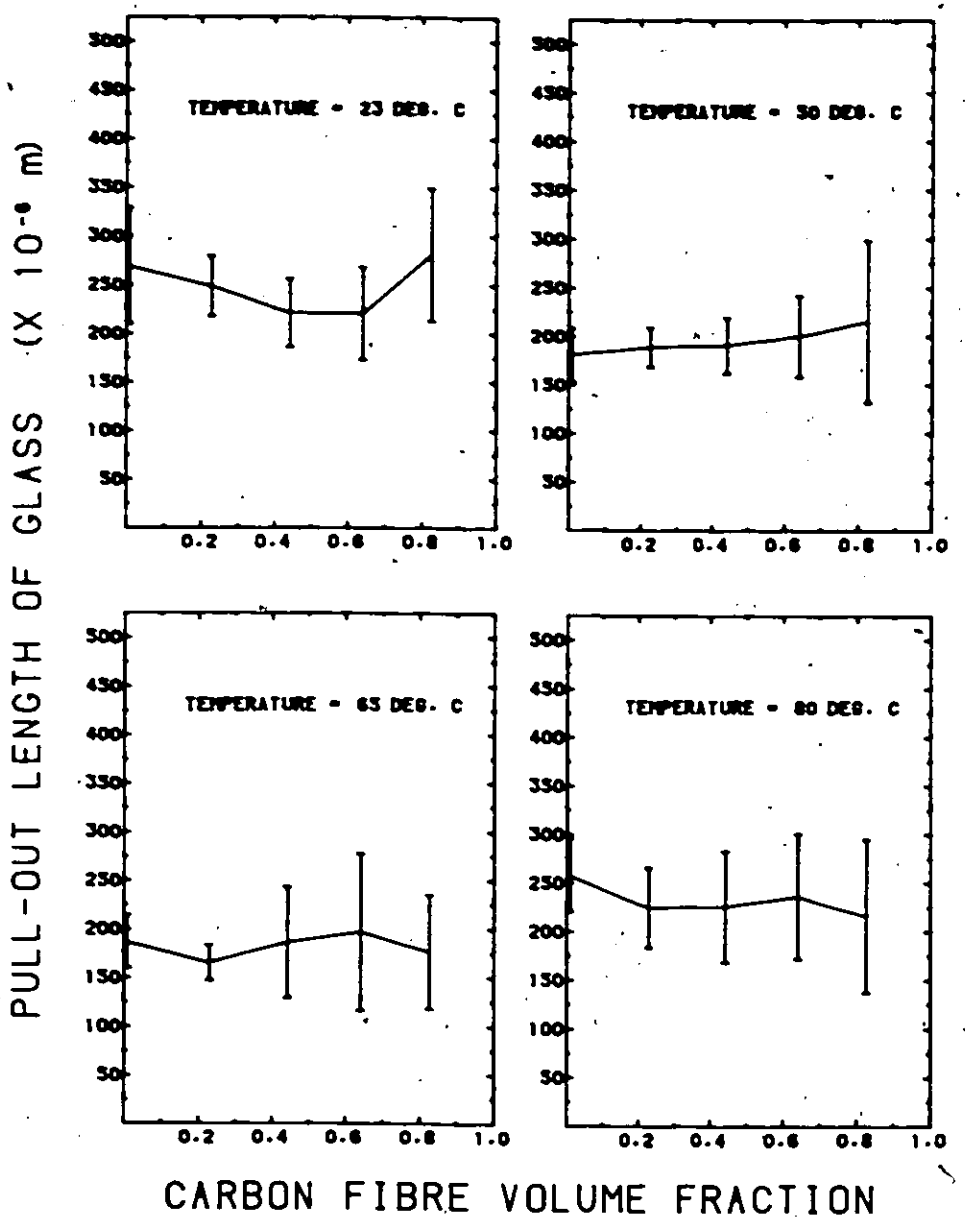

Figure 19: The effect of temperature on pull-out length of glass fibre (mean ±1 standard deviation)

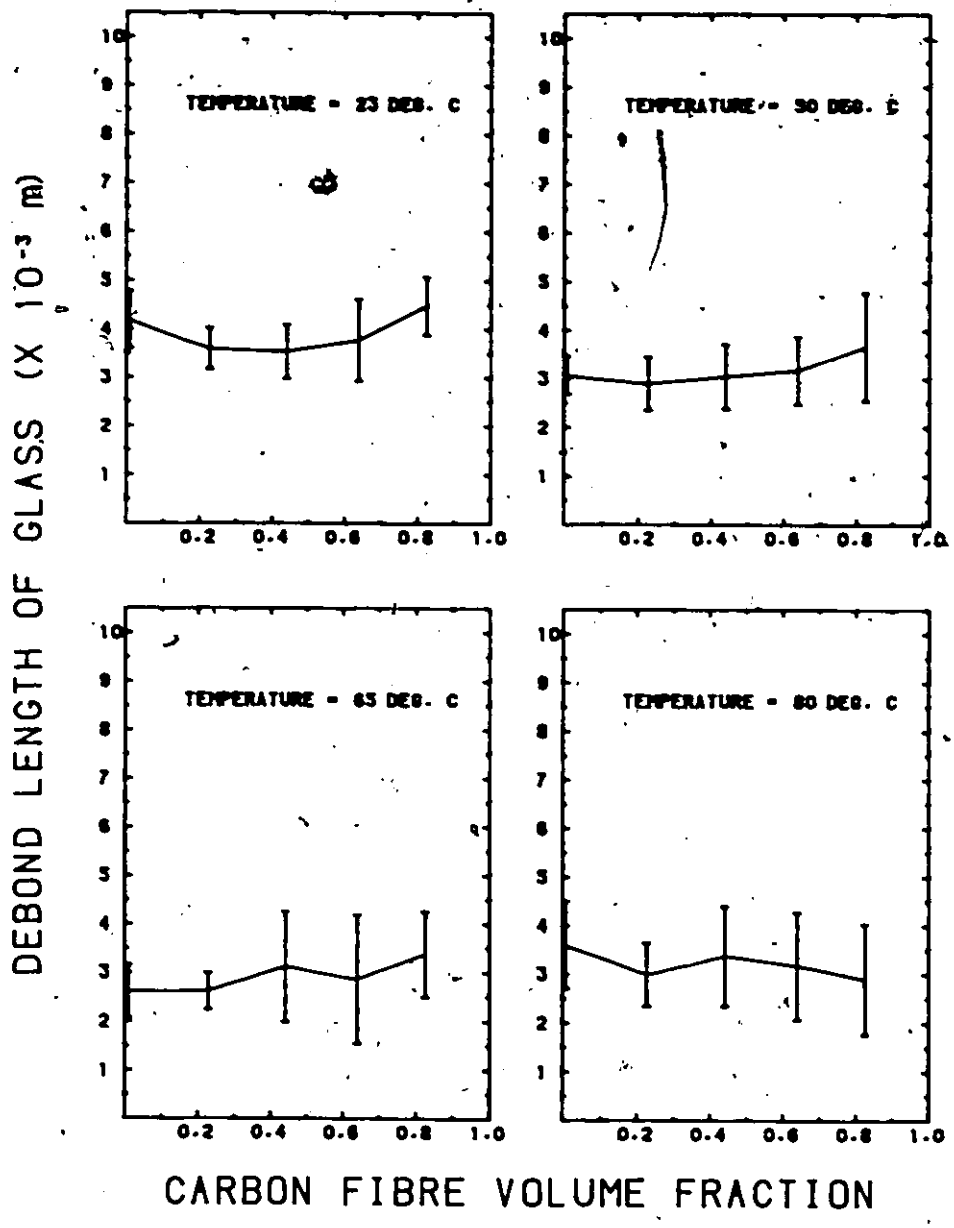

Figure 20: The debond length of glass fibre (mean ±1 standard deviation)

4.2 TENSILE TESTING OF RESIN SPECIMENS

4.2.1 Introduction

The expression for the Post-Debond Friction Energy from Chapter 2 is:

$$\gamma_{pdf} = \frac{V_f \tau y^2}{d} \Delta\varepsilon \qquad (2.21)$$

From the above Equation, it is obvious that there are two unknowns, namely, τ, the interfacial shear stress, and, $\Delta\varepsilon$, the differential failure strain between the matrix and fibre. The shear stress, τ, could be eliminated by substituting Equation (2.3). Therefore, Equation (2.21) becomes,

$$\gamma_{pdf} = \frac{V_f \sigma_f y^2}{2 \ell_c} \Delta\varepsilon \qquad (4.1)$$

In past studies, $\Delta\varepsilon$ was estimated as a constant having a value in the order of 0.01. In this work, an alternative method was used to evaluate $\Delta\varepsilon$ experimentally. Since the failure strain of resin increases with temperature [72] and the failure strain of fibre is not affected by the temperature range tested, testing the bulk resin to investigate the temperature effect would provide better insight into the term $\Delta\varepsilon$. In addition, the elastic modulus of the resin at the testing temperatures was required for calculations of the neutral axis (Appendix C).

The series of experiments and analyses involved are presented in the following sections.

4.2.2 Specimen Fabrication

In order to measure the change of failure strain of bulk resin with temperature, an ASTM Standard Tensile specimen was used. The specimens were made by the same epoxy resin system used also to fabricate the hybrid specimens in this work.

A large quantity of Epon 828 was mixed with suitable quantity of hardener - Anchor 1222. This batch of mixture would be used to cast all the bulk resin tensile specimens needed. This would help to assure consistent properties in all the resin specimens.

The casting procedure of the bulk resin plates is similar to that described in Chapter 3 except that there were no fibres in these plates. A total of five resin plates were cast, cut, and machined into the ASTM Standard Tensile Specimens (Figure 21). 24 tensile specimens were made from these plates.

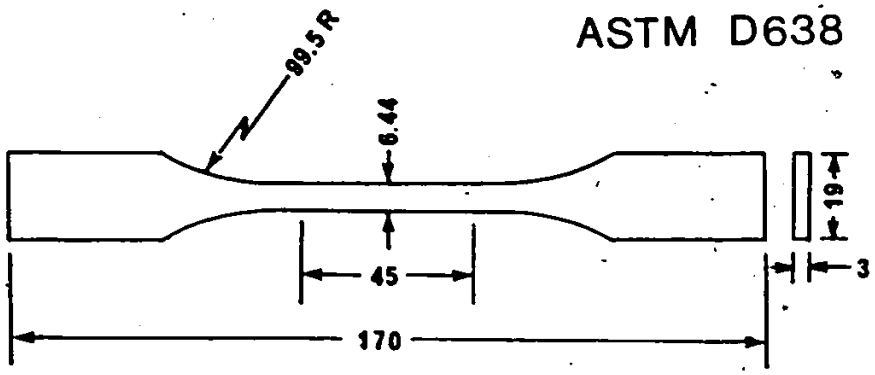

Figure 21: A bulk resin tensile specimen (nominal dimensions in mm)

4.2.3 Specimen Testing

Each specimen was tested in the Instron Universal Tensile Testing Instrument Model #TTCM. The load during the test was measured by a Instron 5000 N Reversible Load Cell. A load deflection curve registering the load and elongation of the specimens during the test was generated by the Instron Chart Recorder for each specimen. The Instron Environmental Chamber Model 3111 was used to provide the desired temperature condition when the specimens were tested at elevated temperatures. A digital thermometer, the Digimite Digital Temperature Indicator with the K-type Thermal Couple Probe was used to check the temperature of

the chamber to make sure it was at the correct temperature when the specimens were tested.

The testing temperatures used for these specimens were room temperature (25 deg. C), 50, 65 and 80 deg. C. Five specimens chosen from different resin plates were carefully tested at each temperature. A total of 20 specimens were tested.

The testing procedure was very similar to that for the hybrid specimens, with the exception that an extensometer was used to measure the strain on the specimens when they were tested at room temperature. This measurement was used to correlate the actual strain of the specimen to the load deflection curve plotted for the specimen. For the other specimens tested at elevated temperatures, the extensometer could not be used to measure the strain. Thus, the strain could only be calculated from the load deflection curve of the specimen. This correlation measure provides a scaling factor for the strain value of the other specimens leading to a better estimate of the failure strain of the specimen.

In order to simulate the strain rate of the resin in the hybrid specimen, the strain rate of the composite at a given cross-head speed was evaluated (Appendix B). This strain rate was related to the strain rate needed for the tensile specimen. A feed rate of 0.67 cm/min was chosen for the tensile test for all temperatures.

4.2.4 Experimental Results

The strain measured by the extensometer during the room temperature test was divided by the gauge length of the specimen to get the actual strain. This strain was compared with the strain computed from load deflection curve plotted for the specimen during the test. A correlation factor was therefore obtained. The value of failure strain of those specimens tested at elevated temperatures were calculated from the load deflection curve with known cross-head speed of the Instron and known speed of the chart of the recorder. The adjusted strains of the specimens could then be calculated by taking into consideration the correlation factor between the actual strain and the strain calculated from the load deflection curve. The failure strains of the resin at different temperatures were then plotted as shown in Figure 22. The modulus of the resin versus temperature was also plotted as shown in Figure 23. The numerical results are given in Table 9 in Appendix E.

From Figure 22, it is obvious that the general nature of the results agree with that of Lubin (Figure 6). The failure strain of resin did increase with temperature (especially at temperatures close to glass transition temperature). Since the failure strain of glass would not be affected within the temperature range tested, it could be concluded that the term $\Delta\varepsilon$, (i.e., essentially the difference of failure strain between fibre and matrix) would

increase with temperature. The change in $\Delta\varepsilon$ could therefore produce significant changes in the Post-Debond Friction Energy with temperature (Equation 4.1).

Another interesting point to note is that the Young's Modulus of the bulk resin decreased with increasing temperature.

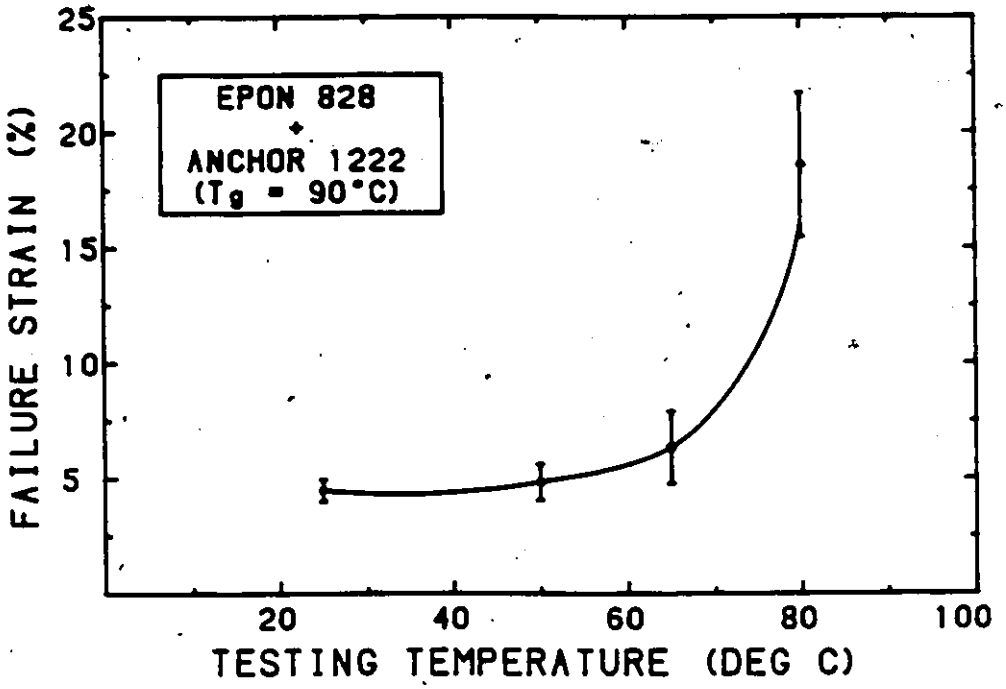

Figure 22: The failure strain of resin at different temperatures (mean ±1 standard deviation)

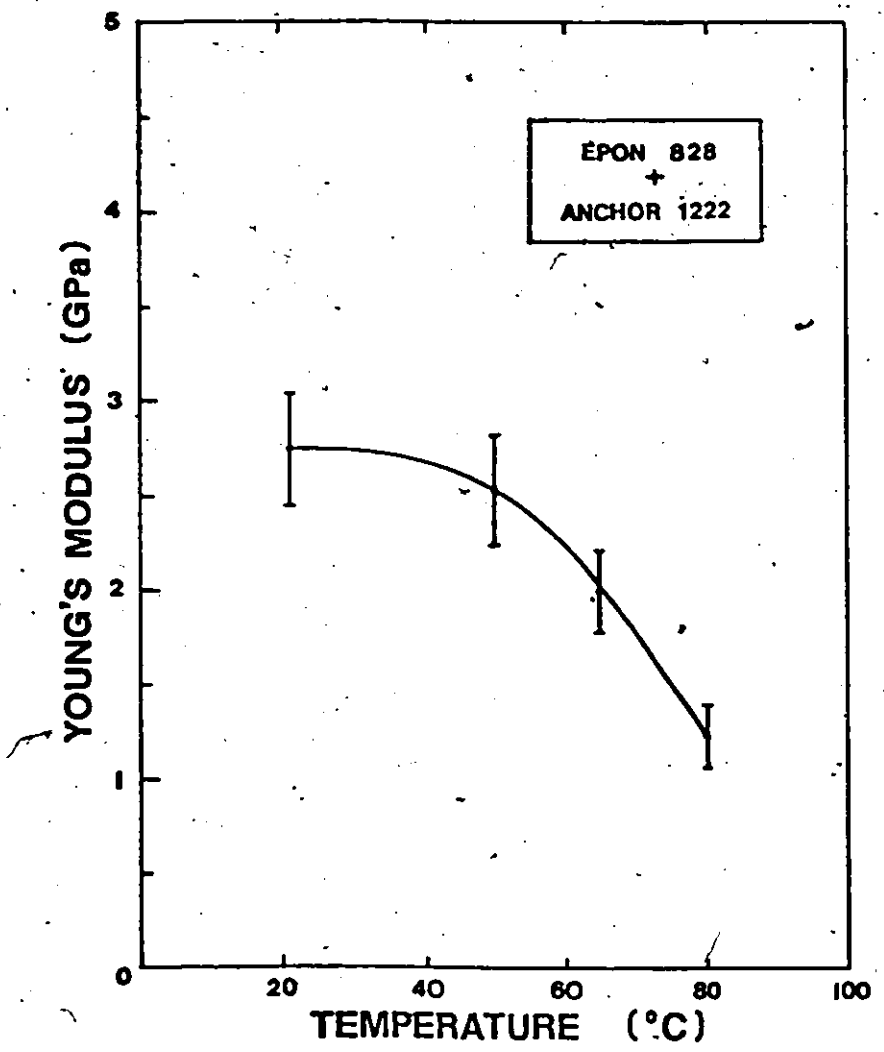

Figure 23: The change of elastic modulus of resin with temperature (mean ±1 standard deviation)

4.2.5 Method to obtain $\Delta\varepsilon$

In the last section, it was shown that the failure strain of bulk resin increased with temperature. This information gave a better understanding of the parameter $\Delta\varepsilon$. However, the failure strain of the bulk resin became extremely high (close to 20%) at high temperature (80 deg. C). It was, moreover, impossible for the matrix resin in the hybrid specimens to attain such a high strain (the failure strain of the composites in this work was typically 3 - 8%); the matrix must have been constrained by the fibres. Therefore, the value of the failure strain of the bulk resin was not used to evaluate $\Delta\varepsilon$.

In order to estimate $\Delta\varepsilon$, the tensile failure strain of the fibre bundles was evaluated. The Equation used was from Appendix B:

$$\epsilon = 12 \frac{c}{L^2}\delta \qquad (B.6)$$

In the above expression, the term 'c', which was the distance from the neutral axis, was not known. In order to evaluate 'c', it was necessary to locate the neutral axis of the composite specimen. The method to locate the neutral axis was outlined in Appendix C. Equations (C.3) to (C.5) from Appendix C are repeated here as follows:

$$k = \sqrt{2pn + (pn)^2} - pn \qquad (C.3)$$

$$p = A/bd \qquad (C.4)$$

$$c = d\,(1-k) \qquad \text{(C.5)}$$

with all the variables shown in Figure 24.

From the above Equations, it is clear that 'c' is different for the various groups of specimens which had varying carbon fibre volume fractions and testing temperatures. With the value of 'c' changing, the resulting strain of the specimen would be changing likewise. Thus, it would be necessary to evaluate the failure strain for all the tested specimens.

The failure strain of the specimen was evaluated at 2 points. The tensile strain of the bundles was calculated first when the crack just reached the fibre bundles (point A, Figure 25). At this stage no fibres were fractured. The 2nd strain value was taken when all the reinforcing fibres were fractured i.e. the specimen had broken into two parts (point B, Figure 25). The average strain was obtained by adding the two strains and dividing by 2. This is then the mean failure strain of the specimen. This strain, when the failure strain of glass fibres was subtracted, was taken as $\Delta\varepsilon$. This procedure was performed for all 187 specimens.

$$\epsilon = \frac{12C}{L^2}\delta$$

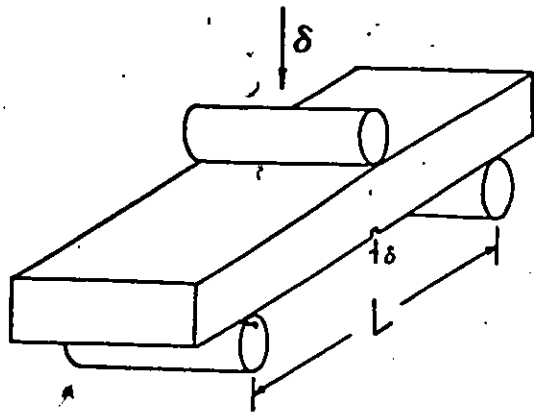

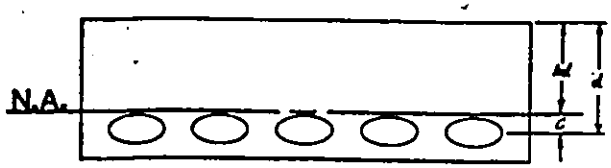

Figure 24: The rate of strain of a three-point bending beam specimen

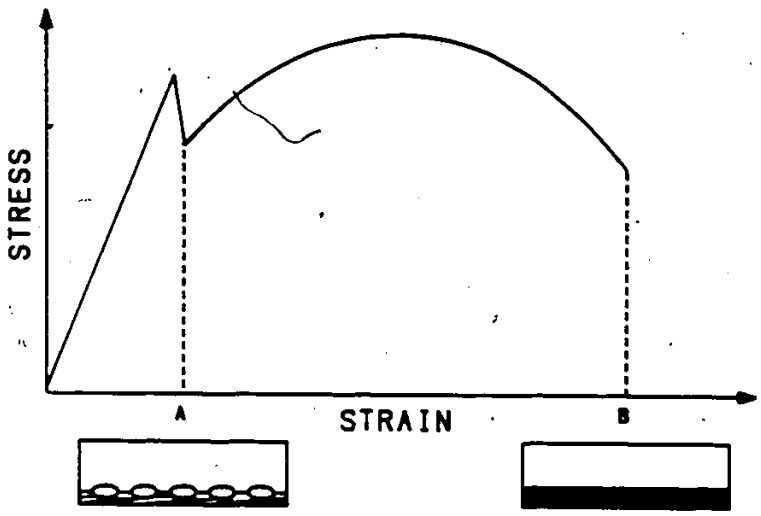

Figure 25: A schematic stress-strain curve and associated crack displacement. An actual curve is given in Figure 14.

Chapter V

EVALUATION OF THEORETICAL FRACTURE ENERGY

In analysing the fracture process of the hybrid specimens, different fracture mechanisms, namely, Fibre Pull-Out Energy, Fibre Debond Energy and Post-Debond Friction Energy, are proposed to account for the energy dissipated. One or more of these microfracture processes may be the controlling factor during different stages in the complete fracture of the composite. The total work to fracture the hybrid specimen is thus the sum of the energy dissipated by these different mechanisms plus the energy required to create new surfaces for glass fibres, carbon fibres and the matrix resin. Therefore, the Theoretical Fracture Energy is:

$$\gamma_T = (\gamma_{po})^c + (\gamma_{po})^g + (\gamma_d)^g + (\gamma_{pdf})^g + \gamma_g + \gamma_c + \gamma_m \qquad (5.1)$$

where: c denotes carbon fibre

g denotes glass fibre

In the following sections, the Theoretical Fracture Energy of the composites was evaluated including the additional assumptions employed for the various energy models.

5.1 EVALUATION OF PULL-OUT ENERGY

The Pull-Out Energy of each specimen was calculated by the equation derived by Cottrell [55]:

$$\gamma_{po} = \frac{W_{po}}{2A} = \frac{V_f \sigma_f \ell_c}{24} \qquad (2.7)$$

where V_f = volume fraction of fibre in composite

σ_f = ultimate tensile strength of fibre

ℓ_c = critical transfer length of fibre

According to Harris et al, [50], the maximum obtainable pull-out length was roughly equal to half of the critical transfer length of the fibre ($\ell_c/2$). The observed pull-out lengths of the fibres of the specimens were assumed to vary linearly with the thickness of each tow, between 0 and $\ell_c/2$. Thus, the average fibre pull-out length, ℓ, is equal to $\ell_c/4$, and the Pull-Out Energy Equation becomes:

$$\gamma_{po} = \frac{V_f \sigma_f \ell}{6} \qquad (5.2)$$

where $\ell = \ell_{max}/2$ with ℓ_{max} equals to the average maximum pull-out length

5.2 EVALUATION OF DEBOND ENERGY

The Equation used to calculate the Debond Energy was taken from the Outwater/Murphy model [46,47]:

$$\gamma_d = \frac{W_d}{2A} = \frac{1}{4} \frac{\sigma_f^2 V_f}{E_f} y \qquad (2.16)$$

5.3 POST-DEBOND FRICTION ENERGY

The Equation to calculate the Post-Debond Friction Energy is given by (Equation 4.1):

$$\gamma_{pdf} = \frac{V_f \sigma_f y^2}{8 \ell} \Delta\varepsilon \qquad (4.1)$$

A final correction is necessary for Equation (4.1). Since ℓ, the fibre pull-out length had been used to evaluate the Pull-Out Energy, a frictional work, and 'y', the debond length also included the pull-out length. To avoid double counting of the pull-out length in evaluating the Post-Debond Friction Energy (which is also a frictional work) the term 'y' in Equation (4.1) is replaced by $(y-\ell)$. Therefore, the final form of Post-Debond Friction Energy Equation becomes:

$$\gamma_{pdf} = \frac{V_f \sigma_f (y - \ell)^2 \Delta\varepsilon}{8 \ell} \qquad (5.3)$$

5.4 FRACTURE SURFACE ENERGY OF GLASS, CARBON AND RESIN

The Fracture Surface Energy of the fibres is extremely small compared to that of the energy absorbed in other mechanisms. A typical value for the surface energy of glass is in the neighbourhood of 2 to 4 Joules/m^2. For carbon, the surface energy is about 4 Joules/m^2. Therefore, these energies are neglected in the total Theoretical Energy.

For the matrix resin, the typical surface energy is also small - about 200 Joules/m^2. The inclusion of this surface energy would only result in a negligible increase of the Theoretical Energy (about 1%). Therefore, it is not included in the calculation of the Theoretical Fracture Energy.

5.5 TOTAL THEORETICAL FRACTURE ENERGY

The Work of Fracture in carbon/epoxy resin composite is defined by the Fibre Pull-Out Mechanism [53,55]. while in glass/epoxy resin composites, Fibre Pull-out, Fibre Debond and Post-Debond Friction between fibre and matrix are the major energy absorbing processes.

The total Theoretical Fracture Energy of the hybrid specimen is then the sum of all the contributions from various mechanisms in the reinforcing fibres. Therefore,

$$\gamma_T = (\gamma_{po})^c + (\gamma_{po})^g + (\gamma_d)^g + (\gamma_{pdf})^g \qquad (5.4)$$

with the fracture energy of the resin being neglected.

Owing to the number of specimens tested, calculating the total Theoretical Fracture Energy and Work of Fracture involved long and tedious manipulation of numbers. A computer program was, therefore, written to handle the calculation problem (Appendix E).

Chapter VI

RESULT ANALYSIS AND DISCUSSION

6.1 WORK OF FRACTURE (WOF)

Figure 15 presented the Experimental Fracture Energy, or Work of Fracture (WOF), of the hybrid composites tested at various temperatures. The WOF was plotted against the carbon fibre volume fraction. The general trend of the result was that as the volume fraction of carbon fibre in the specimens increases, the WOF decreases. This trend was true for all the temperatures tested. This trend implies that as the carbon fibre volume fraction increases, the composite becomes more brittle and less energy was required to fracture the composite. This brittleness of the composite was believed to be contributed mainly by the brittle carbon fibre.

In Figure 26, the WOF of composites with different carbon fibre volume fractions was plotted against the testing temperature. Figures 15 and 26 are combined to form a three-dimensional plot of Work of Fracture versus Carbon Fibre Percentage versus Testing Temperature (Figure 27). The graphs show that the all-carbon fibre specimens were quite insensitive to the change of temperature. The Fracture Energy remains quite constant at all testing

temperatures. For the all-glass fibre specimens, a different trend was observed. There was a very significant increase of Fracture Energy for the all-glass fibre specimens when they were tested at 80 degrees Celsius. For the hybrid specimens, the Fracture Energy, however, remain roughly constant from room temperature up to 65 degrees Celsius. At 80 degrees Celsius, the Fracture Energy of the hybrid specimens tended to increase. But this tendency decreased with increase in carbon fibre volume fraction.

The strengths of both carbon and glass fibres were not affected by the temperature range in which the specimens were tested, and the resin had a glass transition temperature of around 90 degrees Celsius. This implies that the chemical structure of the resin will remain intact unless the environmental temperature rises to 90 degrees Celsius or above. In other words, the resin would not be softened at temperatures below 90 degrees Celsius. However, it is also true that temperature does affect the stiffness of the matrix (Figures 22 and 23, Table 9). But from Figure 26, it is obvious that the WOF remained quite constant (not increasing gradually) until the temperature was 80 degrees Celsius, then the Work of Fracture increased significantly. This effect will be discussed in later sections.

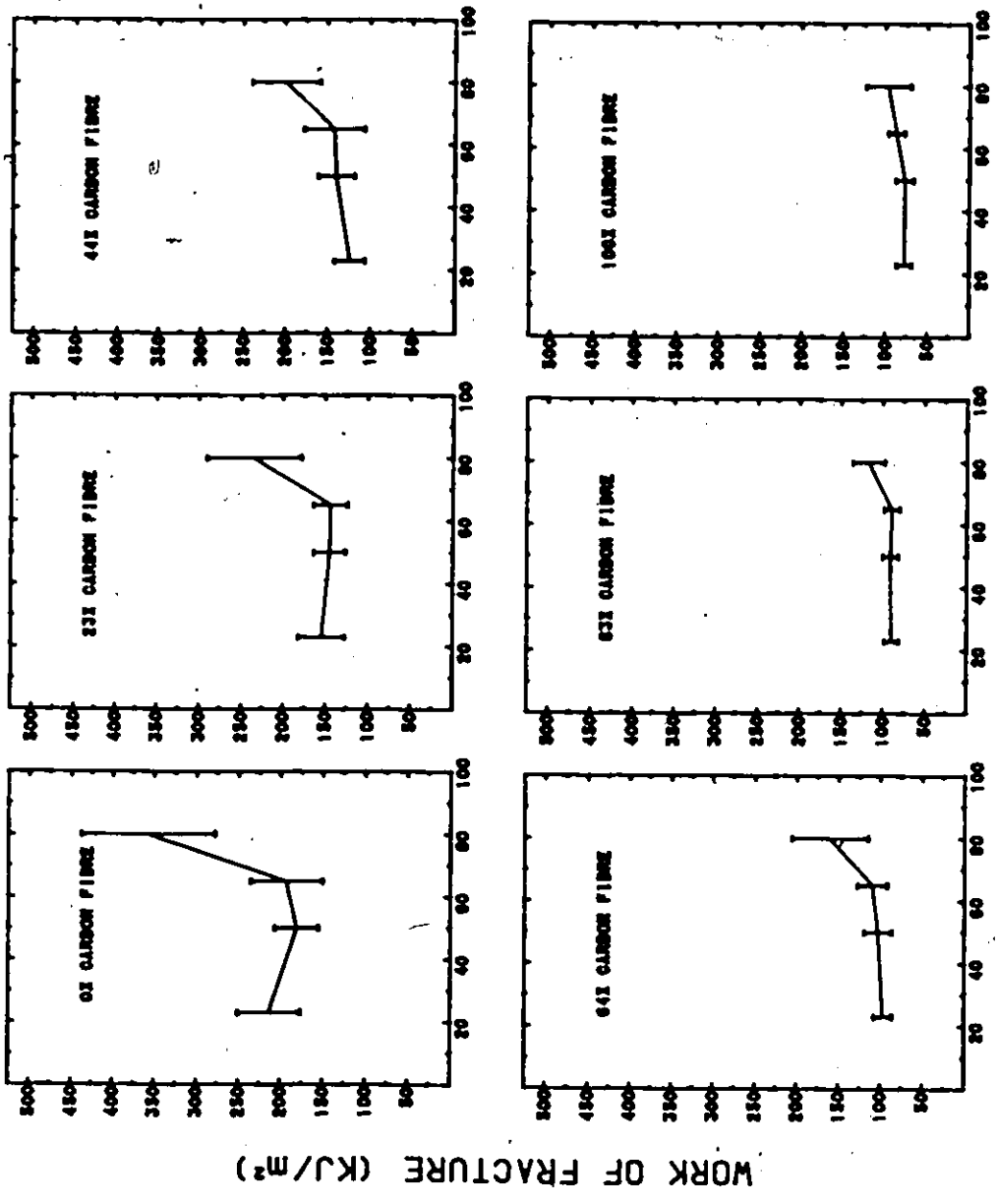

Figure 26: Work of fracture as a function of temperature
(mean ±1 standard deviation)

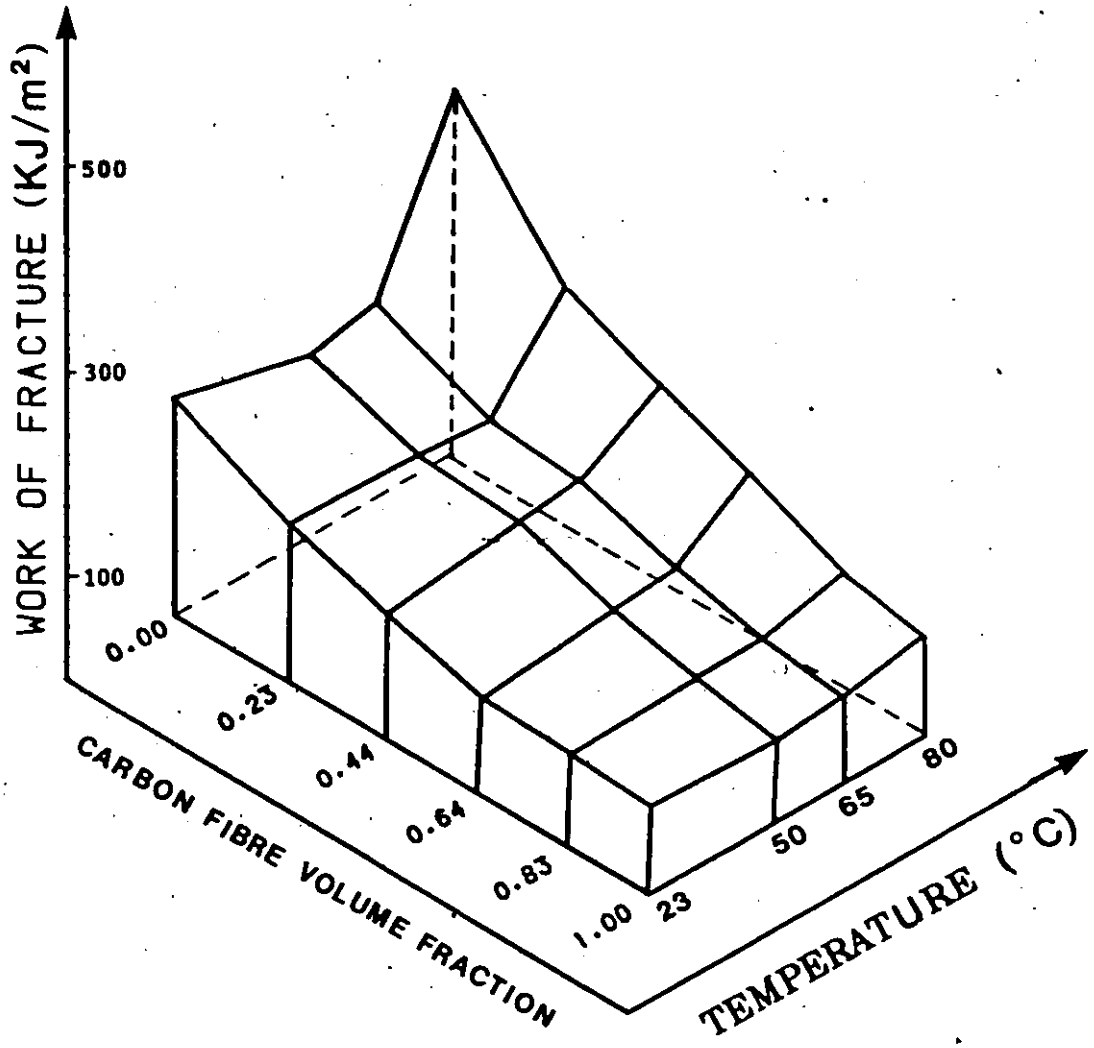

Figure 27: Three-dimensional plot of work of fracture

6.2 PULL-OUT ENERGY

According to Equation (5.2), Pull-Out Energy is a function of fibre volume fraction in total fibre, ultimate strength of the fibre, and the average lengths of fibre which were pulled out from the matrix after the composite was fractured. In the hybrid composite, all the constituent fibres, carbon and glass, contribute to the Pull-Out Energy. They are discussed in the following sections (Figures 28,29).

6.2.1 Carbon Fibre Pull-Out Energy

Pull-out length is the main factor affecting the Pull-Out Energy. In Figures 18 and 30, it could be seen that the pull-out length of carbon was quite insensitive to the temperature changes and changes in carbon fibre volume fraction in total fibre. This pull-out length, in fact, remained approximately constant as temperature and carbon fibre volume fractions were varied. The resulting fracture energy, Carbon Fibre Pull-Out Energy, was approximately a straight line, increasing steadily as carbon fibre volume fraction increased but remaining relatively constant with temperature.

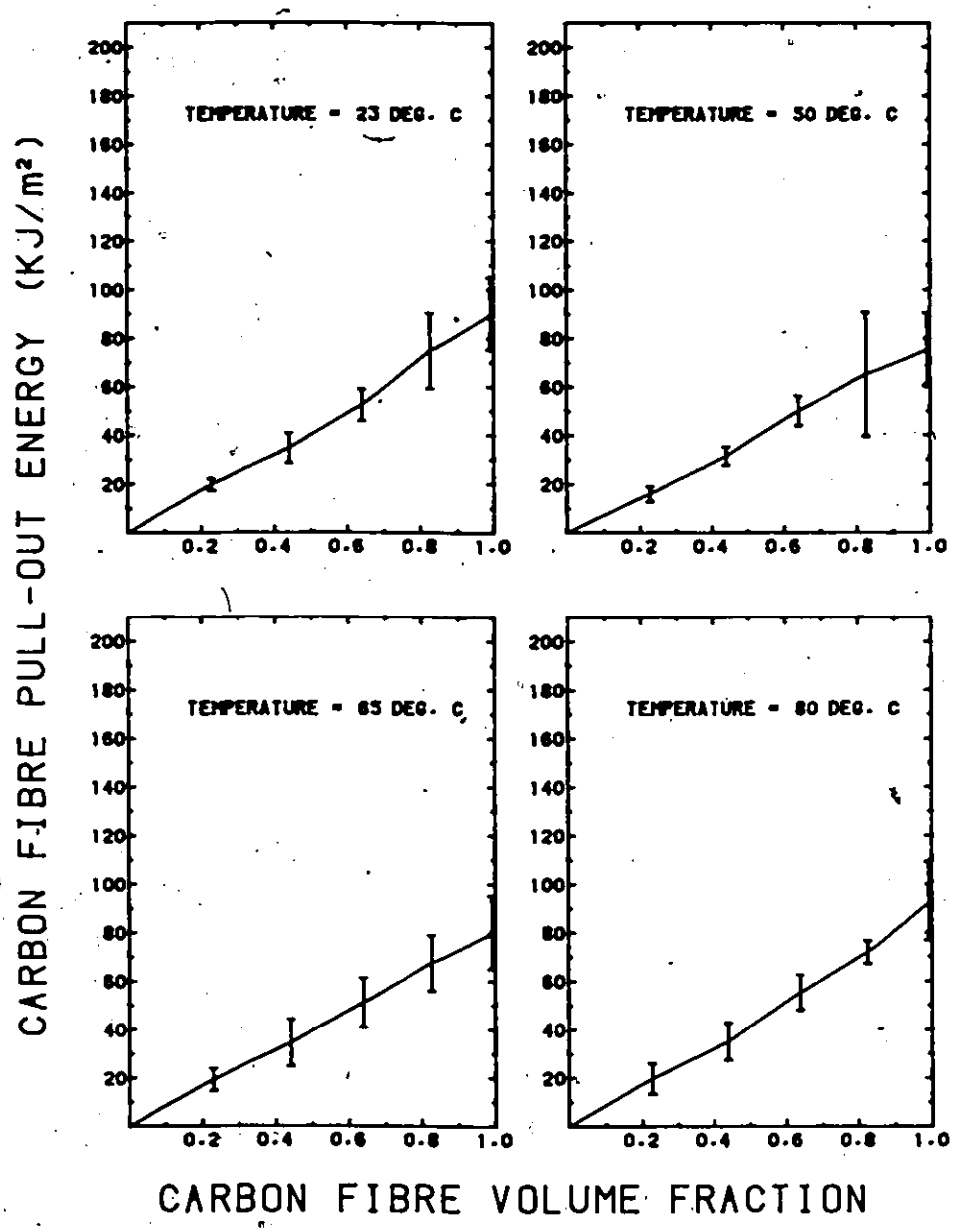

Figure 28: Carbon fibre pull-out energy versus carbon fibre volume fraction (mean ±1 standard deviation)

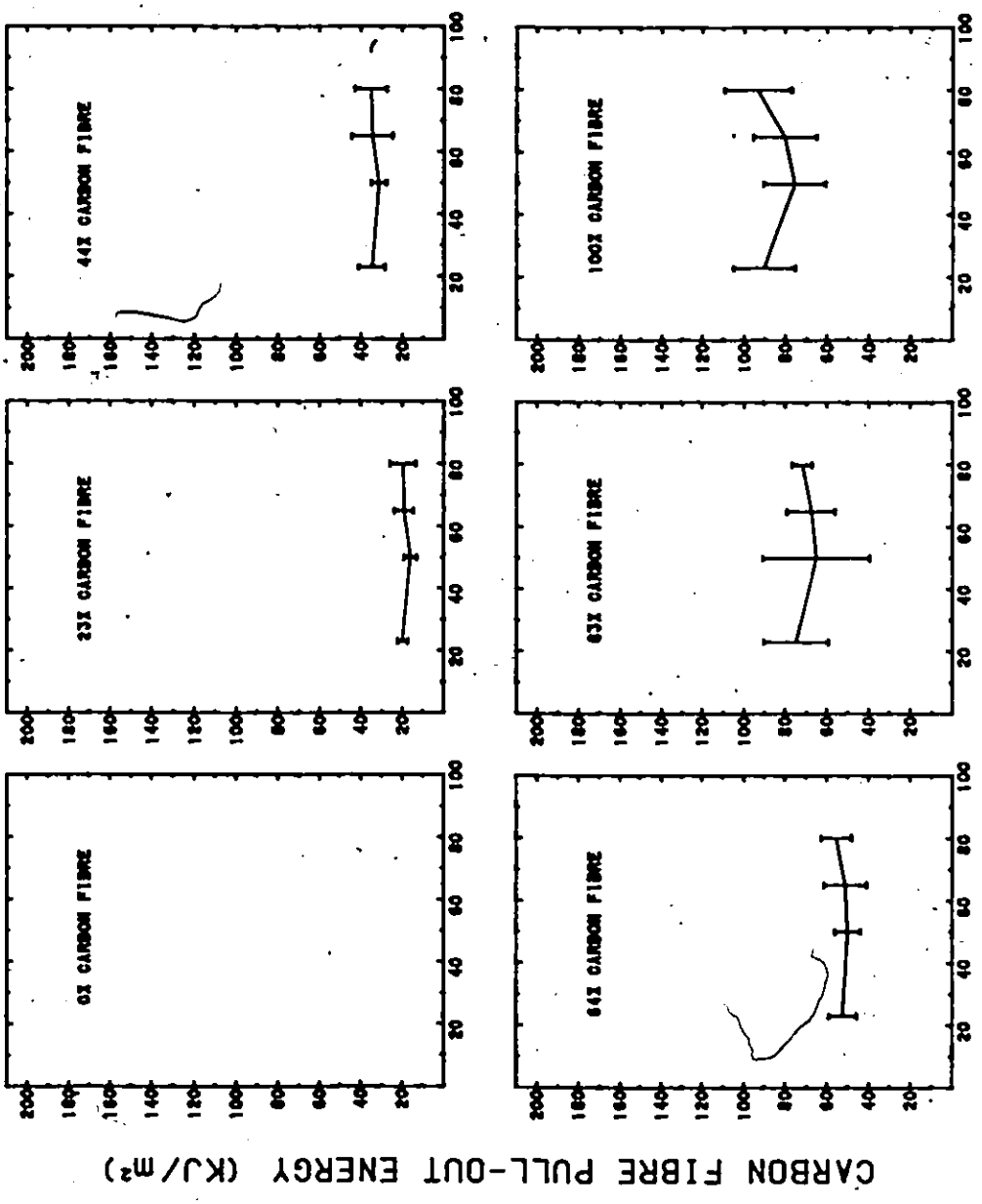

Figure 29: Carbon fibre pull-out energy as a function of temperature (mean ±1 standard deviation)

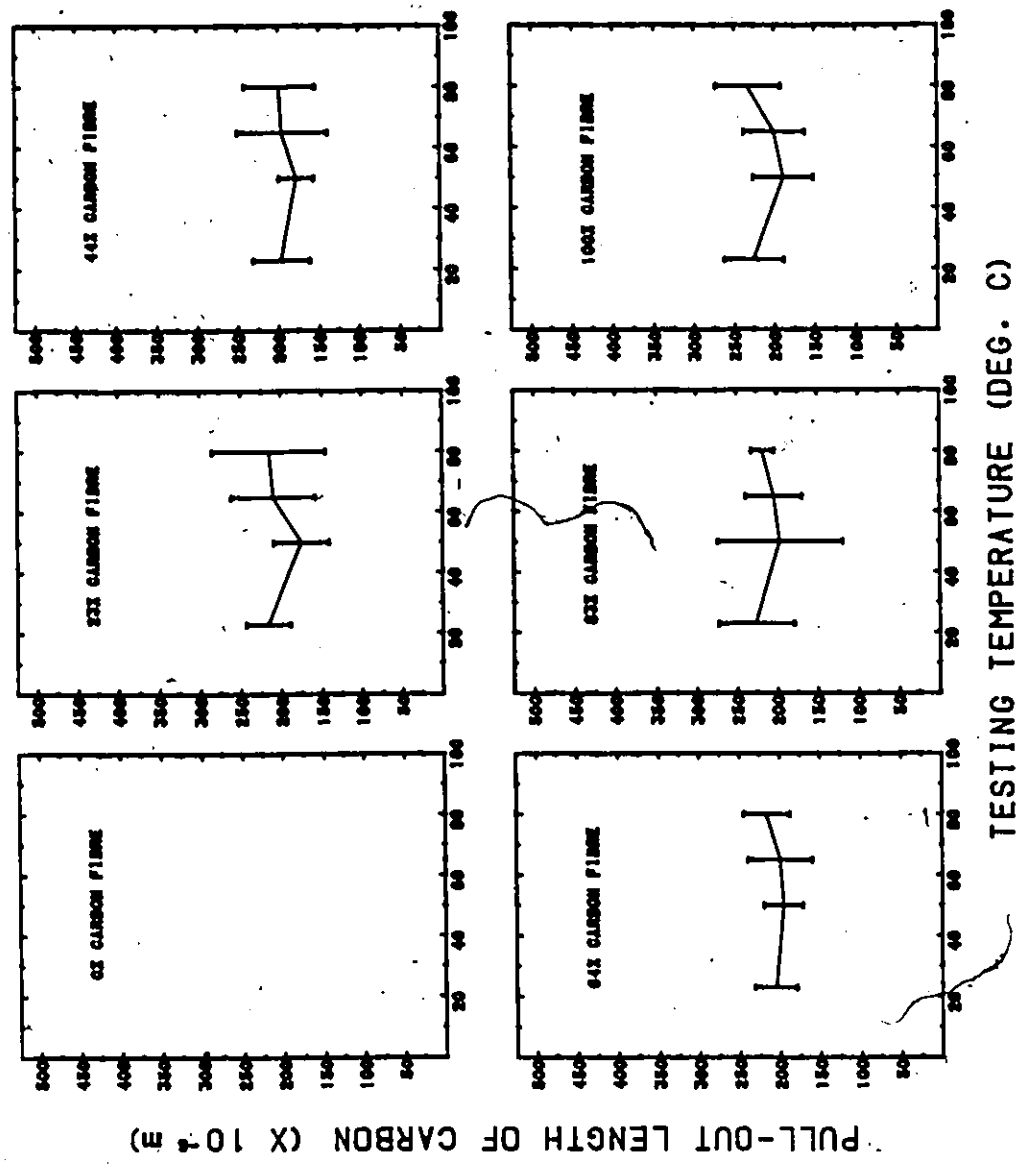

Figure 30: Pull-out length of carbon fibre versus temperature
(mean ±1 standard deviation)

6.2.2 Glass Fibre Pull-Out Energy

In Figure 19, the pull-out length was plotted against the carbon fibre volume fraction at different temperatures. It was found that the pull-out length of the glass fibre was, for all practical purposes, independent of changes in carbon fibre volume fraction in the composite. This is very similar to the behaviour of carbon fibre in the hybrid. Also, when comparing Figures 18 and 19, it can be seen that the value of the average pull-out lengths of glass fibre and carbon fibre are very close. Therefore, it is obvious that the value of pull-out energy of carbon fibre would be higher than that of the glass fibre due to the higher ultimate tensile strength of carbon fibres (Figures 28, 29, 31, 32).

Figure 33 shows the average pull-out length of glass fibre versus testing temperature for different carbon fibre volume fractions. It can be observed that the pull-out length of glass fibre tends to decrease in the temperature range between 50 to 65 deg. Celsius. This tendency becomes very significant in the all-glass fibre specimens and the 23% carbon fibre specimens. For the 44% and 64% carbon fibre specimens, the change of pull-out lengths with temperature becomes less significant. The corresponding change becomes more significant for the 83% carbon fibre hybrids. The reason for this trend is still unknown. Since all the specimens in a specimen group were carefully chosen from different cast hybrid plates, the possibility of specimen variation from group to group was very low.

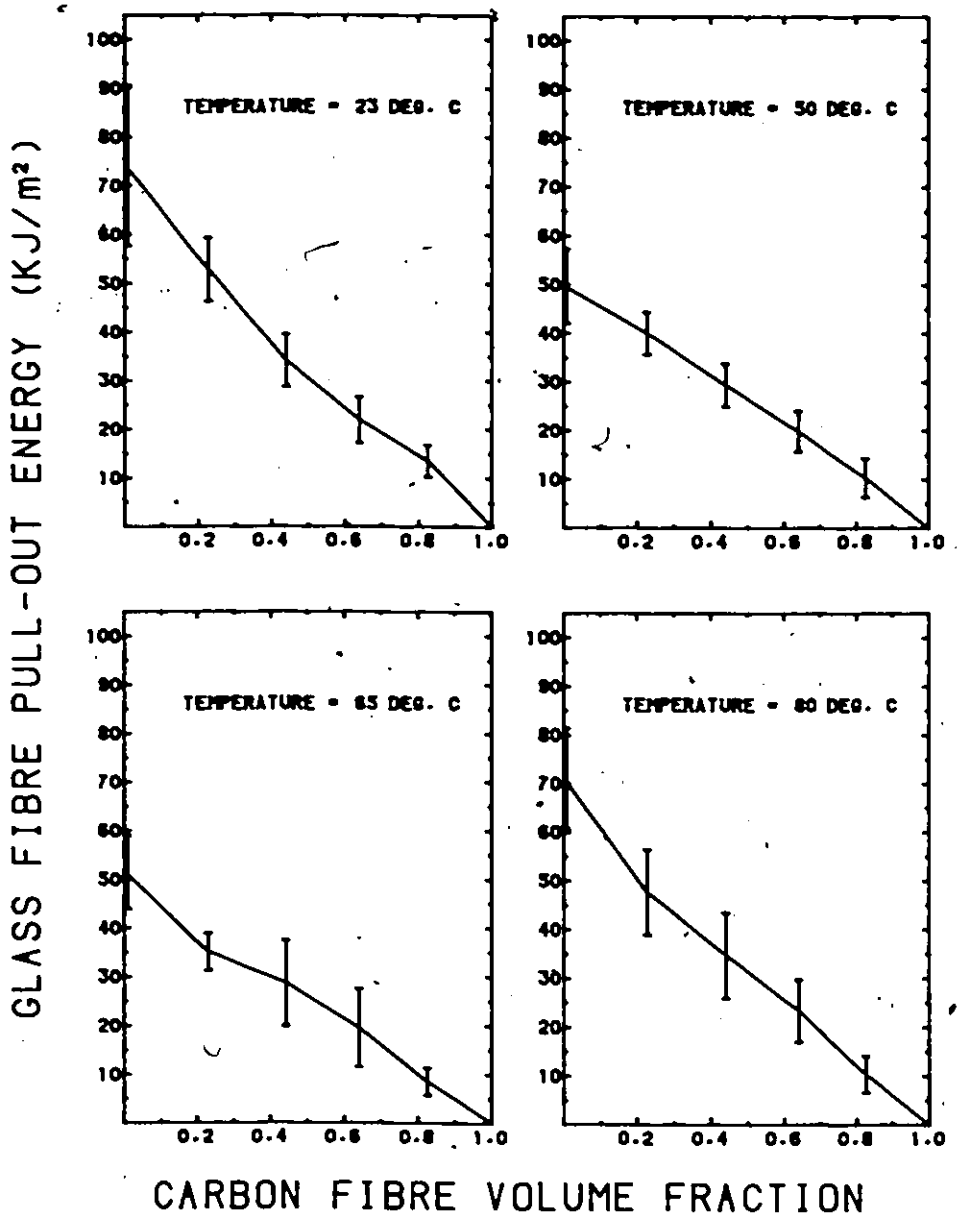

Figure 31: Glass fibre pull-out energy versus carbon fibre volume fraction (mean ±1 standard deviation)

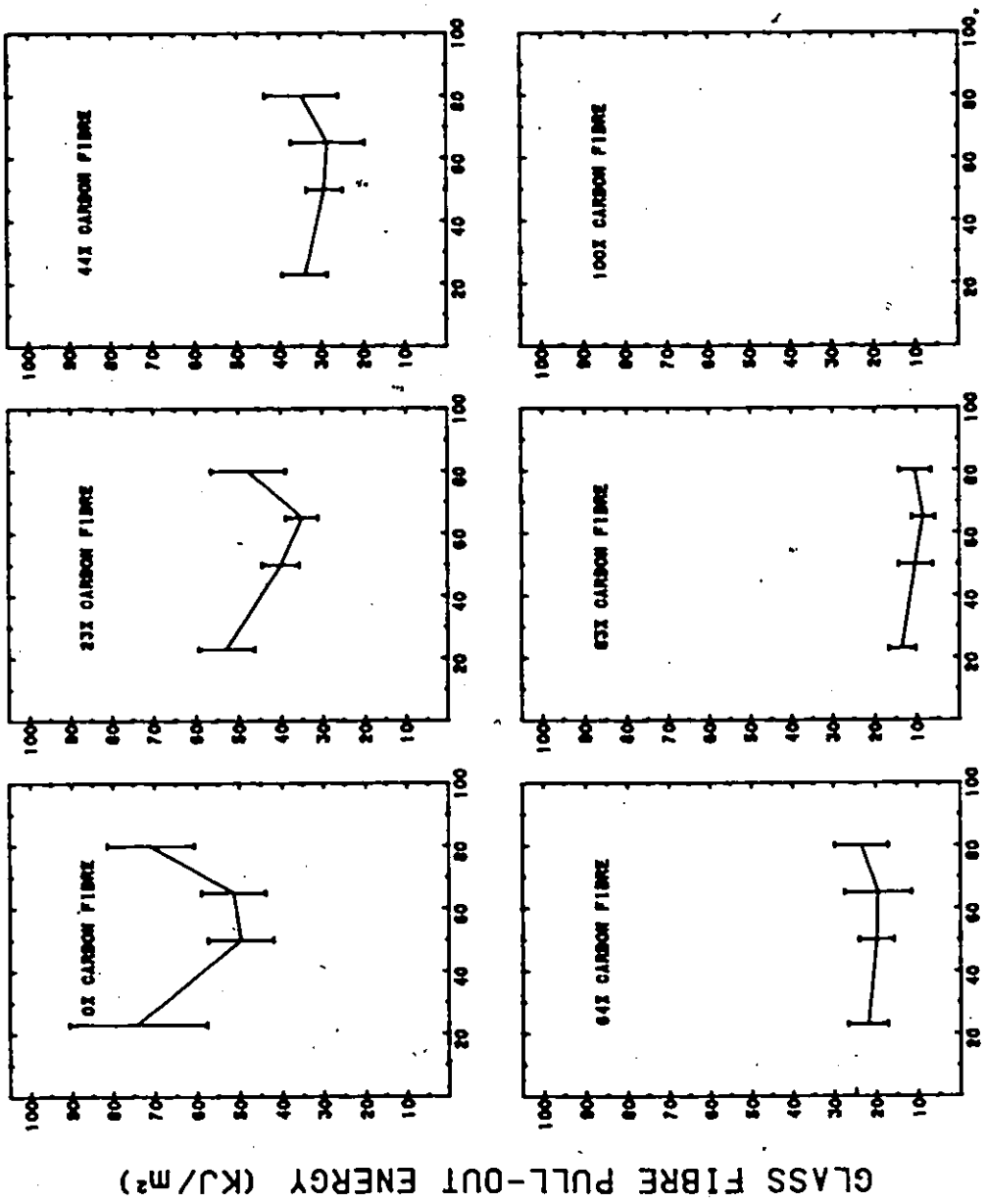

Figure 32: Glass fibre pull-out energy as a function of temperature (mean ±1 standard deviation)

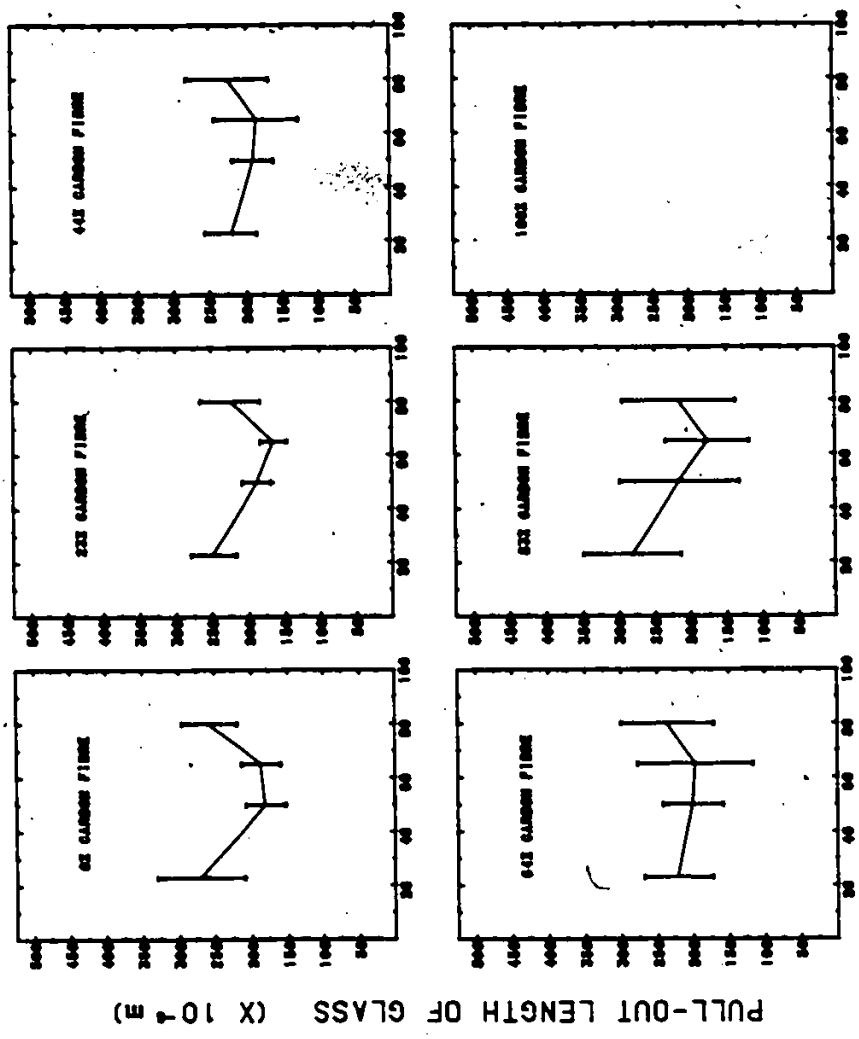

Figure 33: Pull-out length of glass fibre versus temperature (mean ±1 standard deviation)

6.3 DEBOND ENERGY

The debond length of glass fibre in the hybrid composite was quite insensitive to the changes in carbon fibre volume fraction except at room temperature (23 degrees Celsius) where the debond length decreased slightly for specimens with 23% to 44% carbon fibre contents (Figure 20). It was shown that the Debond Energy was a linear function of the glass fibre volume fraction (which was essentially the volume fraction of glass fibre in total fibre) and the fibre debond length. Moreover, the debond length was roughly constant with carbon fibre volume fraction for all temperatures. It could be shown that the Debond Energy of glass fibre would increase linearly with glass fibre volume fraction. This is shown in Figure 34.

Yet, when the debond length was examined in terms of temperature changes, the similar trends which occurred in the glass pull-out length is observed (Figure 35). There was an obvious decrease in debond length for all glass specimens in the temperature range from 50 to 65 degrees Celsius. This tendency continued to occur in the hybrid specimens with 23%, 44% and 64% carbon fibre contents. In the 83% specimens, the debond length tended to decrease as testing temperature was increased. This tendency was again reflected in the Debond Energy curves (Figure 36) when they were plotted against temperature. The physical explanation of this phenomenon is unknown. A closer study on the

temperature effect on the bond strength was, therefore, advised.

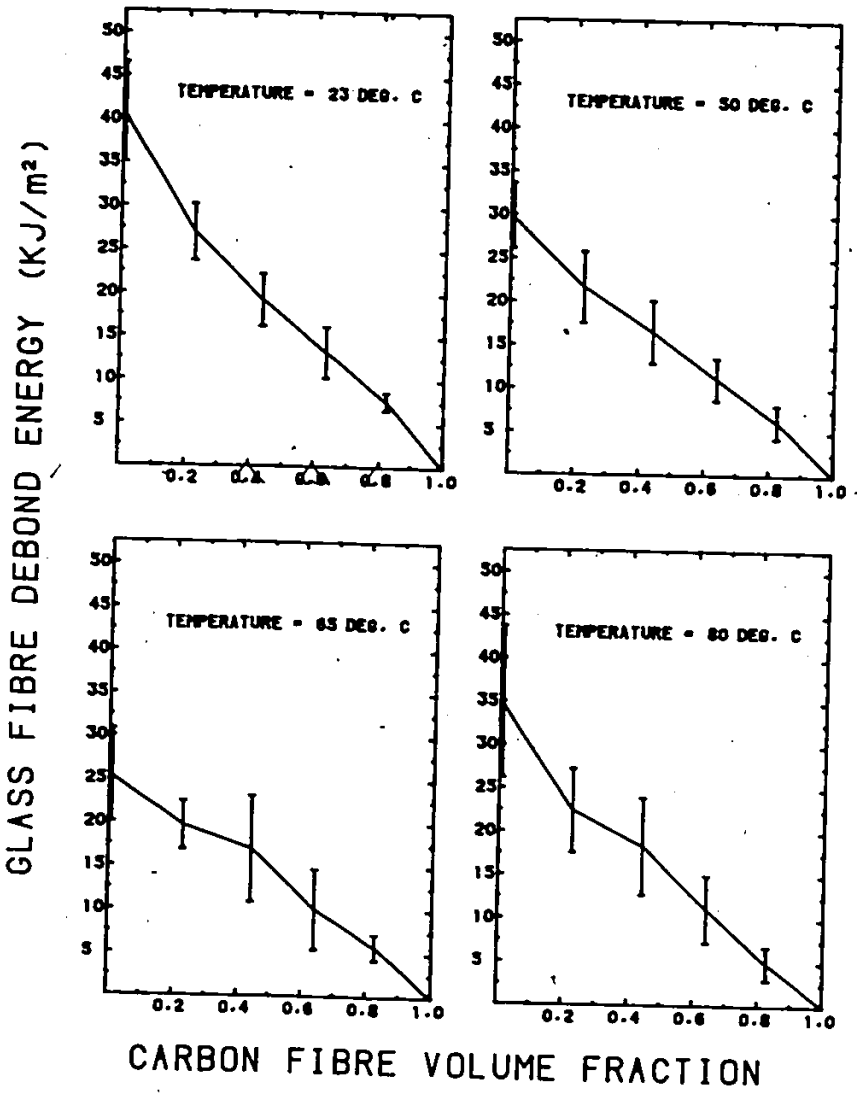

Figure 34: Glass fibre debond energy versus carbon fibre volume fraction (mean ±1 standard deviation)

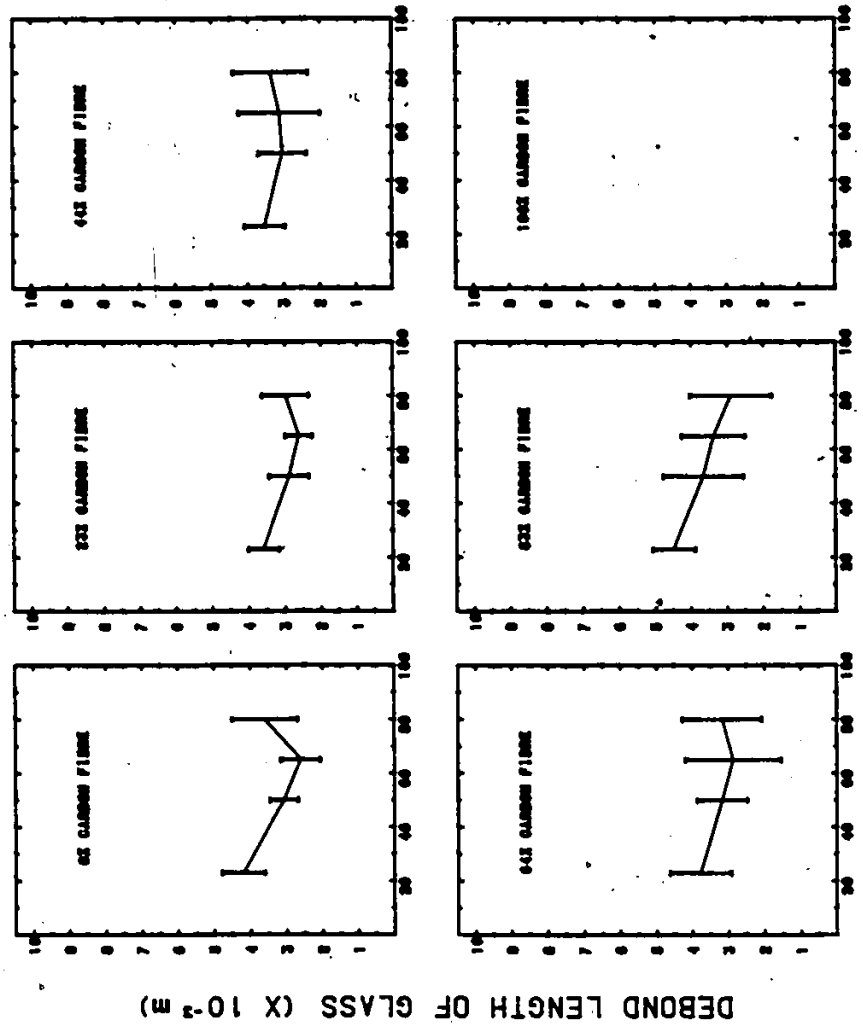

Figure 35: Debond length of glass fibre versus temperature (mean ±1 standard deviation)

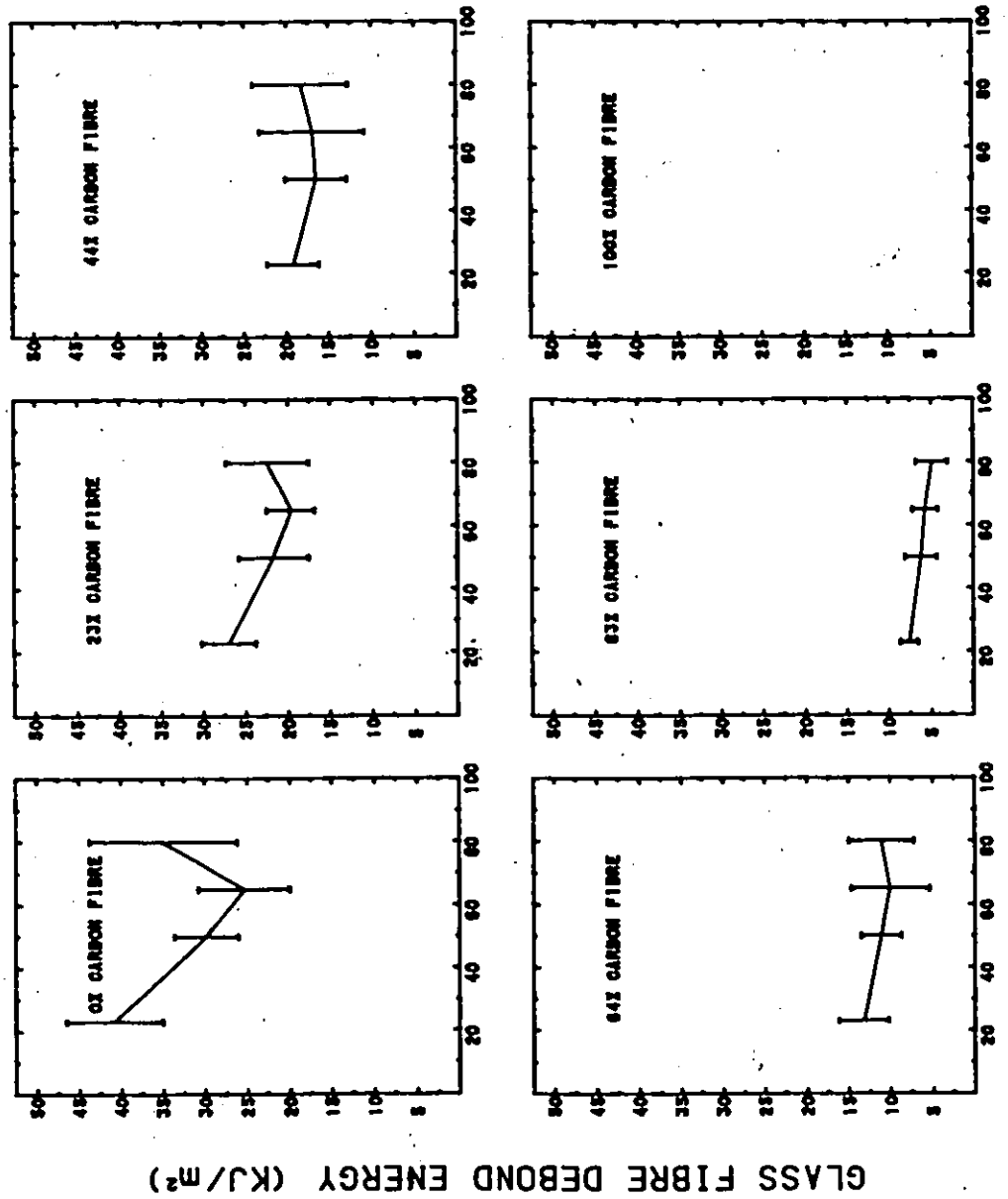

Figure 36: Glass fibre debond energy as a function of temperature (mean ±1 standard deviation)

6.4 THE OVERALL EFFECT OF PULL-OUT AND DEBOND ENERGY

By comparing the values of Pull-Out Energy calculated and the Work of Fracture (WOF), it was observed that the Pull-Out Energy of the all-carbon specimen was the main energy absorption mechanism during the fracture process of the unidirectional carbon fibre/epoxy composites. It was true for all temperatures tested. As glass fibres were introduced to the composites, and as the glass fibre volume fraction was increased, the contribution of Pull-Out Energy became less important. For the all-glass fibre specimens, the Pull-Out Energy only accounted for about one-third of the WOF at room temperature and only one-fifth of the WOF at 80 degrees Celsius. Therefore, it is obvious that for all-glass fibre composites, the Pull-Out mechanism was not the only energy absorption mechanism that was functioning. Some other mechanisms were also acting to increase the toughness of the composite. The same argument also applied for the hybrid composites with Pull-Out Energy contributed by both constituent fibres.

As for all-glass fibre composites and glass/carbon fibre hybrids, the Debond Energy of glass fibres was also one of the energy absorption process which was functioning to contribute to the total fracture energy of the composites. Yet, its value only accounted for less than 20% the WOF measured at room temperature and about 10% of the WOF 80 degrees Celsius. Therefore, it is also obvious that

the Debond Energy of glass fibre was only one of the energy absorption mechanism contributing to the fracture energy of the hybrid composite.

Figure 37 shows the combined effect of glass and carbon fibre Pull-Out and glass fibre Debond Energy for different carbon fibre volume fraction and at different temperatures. It could be seen that these curves were practically horizontal lines. This implies that the overall effects of these mechanisms were quite independent of the carbon fibre volume fraction. In addition, the magnitude of the sum of these three terms was approximately 95 $\pm$20 KJ/m^2 while the work of fracture values reached 350 KJ/m^2. This discrepancy is explained in the next section.

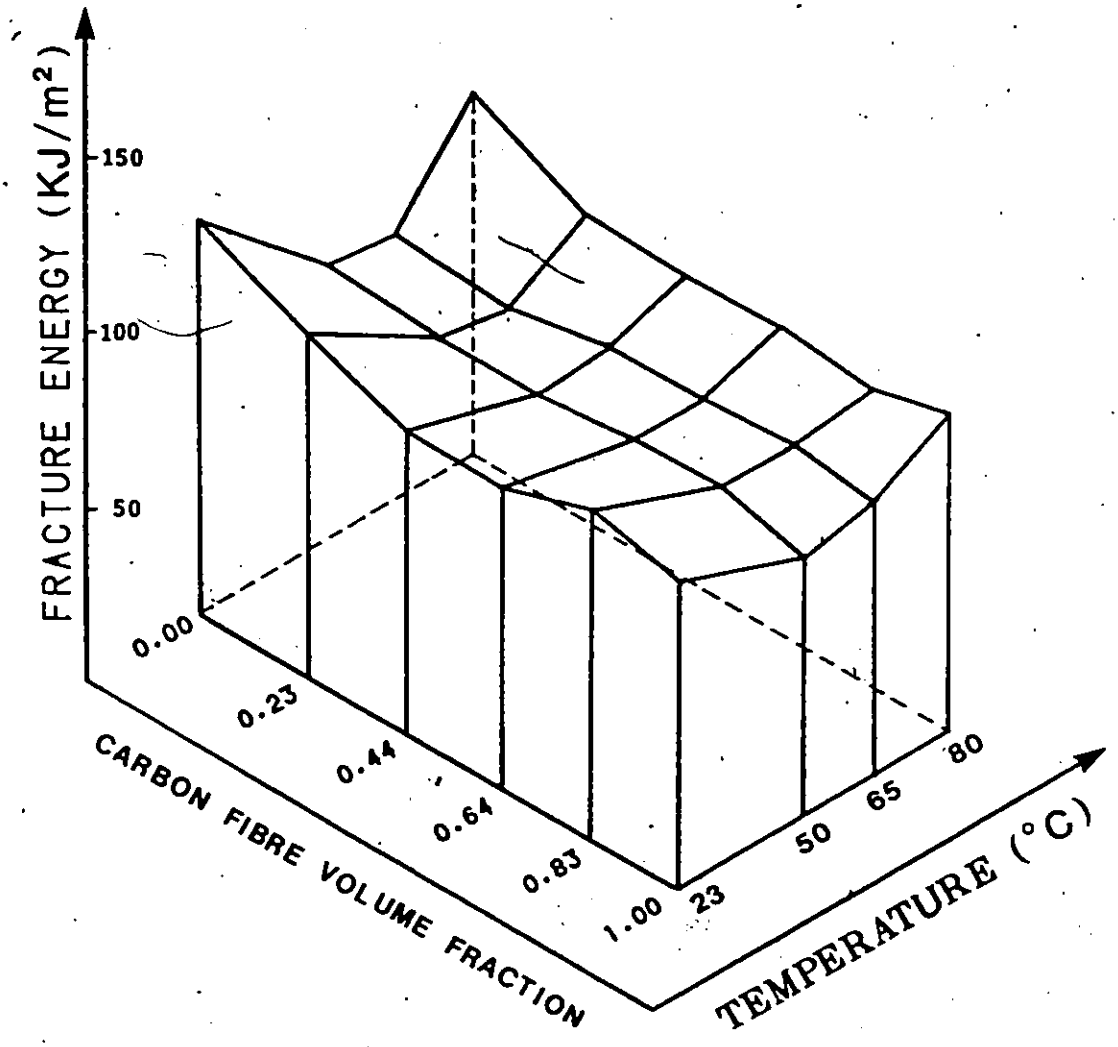

Figure 37: Overall contribution of pull-out & debond energy to theoretical fracture energy

6.5 POST-DEBOND FRICTION ENERGY

From Tables 6 and 7 in Appendix E, it is observed that the Post-Debond Friction Energy was, in general, greater than the Pull-Out Energy and the Debond Energy. Referring to Figure 38, it could be seen that the Post-Debond Friction Energy displayed a similar trend as that of the Work of Fracture (Figure 15), namely, it decreased as carbon fibre volume fraction decreased. This trend was true for all temperatures. At high temperatures, the increase was very significant. When the Post-Debond Friction Energy was examined in terms of temperatures (Figure 39), it showed that this energy increased very rapidly at 80 degrees Celsius for the all-glass specimens.

For the hybrid specimens, the increase of fracture energy was also obvious, though not that significant. The importance of this mechanism was revealed as Figure 39 was compared with Figure 26. The similarity between the two Figures is obvious.

In order to better understand the Post-Debond Sliding Mechanism, it is important to examine its governing parameters. In Equation (5.1), it was quite clear that most of the variables were either material constants or measurable parameters which were not temperature-dependent (although pull-out and debond length did change at 50 and 65 degrees Celsius, the change was not significant since the changes in Fracture Energy at this temperature range were

insignificant). However, the term $\Delta\varepsilon$, which was the relative movement between fibre and matrix after debond, was very likely to be dependent on temperature changes.

The term $\Delta\varepsilon$ was usually taken as the difference in failure strain between fibre and matrix. The failure strain of glass fibre did not change until the temperature was around hundreds of degrees Celsius. As for epoxy resin, it had been shown experimentally in this work that its failure strain increased with temperature (Figure 22). It can therefore be concluded that the term $\Delta\varepsilon$ increased with temperature and its increase was very significant at 80 degrees Celsius for the epoxy system used in this work.

In the physical sense, when the composite was fractured at high temperatures (eg. 80 degrees Celsius), the relative sliding of fibres and resin would increase as the failure strain of the matrix resin increased. In this case, more work was done during this sliding and the composite became tougher.

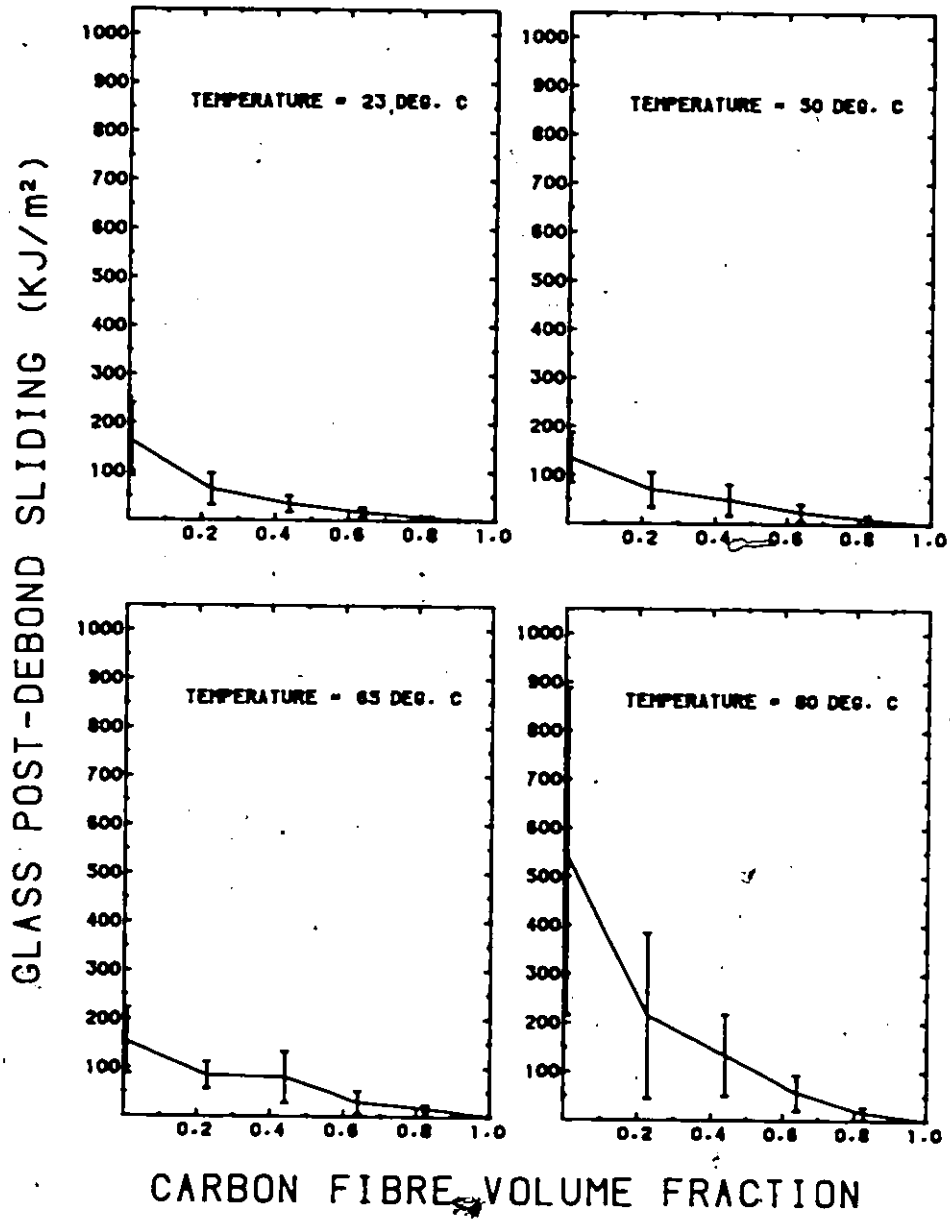

Figure 38: Post-debond friction energy versus carbon fibre volume fraction (mean ±1 standard deviation).

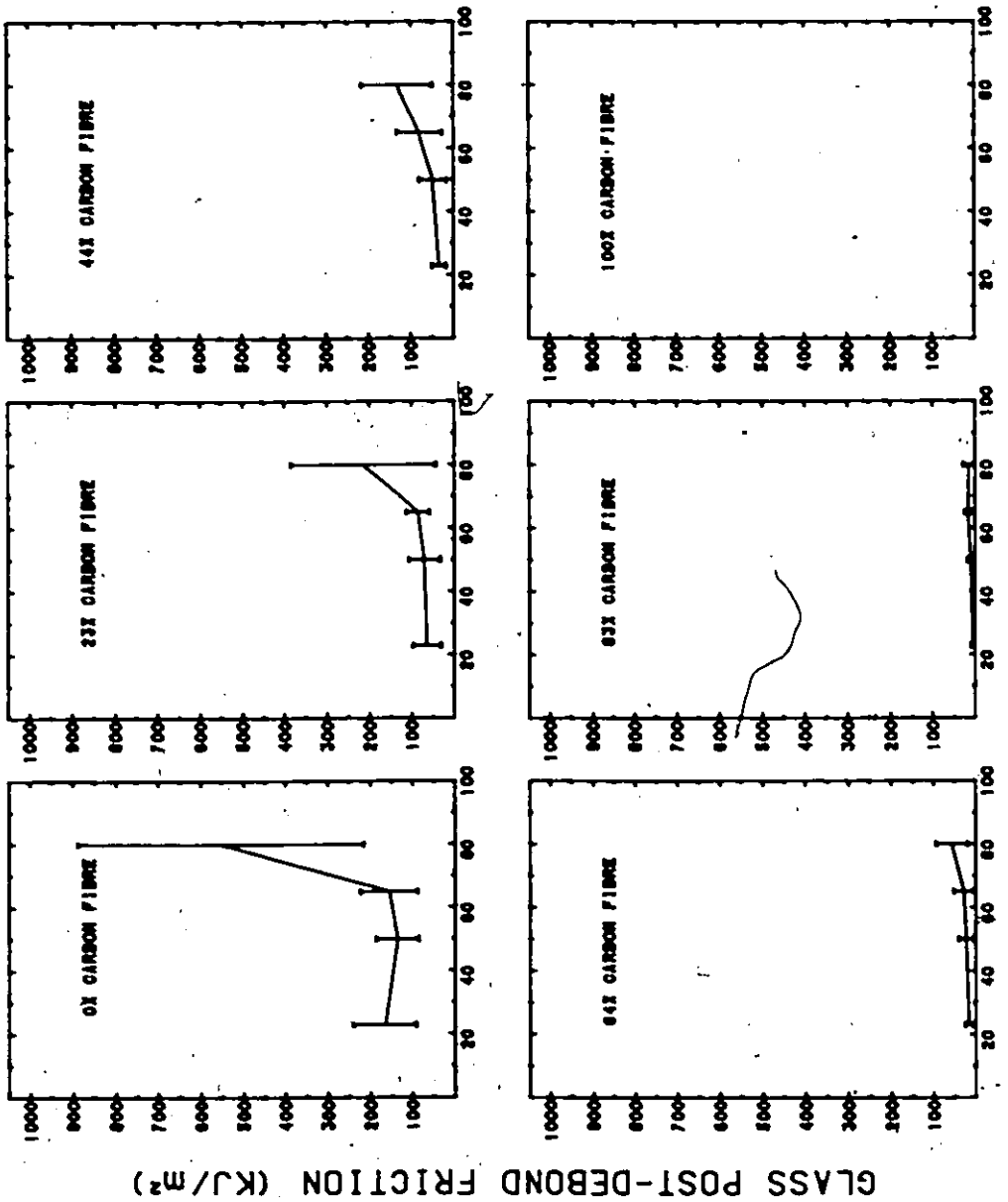

Figure 39: Post-debond friction energy as a function of temperature (mean ±1 standard deviation)

6.6 THEORETICAL FRACTURE ENERGY

The Theoretical Fracture Energy (or TE), according to Equation (5.2), was the sum of all the contributions of fracture energy from all the said mechanisms. In Figures F1 and F2, similar trends to that exhibited by the Work of Fracture and Post-Debond Friction Energy were observed. The similarity of the Experimental Curves, the Theoretical Curves, and the Post-Debond Friction Curves seem to suggest that the Post-Debond Sliding Mechanism is a dominant mechanism in the fracture energy of carbon/glass hybrid reinforced composites (CGHRP) and glass fibre reinforced composites (GFRP).

The Theoretical Fracture Energy is plotted, together with its contributing mechanism and the WOF, versus the carbon fibre volume fraction (Figures 40 to 43).

From these Figures, it can be seen that the agreement between Experimental Fracture Energy (WOF) and Theoretical Fracture Energy is very good. This once again shows that the proposed mechanisms: Fibre Pull-Out, Fibre Debond and Post-Debond Friction, are the chief energy absorbing mechanisms during the fracture of the hybrid composites. However, the agreement between WOF and TE becomes worse at high temperature (80 degrees Celsius). At 80 degrees Celsius, the agreement between theory and experiment is still good for high carbon fibre volume fractions (from all-carbon fibre composites to 44% carbon fibre hybrids). For

hybrid specimens with 23% carbon fibre, the agreement between the Theoretical Curve and the Experimental Curve is still observable. For the all-glass specimens, at 80 degrees Celsius, the Post-Debond Friction Energy increases tremendously and this affects the value of the Theoretical Curve. It is also observed that the Theoretical Energy is far greater than that of the Experimental ones. The Theoretical Fracture Energy as a function of testing temperature and carbon fibre volume fraction are given in Appendix F.

The significant increase of Post-Debond Friction of GFRP at 80 degrees Celsius was due to the increase of failure strain of the matrix resin at this temperature. Because of this increase, the matrix became less stiff. Moreover, a significant amount of energy was absorbed during the relative movement of fibre and matrix. The accompanying softening of the matrix made it extremely difficult to measure the accurate strain of the specimen. Consequently, the calculation of $\Delta\varepsilon$ became very inaccurate at this temperature. Due to the excessive deflection of the specimen, it is believed that the failure strain measured from the load-deflection curve of the specimen was an overestimate of the real deflection of the specimen. This led to an overestimate of the term $\Delta\varepsilon$, and finally led to an overestimate of the Theoretical Energy. Accurate determination of $\Delta\varepsilon$ at high temperature therefore remains a topic for further and more thorough study.

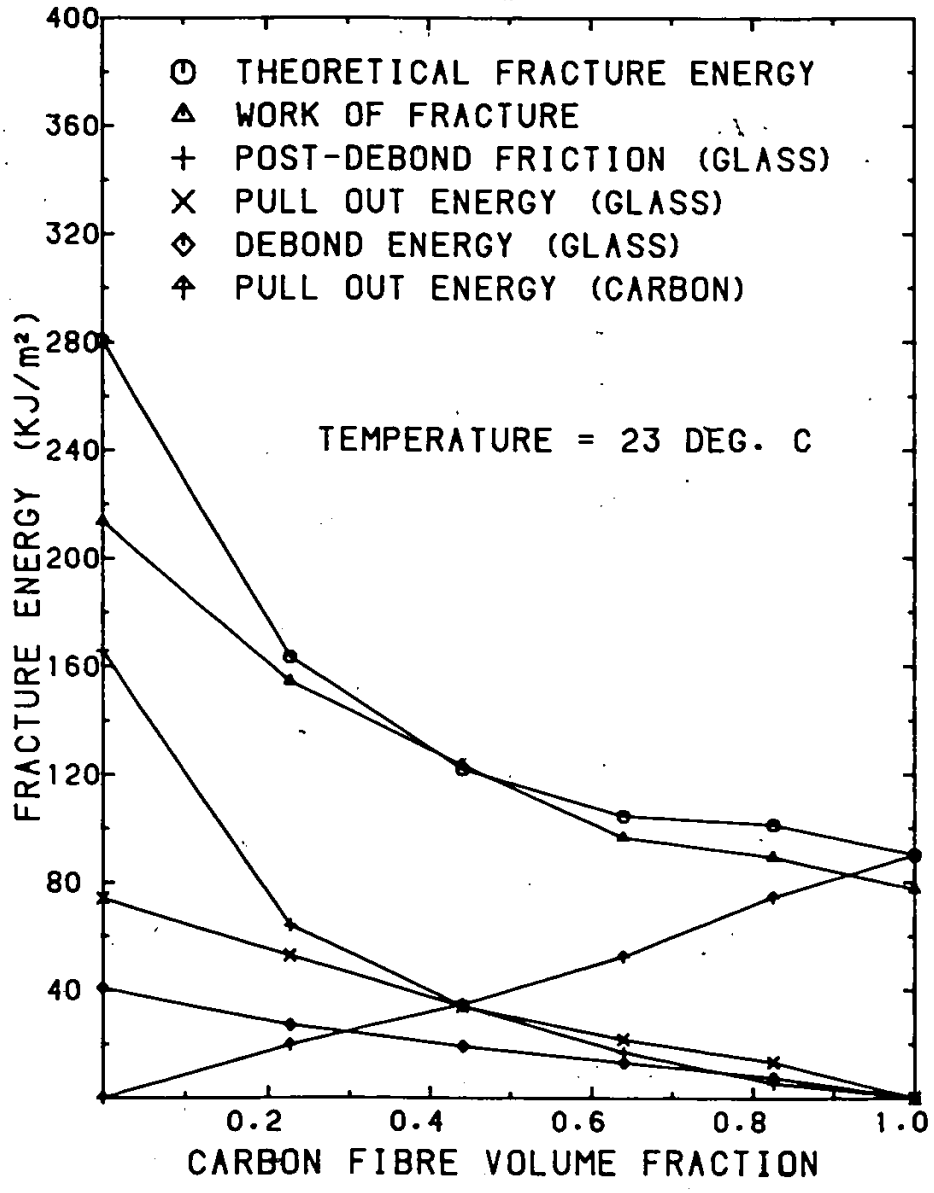

Figure 40: Fracture energy terms versus carbon fibre volume fraction at 23 deg. C.

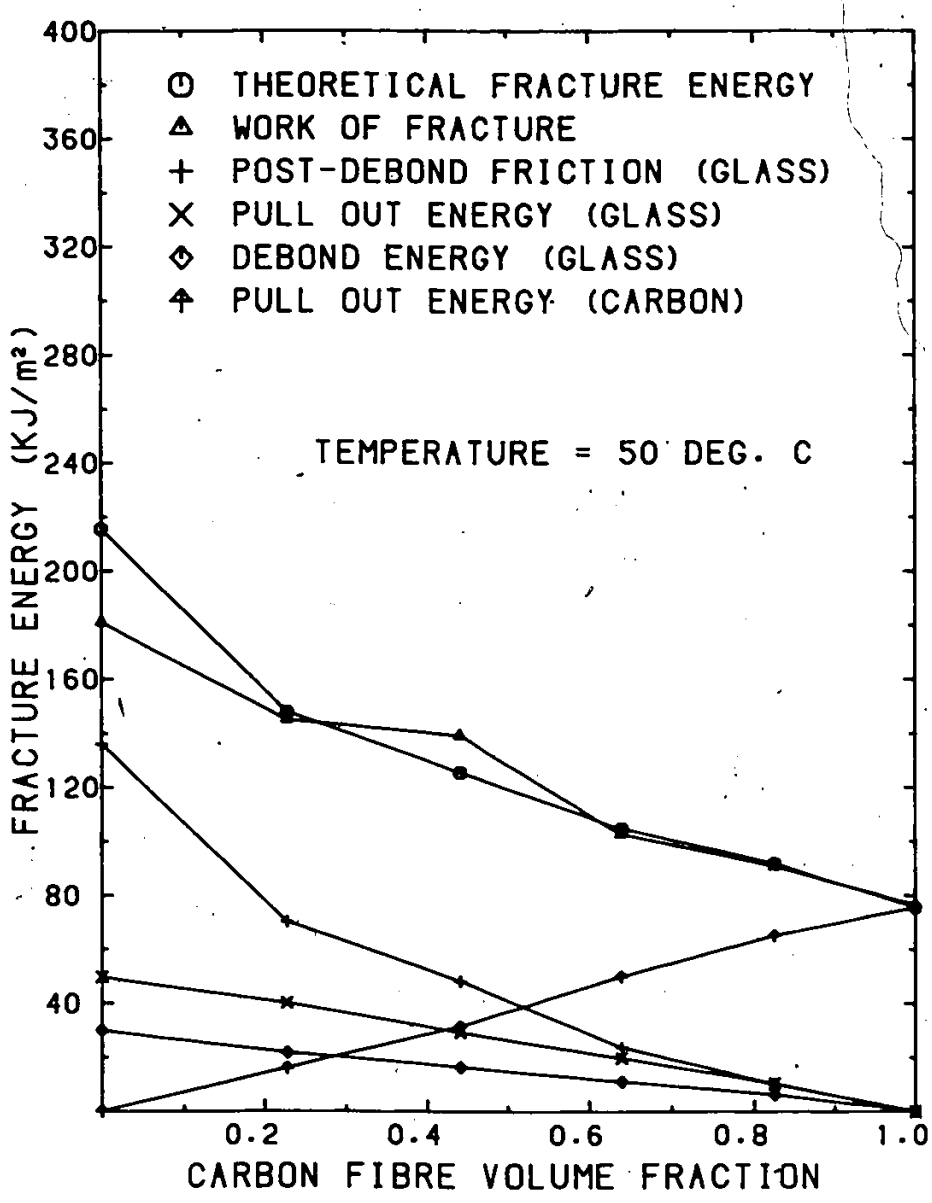

Figure 41: Fracture energy terms versus carbon fibre volume fraction at 50 deg. C.

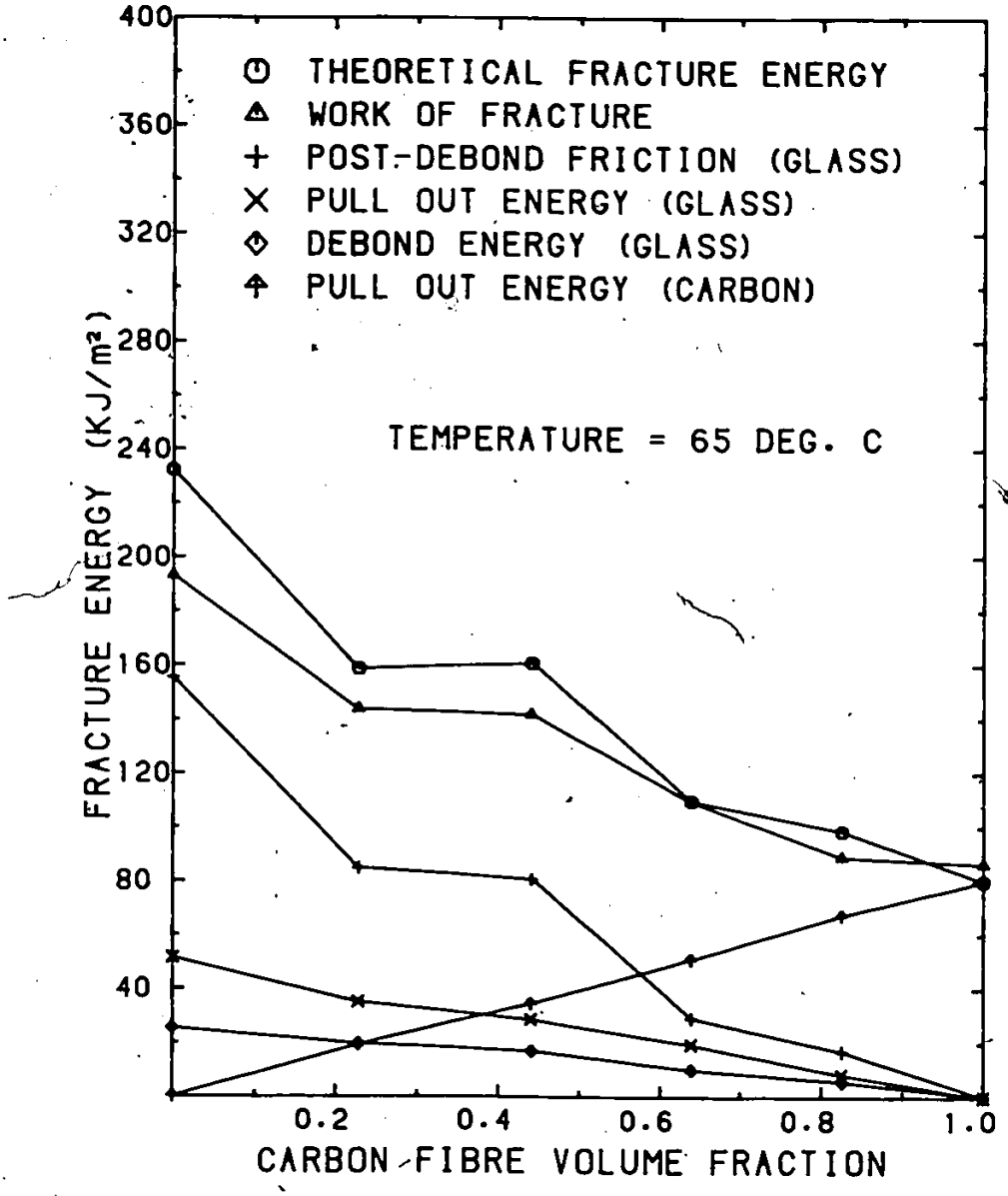

Figure 42: Fracture energy terms versus carbon fibre volume fraction at 65 degrees C.

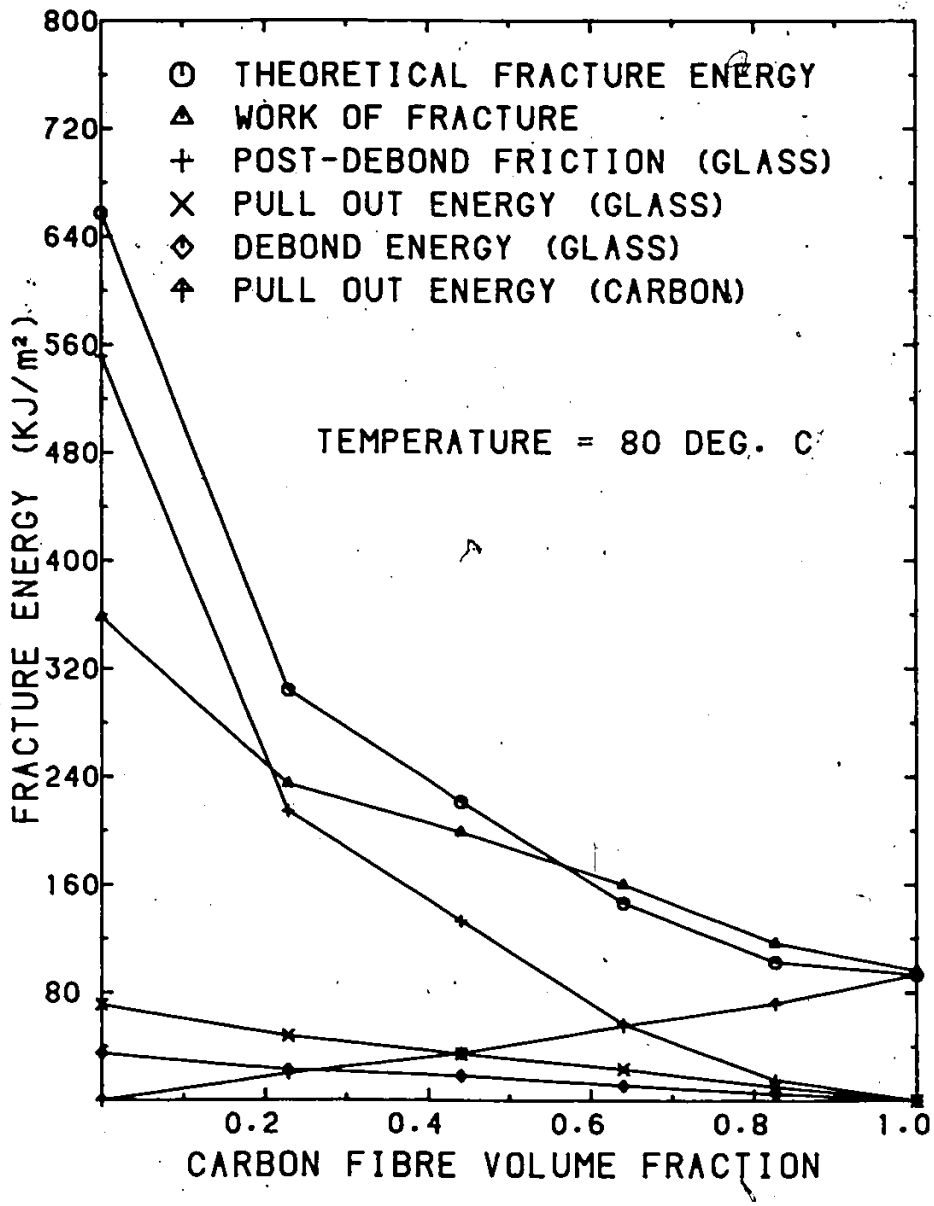

Figure 43: Fracture energy terms versus carbon fibre volume fraction at 80 deg. C.

Chapter VII

CONCLUSIONS AND RECOMMENDATIONS

The results of this thesis have contribute significantly to the understanding of the relationships between toughness and fracture mechanisms in fibre reinforced composites. The following conclusions are drawn:

1. The Pull-out Energy of carbon fibre, Pull-Out Energy of glass fibre, Debond Energy of glass fibre and Post-Debond Friction between glass fibre and the epoxy resin were the main contributors to the Fracture Energy of the CGHRP.
2. The Pull-Out Energy of carbon fibre was greater than that of the glass due to the higher strength of carbon fibre.
3. The Pull-Out Energy was greater than the Debond Energy even though the Debond length was generally more than 10 times longer than the fibre pull-out length. This was, in a sense, in agreement with Kelly's theory [54].
4. Fibre Pull-Out was the chief energy absorbing mechanism for CFRP.
5. For GFRP, Fibre Pull-Out, Fibre Debond and Post-Debond Friction were the contributing mechanisms to the Fracture Energy of the composite.

6. Post-Debonding Sliding was an important energy absorbing mechanism contributing to the Fracture Energy of glass fibres in the hybrid composite. It affected the trend of the Theoretical Fracture Energy.
7. The differential failure strain of the Post-Debond Sliding Mechanism was temperature-dependent.
8. The differential failure strain was also dependent on the stiffness of the matrix and the total matrix volume fraction in the composite (Appendix C).
9. The Post-Debond Friction Energy increased with temperature mainly due to an increase in the differential failure strain with temperature.
10. The Fracture Energy of hybrid composite was significantly influenced by the effect of temperature in the vicinity of, or above, the glass transition temperature of the epoxy matrix. For temperatures much lower than the transition temperature (at least 20 deg. C. according to this work), the temperature effect was not too significant.

The following are recommendations that the author believes should be studied:

1. A study on the environmental effects (i.e. combined effect of both humidity and temperature) on the fracture energy of the hybrid composites will provide a better picture of how the microfracture mechanisms work.
2. A more refined method to determine the failure strain of the specimens will lead to an improvement in evaluating the differential failure strain at elevated temperatures.
3. Some studies should be done to examime the reasons leading to the decrease of fracture energy of the hybrid composites at 50 and 60 deg. C. In this case, a temperature study on the bond-strength between the fibre and matrix is recommended.

BIBLIOGRAPHY

1. Loewenstein, K. L., "Glass Systems." Composite Materials, ed. by L. Holliday. EMSS, Elsevier, 1966 pp.129-220

2. Gordon, J. E., "The New Science of Strong Materials." Penguin Books. 1968.

3. Evans, C. C., "Whiskers." M & B Monographs ME/8, Mills & Boon Limited, 1972. pp.1-13

4. Lawn, B. R. & Wilshaw, T. R., "Fracture of Brittle Solids." Cambridge University Press, 1975. pp.1-15

5. Edison, T. A.: U.S. Patent 223,398 "Electric Lamp." Jan. 27, 1880.

6. Watt, W., Phillip, L. N. & Johnson, W., "High-strength High-modulus Carbon fibres." The Engineer 221 no. 5757, 1966. pp.815-816

7. Watts, A. A., "Commercial Applications for Advanced Composites." ASTM STP 704, 1980

8. Clements, L. L. "Properties of Commercial Fibers used for Filament-wound Composites." Lawrence Livermore Lab. UCIP-17873, Oct., 10, 1978.

9. Lee, H. & Neville, K., "Handbook of Epoxy Resins." McGraw-Hill, 1967. pp.1-8

10. Hull, D. "An Introduction to Composite Materials" Cambridge University Press (1981) pp.29

11. Vinson, J. R. & Chou, T. W., "Composite Materials and their use in Structures." Applied Science Pub., 1975. pp.35

12. Piggott, M. R., "Load Bearing Fibre Composites." Pergamon International Library: International series on the strength and fracture of materials and structures. 1980.

13. Pinckney, R. L. "Application of Carbon Fibres to Helicopters." Carbon Fibre: Their Place in Modern Technology. 2nd International Conference on Carbon Fibre (The Plastics Institute, London, Feb. 18-20, 1974.) paper no.38

14. Phillips, L. N. & Murphy, D. J., "Carbon Fibre Reinforced Plastics - The new Technology." Royal Aircraft Establishment. 1977

15. Hammond, M. G. & Farrell, K., "Graphite Epoxy Composite Material - Components for Communication Satellites." Proceedings of the 1978 International Conference on Composite Materials, April 1978 pp.1392

16. Dunbar, D. R., Robertson, A. R. & Kerrison, "Graphite/Epoxy Booms for the Space Shuttle Remote Manipulator." Proceedings of the 1978 International Conference on Composite Materials, April 1978 pp.1360

17. Dharan, C. K. H., "Design of Automotive Components with Advance Composites." Proceedings of the 1978 International Conference on Composite Materials, April 1978 pp.1446

18. Salkind, M. & Holister, G. ed. "Applications of Composite Materials." ASTM STP 524, 1973

19. Rogers, C. "Structural Design with Composites." Fundamental Aspects of Fiber Reinforced Plastics, Ed. by R. Schwartz and H. Schwartz, Wiley. N.Y. 1968 pp.141-160

20. Salkind, M. J. "Fibre Composite Structures." Proceedings of the 1975 International Conference on Composite Materials, April 1975 vol.2 pp.5-30

21. Jones, R. M. "Mechanics of Composite Materials." McGraw Hill 1975. pp.18-20

22. Pimm, J. H. "Difects Experience in the Production of Advaned Composite Outer Wings for the A-7D Attack Aircraft." Proceedings of the 1978 International Conference on Composite Materials, April 1978 pp.1621-1635

23. June, R. & Lager, J. "Applications of Composite Materials." ed. by M. Salkind & G. Holister, ASTM STP 524, 1973. pp.1-42

24. Ludwig, W. & Sicari, J. Materials and Processes for the 70's, SAMPE, Azusa, Ca., 1973. pp.336-355

25. Brooks, W. & Dow, M. "Materials and Processes for the 70's." SAMPE, Azusa, Ca., 1973 pp.539-558

26. Wong, D. G. & Vollersen, C. A., "Advanced Material Applications on the Trident I Missile." Composite materials: Testing and Design (5th Conference) ASTM STP 674, S. W. Tsai, ed., ASTM, 1970. pp.14-29

27. Sturgeon, D., Riewald, P. & Lacy, R. New Industries and Applications for Advanced Materials Technology. SAMPE, Azusa, Ca., 1974 pp.304-319

28. Zweben, C. H. "Hybrid Fibre Composite Material." Proceedings of the 1975 International Conference on Composite Materials, April 1975, vol.1 pp.345

29. Lovell, D. R., "Reinforcement of GRP & Wood with Carbon Fibre." Carbon Fibre: Their Place in Modern Technology. 2nd International Conference on Carbon Fibre (The Plastics Institute, London, Feb. 18-20, 1974.) paper no.43

30. Phillips, L. N. Composites 1 no.1, 1969. pp.50-51

31. Zweben, C. & Norman, J. C., "Kevlar 49/THORNEL 300 Hybrid Fibric Composites for Aerospace Applications." SAMPE Quarterly, July, 1976. pp.1-10

32. Salkind, M. J. "The Twin Beam Composite Rotor Blade." Fibre Science and Technology 8 no.2, April, 1975. pp.95-102

33. Anon., "Carbon Fibres in Heliopter Blades." Composite 5 no.4 (July, 1974) pp.144

34. Novak, R. C. "Material Variables Affecting the Impact Resistance of Graphite & Boron Composites - Part II" AFML TR-74-196-part II, 1974.

35. Pike, R. A. & Novak, R. C., "The Pendulum Test: A method for Assessing the Impact Response of Composite Material." 31st Annual Technical Conference, 1976. Reinforced Plastics/Composites Institute, The Society of the Plastic Industry. Paper 12-D

36. Lucas, J. J. "Impact Tests of a Graphite/Epoxy Helicopter Tail Roter Blade." Fibre Science and Technology, vol.7 no.4, 1974 pp.295-310

37. Miner, L. H., Lacy, R. I. & Woodrick, J. V. "Kevlar Aramid Composites for Marine Applications." 31st Annual Technical Conference, 1976. Reinforced Plastic/Composite Institute, The Society of the Plastic Industry, Paper 22-E

38. Parker, B. M. "Boron Fibre and Boron Reinforced Composites." Composite 5, Jan., 1974 pp.7-15

39. Anon., "New Materials Fly Better and Cheaper." Mechanical Engineering, May, 1982.

40. Perry, J. L. & Adams, D. F. "Charpy Impact Experiments on Graphite/Epoxy Hybrid Composites." Composites 6 July, 1975. pp.166-172

41. Riewald, P. G. & Zweben, C. "Kevlar 49 Hybrid Composites for Commercial and Aerospace Applications." 30th Annual Technical Conference, 1975. Reinforced Plastics/Composites Institute. The Societty of the Plastic Industry, Paper 14-B

42. Lovelace, A. M. "A Perspective on Composites." Proceedings of the 1978 International Conference on Composite Materials, April 1978 pp.3-8

43. Kliger, H. S. "Ultra High Modulus Graphite Hybrides for combined Torsional and Extensional Rigidity." 31st Annual Technical Conference, 1976. Reinforced Plastics/Composites Institute. The Society of the Plastic Industry, Paper 12-A

44. Short, D. & Summerscales, S., "Hybrid - a review. Part I. Techniques, design and construction." Composite 10, Oct., 1979 pp.215-223

45. Tattersall, H. G. & Tappin, G., "The Work of Fracture its Measurement in Metals, Ceramics and other Materials." Journal of Materials Science 1 (1966) pp.296-301

46. Outwater, J. O. & Murphy, M. C., "On the Fracture Energy of Unidirectional Laminates." 24th Annual Technical Conference on Reinforced Plastics/Composites Division, paper 11C (Society of Plastics Industry, Inc., 1969)

47. Outwater, J. O. & Murphy, M. C., "On the Fracture Energy of Unidirectional Laminates." Modern Plastics 7 (1970) pp.160

48. Beaumont, P. W. R. & Harris, B., "The Energy of Crack Propagation in Carbon Fibre Reinforced Resin Systems." Journal of Materials Science 7 (1972) pp.1265-1279

49. Gershon, B. & Marom, G. "Fracture Toughness and Mechanical Properties of Glass Fibre-Epoxy Composites." Journal of Materials Science 10 (1975) pp.1549-1556

50. Harris, B., Morley, J. & Phillips, D. C., "Fracture Mechansims in Glass Reinforced Plastics." Journal of Materials Science 10 (1975) pp.2050-2061

51. Kirk, J., Munro, M. & Beaumont, P. W. R. "The Fracture Energy of Hybrid Carbon & Glass Fibre." Journal of Materials Science 13 (1978) pp.2197-2204

52. Munro, M. "Impact Fracture Energy of Hybrid Glass/Carbon/Epoxy Composites." Strength and Fracture of Composites - CFC4, Alton, Ontario, October, 1980.

53. Kelly, A., "The Strengthening of Metals by Dispersed Particles." Proceedings of the Royal Society of London, A282 pp.63-79

54. Kelly, A., "Strong Solids." Oxford University Press., 1973

55. Cottrell, A. H., "Strong Solids." Proceedings of the Royal Society of London, A282 (1964) pp.2-9

56. Cooper, G. A. "The Fracture Toughness of Composites Reinforced with Weakened Fibres." Journal of Materials Science 5 (1970) pp.645-654

57. Harris, B., Beaumont, P. W. R. & Moncuniel deFerran, E., "Strength and Fracture Toughness of Carbon Fibre Polyester Composites." Journal of Materials Science 6 (1971) pp.238-251

58. Phillips, D. C., "The Fracture Energy of Carbon Fibre Reinforced Glass." Journal of Materials Science 7 (1972) pp.1175-1191

59. Sambell, R. A. J., Briggs, A., Phillips, D. C., & Bowen, D. H. "Carbon Fibre Composites with Ceramic and Glass Matrices." Journal of Materials Science 7 (1972) pp.676-681

60. Piggott, M. R., "The Effect of Aspect Ratio on Toughness in Composites." Journal of Materials Science 9 (1974) pp.494-502

61. Kelly, A. "Interface Effects and the Work of Fracture of a Fibrous Composite." Proceedings of the Royal Society of London, A319 (1970) pp.95-110

62. Marston, T. U., Atkins, A. G. & Felbeck, D. K., "Interfacial Fracture Energy and the Toughness of Composites." Journal of Materials Science 9 (1974) pp.447-455

63. Cook, J. & Gordon, J. E., "A Mechanism for the Control of Crack Propagation in all-brittle systems." Proceedings of the Royal Society of London, A282, 1964. pp.508-520

64. Piggott, M. R., "Theoretical Estimation of Fracture Toughness of Fibrous Composites." Journal of Materials Science 5 (1970) pp.669-675

65. Cooper, G. A. & Piggott, M. R., "Cracking and Fracture in Composites." Fracture 1977, Vol.1, ICF4, Waterloo, Can., June 19-24, 1977 pp.557-605

66. Munro, M. & Beaumont, P. W. R., "Fracture Mechanisms and Toughening of Fibre Composites." ICM 3 vol.3, Cambridge, England, Aug., 1979. pp.253-261

67. Hing, P. & Groves, G. W., "The Strength and Fracture Toughness of Polycrystalline Magnesium Oxide containing Metallic Particles and Fibres." Journal of Materials Science 7 (1972) pp.427-434

68. Cooper, G. A. & Kelly, A., "Tensile Properties of Fibre-reinforced Metals: Fracture Mechanics." Journal of the Mechanics and Physics of Solids. Vol.15 (1967) pp.279-297

69. Helfet, J. L. & Harris, B., "Fracture Toughness of Composites Reinforced with Discontinuous Fibres." Journal of Materials Science 7 (1972) pp.494-498

70. Wells, J. K. & Beaumont, P. W. R., "Fracture Energy Maps for Fibre Composites." Journal of Materials Science 17 (1982) pp.397-405

71. Beaumont, P. W. R. & Anstice, P. C., "A Failure Analysis of the Micromechanisms of Fracture of Carbon Fibre and Glass Fibre Composites in Monotonic Loading." Journal of Materials Science 15 (1980) pp.2619-2635

72. Lubin, G. (ed.) "Handbook of Fiberglass and Advanced Plastics Composites." Robert E. Krieger Pub. Co. 1975.

73. Lynch, C. T. & Kersaw, J. P. "Metal Matrix Composite." Cleveland, CRC Press, 1972. pp.5

74. "Commerical Data for Fibre Glass" Owens/Corning Fiberglas Pub. No.5-ASP-6870 Litho, May 1975

75. Morey, G. W. "The Properties of Glass - 2nd Ed." Reinhold Pub. Corp. 1954. pp.314-326

76. Cooper, G. A. "Optimization of the Three-Point Bend Test for Fracture Energy Measurement." Journal of Materials Science 12 (1977) pp.227-289

Appendix A

CALCULATION OF THE WORK OF FRACTURE ENERGY

Figure A1 shows a typical load-deflection curve obtained during the experiment.

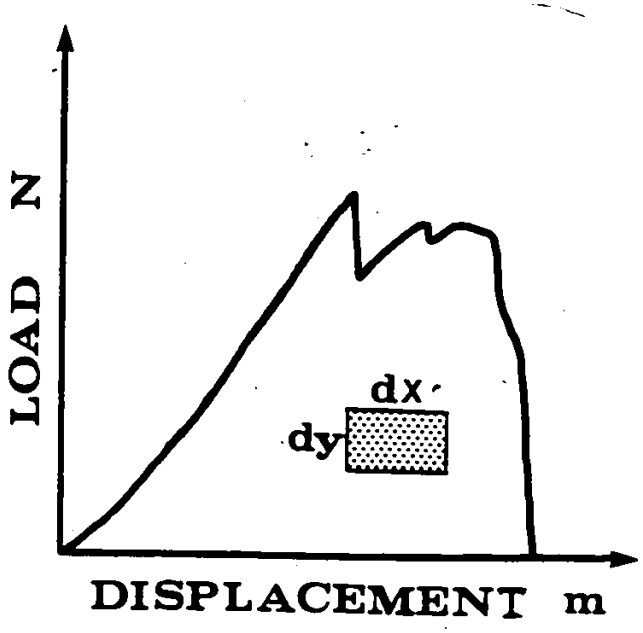

Figure A1: Load-deflection curve of a typical specimen

Yet, the unit of the abscissa represents the rate of travel of the chart on the Chart Recorder. Thus, it is necessary to relate the chart speed with the crosshead speed so as to get the equivalent distance travelled by the indentor. From Figure A1, if the chart travels dx mm, the crosshead would travel:

$$\text{Feed} = \frac{\nu_x}{\nu_c}\, dx \text{ mm} \qquad (A.1)$$

where ν_x = cross-head speed

ν_c = chart speed

The unit of the ordinate axis was in Newton and was 240 mm long. Let FSL equal the full scale load or maximum load on the axis. A distance of dy mm on the ordinate would represent:

$$\text{Force} = \left(\frac{FSL}{240}\right) dy \text{ N.} \qquad (A.2)$$

Therefore, 1 square mm under the load deflection curve would correspond to:

$$\frac{\nu_x}{\nu_c}\,\frac{FSL}{240}$$

with $(dx\ dy) = 1\ mm^2$, and

$$\text{Toughness} = U = A_c\,\frac{\nu_x}{\nu_c}\,\frac{FSL}{240} \qquad (A.3)$$

where A_c = area under the load-deflection curve

Therefore,

$$\gamma_f = WOF = \frac{U}{2A} \qquad (A.4)$$

where A = cross-sectional area of fibres

Appendix B

STRAIN RATE OF A BEAM UNDER THREE-POINT BEND TEST

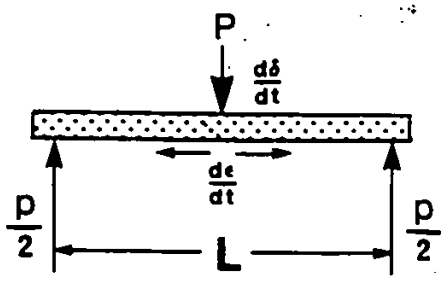

Figure B1: Three-point bending of a beam

According to the Beam Theory, from Figure B1, the maximum deflection of the beam occurs at the mid-point and was given by:

$$\delta = \frac{PL^3}{48EI} \qquad (B.1)$$

where: P = load applied

L = span of the beam

E = Young's Modulus of material.

I = Moment of Inertia

The maximum moment was given by:

$$M = \frac{PL}{4} \qquad (B.2)$$

and the maximum stress was:

$$\sigma = \frac{Mc}{I} \qquad (B.3)$$

where c = distance from the neutral axis

From Hooke's Law, $E = \frac{\sigma}{\epsilon}$

Therefore, the maximum strain of the beam became:

$$\epsilon = \frac{Mc}{EI} \qquad (B.4)$$

Substituting Equation (B.2) into (B.4), get:

$$\epsilon = \frac{PLc}{4EI} \qquad (B.5)$$

Rearranging (B.1) and substituting into (B.5), get:

$$\epsilon = \frac{12c}{L^2}\delta \qquad (B.6)$$

In terms of time derivatives,

$$\frac{d\epsilon}{dt} = \frac{12c}{L^2}\frac{d\delta}{dt} \qquad (B.7)$$

Appendix C

TO FIND THE NEUTRAL AXIS OF A COMPOSITE BEAM

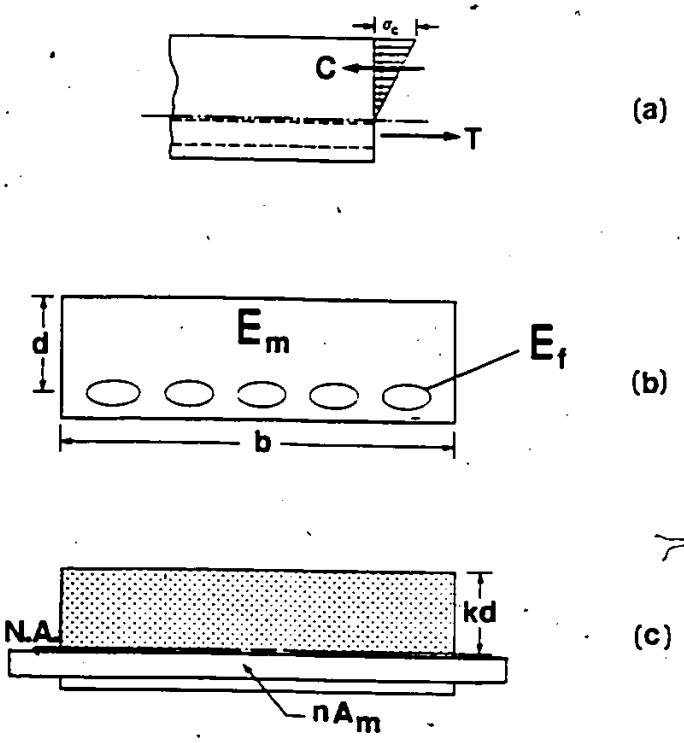

Figure C1: Bending and area transformation of a composite beam

Assumptions:

1. Perfect Bonding between fibre and matrix
2. No slip between fibre and matrix when stressed.

The ratio of the Young's Modulus of the fibre to that of the matrix was defined as:

$$n = \frac{E_f}{E_m} \qquad (C.1)$$

The area of the fibre, A_f, was transformed into an area of matrix, nA_m, equivalent as far as elastic properties were concerned. The transformed cross-section was that shown in Figure C1(c).

The moment of the shaded area above the neutral axis, N.A., with respect to N.A. was equal to that of the area below N.A. Therefore,

$$(\overline{b\ k\ d})\ {}^{kd}/_{2} = nA_{eq}\ (d - dk) \qquad (C.2)$$

Solving 'k', get:

$$k = \sqrt{2pn + (pn)^2} - pn \qquad (C.3)$$

$$p = {}^{A}/_{bd} \qquad (C.4)$$

'k' was the value which defined the position of the neutral axis. From Figure C1, it could be seen that:

$$c = d\ (1-k) \qquad (C.5)$$

If more than one kind of fibres were present in the composite beam, the area of the fibres with greater modulus

would have to transform into the equivalent area of the fibre having lower modulus similar to what was mentioned. Therefore, the equivalent area of the hybrid fibres in terms of the area of the fibre with lower modulus was given by:

$$A_{eq} = n'A_c + A_g \qquad (C.6)$$

where $n' = E_c/E_g$

E_c = modulus of the stiffer fibre

E_g = modulus of the less stiff fibre

This equivalent area of reinforcing fibres would be further transformed into equivalent area of the matrix, nA_{eq}, which was outlined above.

Appendix D

COMPUTER PROGRAM

In Table 4, a computer program which is written to compute the Work of Fracture and other Theoretical Fracture Energy of the specimens is listed.

The program first calculates the Work of Fracture of each specimen. Then, it evaluates the failure strain, the average debond and pull-out length for each and every specimen. After all these necessary parameters are evaluated, they are substituted into the Energy Equations to evaluate the respective Theoretical Fracture Energy for individual specimen. This program also calculates the mean and standard deviation of all the Fracture Energy for specimens with same carbon volume fraction and tested in same temperature. These values are tabulated or plotted in this thesis.

TABLE 4

Program to Calculate Fracture Energy

```
C     PC = CARBON FIBRE PERCENTAGE IN THE SPECIMEN
C     NUM = SPECIMEN NUMBER
C     TEMP = TESTING TEMPERATURE
C     VXH = CROSSHEAD SPEED OF THE INSTRON TESTING MACHINE
C     VC = CHART SPEED DURING THE TEST
C     FSL = FULL SCALE LOADING ( LOADING FACTOR )
C     VFG = VOLUME FRACTION OF GALSS IN THE SPECIMEN
C     VFC = VOLUME FRACTION OF CARBON IN THE SPECIMEN
C     PFG = STRENGTH OF GLASS ( 1.65E09 MPA )
C     PFC = STRENGTH OF CARBON ( 2.40E09 MPA )
C     DL = DEBONDED LENGTH OF EACH GLASS TOW IN THE SPECIMEN
C     Y = AVERAGE DEBONDED LENGTH OF GLASS WITHIN 1 SPECIMEN
C     EG = MODULUS OF ELASTICITY OF GLASS ( 70.0E09 MPA )
C     EC = MODULUS OF ELASTICITY OF CARBON ( 240.0E09 MPA )
C     LG = AVERAGE PULL-OUT LENGTH OF ALL THE GALSS TOW IN
C          ONE SPECIMEN.
C     LC = AVERAGE PULL-OUT LENGTH OF ALL THE CARBON TOW IN
C          ONE SPECIMEN.
C     YLC = AVERAGE OF THE INDIVIDUAL TOW OF THE TERM
C           Y**2/LG
C     STRAIN = DIFFERENCE OF STRAIN BETWEEN FIBRE AND RESIN
C
C     ENERGY TERMS
C     ============
C          DEG = DEBOND ENERGY OF GLASS
C        PDFEG = POST-DEBOND FRACTION ENERGY OF GLASS
C         POEG = PULL-OUT ENERGY OF GLASS
C         POEC = PULL-OUT ENERGY OF CARBON
C
C
      INTEGER A,C,PC,G,T,TEMP,Z,GP,CD,
     &        GROUP(9,4,6),COND(9,4,6)
C
      REAL MFE(4,6),MTE(4,6),DL(5),POCM(5),POGM(5),
     &     MPOC(4,6),MPOG(4,6),MDG(4,6),MPDG(4,6),
     &     LC(9,4,6),LG(9,4,6),STRAIN(9,4,6),ER(4),
     &     FST(9,4,6),MFST(4,6),SDFST(4,6)
C
      DIMENSION FE(9,4,6),YLG(9,4,6),NUMSP(9,4,6),
     &          TE(9,4,6),DEG(9,4,6),PDFEG(9,4,6),
     &          POEG(9,4,6),POEC(9,4,6),Y(9,4,6),
     &          SDPOC(4,6),SDPOG(4,6),SDDG(4,6),
     &          SDPDG(4,6),SDFE(4,6),SDTE(4,6)
C
C        DEFINE VALUES OF VARIABLES
C        ==========================
C
                  CAP = 500.
                  PFC = 2.4E9
```

```
                      PFG = 1.65E9
                      EG = 70.0E9
                      NOC = 6
                      NTT = 4
                      NOS = 9
                      CF = 1.1E-03
                      SL = 20.0E-03
                      ER(1) = 2.75
                      ER(2) = 2.54
                      ER(3) = 1.997
                      ER(4) = 1.101
C
C
C     WHERE: NOC-1 = NUMBER OF CARBON TOW PRESENT IN THE
C                    SPECIMEN
C            NTT = TESTING TEMPERATURE.
C                  ( IF NTT = 1, TEMPERATURE = 23 DEG C
C                    IF NTT = 2, TEMPERATURE = 50 DEG C
C                    IF NTT = 3, TEMPERATURE = 65 DEG C
C                    IF NTT = 4, TEMPERATURE = 80 DEG C )
C            NOS = CALL NUMBER OF THE SPECIMEN
C                  ( NOS = ORIGINAL SPECIMEN NUMBER - 249 )
C            CF = DISTANCE FORM THE NEUTRAL AXIS APTER CRACK
C                 HAS PASS THE FIBRE TOW
C            SL = DISTANCE BETWEEN THE SUPPORTS IN THE 3 PT
C                 BENDING JIG ( EQUALS TO 2 CM )
C            ER(NTT) = MODULUS OF ELASTICITY OF RESIN AT
C                      DIFFERENT TEMPERATURES
C
C
      DO 1 K = 1,NOC
      DO 1 J = 1,NTT
      DO 1 I = 1,NOS
    1    NUMSP(I,J,K) = 0
C
C
 1000 READ(5,50) TEMP
      IF(TEMP.EQ.99) GO TO 1001
C
C
        READ(5,51) VC,FSL
        IF(TEMP.EQ.23) T = 20
        IF(TEMP.EQ.50) T = 40
        IF(TEMP.EQ.65) T = 60
        IF(TEMP.EQ.80) T = 80
        J = T/20
 1002   READ(5,52) NUM,PC,A,GP,CD,DC1,DC2
        IF(NUM.EQ.999) GO TO 1000
C
C     EVALUATE DIFFERENT VARIABLES
C     ============================
C
          IF(NUM.GT.359) VXH = 0.2683
          IF(NUM.LE.359) VXH = 0.28
```

```
            AC = 5000*3.141592654/4*(8.0E-6)**2
            AG = 1600*3.141592654/4*(13.0E-6)**2
            I = 1
            K = PC/20+1
            C = K-1
            G = 5-C
            VFC = AC*C/(AC*C+AG*G)
            VFG = 1-VFC
 1980       IF(NUMSP(I,J,K).EQ.0) GO TO 1981
            IF(NUMSP(I,J,K).NE.0) I = I+1
               GO TO 1980
 1981       NUMSP(I,J,K) = NUM
            GROUP(I,J,K) = GP
             COND(I,J,K) = CD
C
C      EVALUATE THE WORK OF FRACTURE ENERGY
C      ====================================
C
            TOUG = A*VXH/VC*1.E-3*FSL*CAP*9.81/240.0
            FE(I,J,K) = TOUG*0.5/(C*AC+G*AG)/1.E03
C
C      CALCULATE THE CHANGE IN STRAIN IN EACH SPECIMEN
C      ===============================================
C
                FEED1 = DC1*VXH/VC*0.01
                FEED2 = DC2*VXH/VC*0.01
                CALL NAXIS(PC,ER(J),CI)
                ST1=FEED1*12*CI/SL**2
                ST2=FEED2*12*CF/SL**2
                FST(I,J,K) = (ST1+ST2)/2
                STRAIN(I,J,K) = FST(I,J,K)-0.015
C
C      CALCULATE THE AVERAGE PULL-OUT AND DEBOND LENGTH
C      ================================================
C
            SUMY = 0
            SUMC = 0
            SUMG = 0
            SUMDL = 0
            READ(5,53) (DL(Z),Z = 1,5)
            DO 4 Z = 1,5
               POCM(Z) = 0
               POGM(Z) = 0
    4          SUMY = SUMY+DL(Z)
C
            IF(G.EQ.0) GO TO  20
            IF(G.EQ.5) GO TO  21
C
            IF(G.EQ.1) READ(5,53)
           &   POCM(1),POCM(2),POGM(3),POCM(4),POCM(5)
            IF(G.EQ.2) READ(5,53)
           &   POCM(1),POGM(2),POCM(3),POGM(4),POCM(5)
            IF(G.EQ.3) READ(5,53)
           &   POGM(1),POCM(2),POGM(3),POCM(4),POGM(5)
```

```
      IF(G.EQ.4)READ(5,53)
     &    POGM(1),POGM(2),POCM(3),POGM(4),POGM(5)
      DO 7 Z = 1,5
         SUMC = SUMC+POCM(Z)
         SUMG = SUMG+POGM(Z)
         IF(POGM(Z).NE.0) SUMDL=SUMDL
     &      +(DL(Z)-POGM(Z))**2/(POGM(Z)/2)
    7 CONTINUE
      LC(I,J,K) = SUMC/C/2
      LG(I,J,K) = SUMG/G/2
      Y(I,J,K) = SUMY/G
      YLG(I,J,K) = SUMDL/G
      GO TO 1002
C
   20 READ(5,53) (POCM(Z),Z = 1,5)
      DO 5 Z = 1,5
    5    SUMC = SUMC+POCM(Z)
      LC(I,J,K) = SUMC/C/2
      LG(I,J,K) = 0
      Y(I,J,K) = 0
      YLG(I,J,K) = 0
      GO TO 1002
C
   21 READ(5,53) (POGM(Z),Z = 1,5)
      DO 6 Z = 1,5
         SUMG = SUMG+POGM(Z)
    6    SUMDL = SUMDL+(DL(Z)-POGM(Z))**2/(POGM(Z)/2)
      LC(I,J,K) = 0
      LG(I,J,K) = SUMG/G/2
      Y(I,J,K) = SUMY/G
      YLG(I,J,K) = SUMDL/G
      GO TO 1002

 1001 CONTINUE
   50 FORMAT(1I2)
   51 FORMAT(F9.1,F11.9)
   52 FORMAT(T1,I3,T10,I3,T19,I5,T28,I1,T37,I1,T44,F4.1,
     &       T54,F4.1)
   53 FORMAT(5F9.5)
C
C
C    CALCULATING THE AVERAGE AND STD. DEV.
C    *************************************
C
C
      DO 71 J = 1,NTT
      DO 71 K = 1,NOC
      DO 71 I = 1,NOS
         IF(NUMSP(I,J,K).EQ.0) GO TO 71
         CALL CALVFC(K,VFC)
         DEG(I,J,K) = (1-VFC)*Y(I,J,K)*PFG**2/(4*EG)/1.E6
         PDF1 = (1-VFC)*PFG*STRAIN(I,J,K)/8/1.E6
         PDFEG(I,J,K) = PDF1*YLG(I,J,K)
         POEG(I,J,K) = (1-VFC)*PFG*LG(I,J,K)/6/1.E6
```

```
      POEC(I,J,K) = VFC*PFC*LC(I,J,K)/6/1.E6
      TE(I,J,K)=DEG(I,J,K)+PDFEG(I,J,K)
     &          POEG(I,J,K)+POEC(I,J,K)
   71 CONTINUE
C
      CALL STD(NOS,NTT,NOC,NUMSP,FE,MFE,SDFE)
      CALL STD(NOS,NTT,NOC,NUMSP,POEC,MPOC,SDPOC)
      CALL STD(NOS,NTT,NOC,NUMSP,POEG,MPOG,SDPOG)
      CALL STD(NOS,NTT,NOC,NUMSP,DEG,MDG,SDDG)
      CALL STD(NOS,NTT,NOC,NUMSP,PDFEG,MPDG,SDPDG)
      CALL STD(NOS,NTT,NOC,NUMSP,TE,MTE,SDTE)
      STOP
      END
C
C
      SUBROUTINE CALVFC(K,VFC)
                 AC = 5000*3.141592654/4*(8.0E-6)**2
                 AG = 1600*3.141592654/4*(13.0E-6)**2
                 C = K-1
                 G = 5-C
                 VFC = AC*C/(AC*C+AG*G)
                 RETURN
                 END
C
      SUBROUTINE STD(II,JJ,KK,NUMSP,X,MX,SDX)
                 REAL X(9,4,6),SX(4,6),MX(4,6),
     &                SUM(4,6),SDX(4,6)
                 INTEGER NUMSP(9,4,6),M(4,6)
                 DO 111 J = 1,JJ
                 DO 111 K = 1,KK
                    SX(J,K) = 0
                    SUM(J,K) = 0
                    M(J,K) = 0
                    DO 222 I = 1,II
                       IF(NUMSP(I,J,K).EQ.0) GO TO 222
                          SX(J,K) = SX(J,K)+X(I,J,K)
                          M(J,K) = M(J,K) + 1
  222               CONTINUE
                    IF(M(J,K).EQ.0) GO TO 111
                       MX(J,K) = SX(J,K)/M(J,K)
                    DO 333 I = 1,II
                       IF(NUMSP(I,J,K).EQ.0) GO TO 333
                          SA = (X(I,J,K)-MX(J,K))**2
                          SUM(J,K) = SUM(J,K)+SA
  333               CONTINUE
                    SDX(J,K) = SQRT(SUM(J,K)/(M(J,K)-1))
  111            CONTINUE
                 RETURN
                 END
C
C
      SUBROUTINE NAXIS(PC,EM,CNA)
                 INTEGER PC
                 AM = 0.5E-03
```

```
      BM = 0.2E-03
      PI = 3.141592654
      AXF = PI*AM*BM
      A1C = PI*(8.0E-06)**2/4
      A1G = PI*(13.0E-6)**2/4
      B = 10.337E-03
      D = 2.4E-03
      NNC = 5000
      IF(PC.EQ.0) NNC = 0
      NNG = 1600
       IF(PC.EQ.100) NNG = 0
      C = PC/20
      G = 5-C
      EG = 70
      EC = 240
C
   10 AEQ = (C*EC/EG*A1C*NNC+G*A1G*NNG)
      PN = EG/(B*D)*AEQ/EM
      CNA = D*(1-SQRT(2*PN+PN**2)+PN)
      IF(CNA.GE.BM) GO TO 110
        X = AM*SQRT(1-(CNA/BM)**2)
        AS = AXF/2-CNA*X-AM*BM*ARSIN(CNA/BM)
        NCC = 5000*AS/AXF
        NGC = 1600*AS/AXF
        IF((IABS(NNC+NCC-5000).LE.5).AND.
     &     (IABS(NNG+NGC-1600).LE.2)) GO TO 110
           NNC = 5000-NCC
           NNG = 1600-NGC
           GO TO 10
  110     CONTINUE
       RETURN
       END
```

Appendix E

TABLE OF EXPERIMENTAL RESULTS

TABLE 5

The Work of Fracture of Hybrid Composites

Testing Temp. (deg. C.)	Num. of Specimens Tested	Carbon Volume Fraction	Work of Fracture (KJ/m^2)
23	8	0.00	213.69 ±39.83
23	8	0.23	154.37 ±29.39
23	7	0.44	123.53 ±19.10
23	8	0.64	96.63 ±11.65
23	7	0.83	89.49 ± 9.09
23	8	1.00	77.48 ± 9.54
50	8	0.00	180.92 ±27.60
50	8	0.23	144.99 ±20.34
50	7	0.44	139.31 ±23.14
50	8	0.64	102.77 ±17.90
50	7	0.83	90.77 ± 9.86
50	9	1.00	76.76 ±11.15
65	8	0.00	192.99 ±45.70
65	8	0.23	143.77 ±21.66
65	7	0.44	141.80 ±38.69
65	8	0.64	109.53 ±19.25
65	9	0.83	89.15 ± 9.73
65	8	1.00	86.63 ±10.31
80	8	0.00	357.85 ±85.86
80	8	0.23	234.27 ±59.99
80	7	0.44	198.74 ±44.04
80	8	0.64	160.13 ±48.61
80	7	0.83	116.85 ±20.84
80	8	1.00	96.37 ±28.50

TABLE 6

Debond Energy and Post-Debond Friction Energy of Glass Fibres

Testing Temp. (deg. C.)	Carbon Volume Fraction	Glass Fibre Debond Energy (KJ/m^2)	Glass Fibre Post-Debond Friction Energy (KJ/m^2)
23	0.00	40.75 ± 5.75	165.66 ± 74.46
23	0.23	26.96 ± 3.24	63.89 ± 32.66
23	0.44	19.18 ± 3.03	33.97 ± 16.24
23	0.64	13.20 ± 2.98	17.01 ± 9.82
23	0.83	7.60 ± 1.02	5.57 ± 4.74
23	1.00	0.00 ± 0.00	0.00 ± 0.00
50	0.00	29.84 ± 3.77	135.89 ± 50.98
50	0.23	21.67 ± 4.13	70.14 ± 36.64
50	0.44	16.51 ± 3.62	48.25 ± 32.11
50	0.64	11.10 ± 2.44	23.84 ± 17.14
50	0.83	6.20 ± 1.90	10.14 ± 8.92
50	1.00	0.00 ± 0.00	0.00 ± 0.00
65	0.00	25.38 ± 5.40	155.32 ± 67.72
65	0.23	19.64 ± 2.82	84.81 ± 27.82
65	0.44	16.96 ± 6.14	80.69 ± 53.33
65	0.64	10.05 ± 4.64	29.21 ± 23.71
65	0.83	5.74 ± 1.50	16.98 ± 8.24
65	1.00	0.00 ± 0.00	0.00 ± 0.00
80	0.00	34.96 ± 8.78	551.53 ±336.83
80	0.23	22.42 ± 4.87	214.04 ±170.12
80	0.44	18.34 ± 5.61	133.16 ± 83.74
80	0.64	11.12 ± 3.85	56.66 ± 36.76
80	0.83	4.92 ± 1.92	15.38 ± 12.59
80	1.00	0.00 ± 0.00	0.00 ± 0.00

TABLE 7

Pull-Out Energy of Glass Fibres and Carbon Fibres

Testing Temp. (deg. C.)	Carbon Volume Fraction	Glass Fibre Pull-Out Energy (KJ/m^2)	Carbon Fibre Pull-Out Energy (KJ/m^2)
23	0.00	74.13 ±16.48	0.00 ± 0.00
23	0.23	52.78 ± 6.57	19.71 ± 2.50
23	0.44	33.98 ± 5.45	34.70 ± 6.18
23	0.64	21.87 ± 4.73	52.43 ± 6.62
23	0.83	13.48 ± 3.27	74.71 ±15.56
23	1.00	0.00 ± 0.00	90.16 ±14.89
50	0.00	49.71 ± 7.65	0.00 ± 0.00
50	0.23	40.04 ± 4.37	16.00 ± 3.13
50	0.44	29.32 ± 4.42	31.43 ± 3.77
50	0.64	19.86 ± 4.17	49.95 ± 6.13
50	0.83	10.32 ± 4.01	65.08 ±25.61
50	1.00	0.00 ± 0.00	75.57 ±15.00
65	0.00	51.41 ± 7.56	0.00 ± 0.00
65	0.23	35.04 ± 3.88	19.13 ± 4.70
65	0.44	28.58 ± 8.80	34.44 ± 9.78
65	0.64	19.49 ± 8.01	51.00 ±10.14
65	0.83	8.46 ± 2.81	67.45 ±11.53
65	1.00	0.00 ± 0.00	80.12 ±15.22
80	0.00	70.99 ±10.40	0.00 ± 0.00
80	0.23	47.64 ± 8.75	19.63 ± 6.37
80	0.44	34.68 ± 8.82	35.06 ± 7.65
80	0.64	23.41 ± 6.40	55.30 ± 7.28
80	0.83	10.36 ± 3.79	71.91 ± 4.71
80	1.00	0.00 ± 0.00	93.11 ±16.22

TABLE 8

Theoretical Fracture Energy of Hybrid Composites

Testing Temp. (deg. C.)	Num. of Specimens Tested	Carbon Volume Fraction	Theoretical Fracture Energy (KJ/m^2)
23	8	0.00	280.53 ± 89.85
23	8	0.23	163.34 ± 37.99
23	7	0.44	121.83 ± 23.25
23	8	0.64	104.51 ± 15.21
23	7	0.83	101.35 ± 19.78
23	8	1.00	90.16 ± 14.89
50	8	0.00	215.44 ± 55.21
50	8	0.23	147.84 ± 41.56
50	7	0.44	125.51 ± 34.57
50	8	0.64	104.74 ± 23.42
50	7	0.83	91.74 ± 26.61
50	9	1.00	75.57 ± 15.00
65	8	0.00	232.10 ± 78.36
65	8	0.23	158.63 ± 35.16
65	7	0.44	160.68 ± 70.72
65	8	0.64	109.76 ± 38.39
65	9	0.83	98.63 ± 18.92
65	8	1.00	80.12 ± 15.22
80	8	0.00	657.48 ±351.59
80	8	0.23	303.74 ±183.17
80	7	0.44	221.25 ± 97.07
80	8	0.64	146.49 ± 45.56
80	7	0.83	102.58 ± 20.50
80	8	1.00	93.11 ± 16.22

TABLE 9

Failure Strain and Modulus of Bulk Resin with Temperature

Testing Temperature (deg. C.)	Failure Strain (%)	Young's Modulus (GPa)
25	0.0449 ± 0.0048	2.750 ± 0.290
50	0.0484 ± 0.0079	2.540 ± 0.280
65	0.0636 ± 0.0151	1.997 ± 0.219
80	0.1858 ± 0.0312	1.101 ± 0.156

Appendix F

THE PLOTS OF THEORETICAL FRACTURE ENERGY

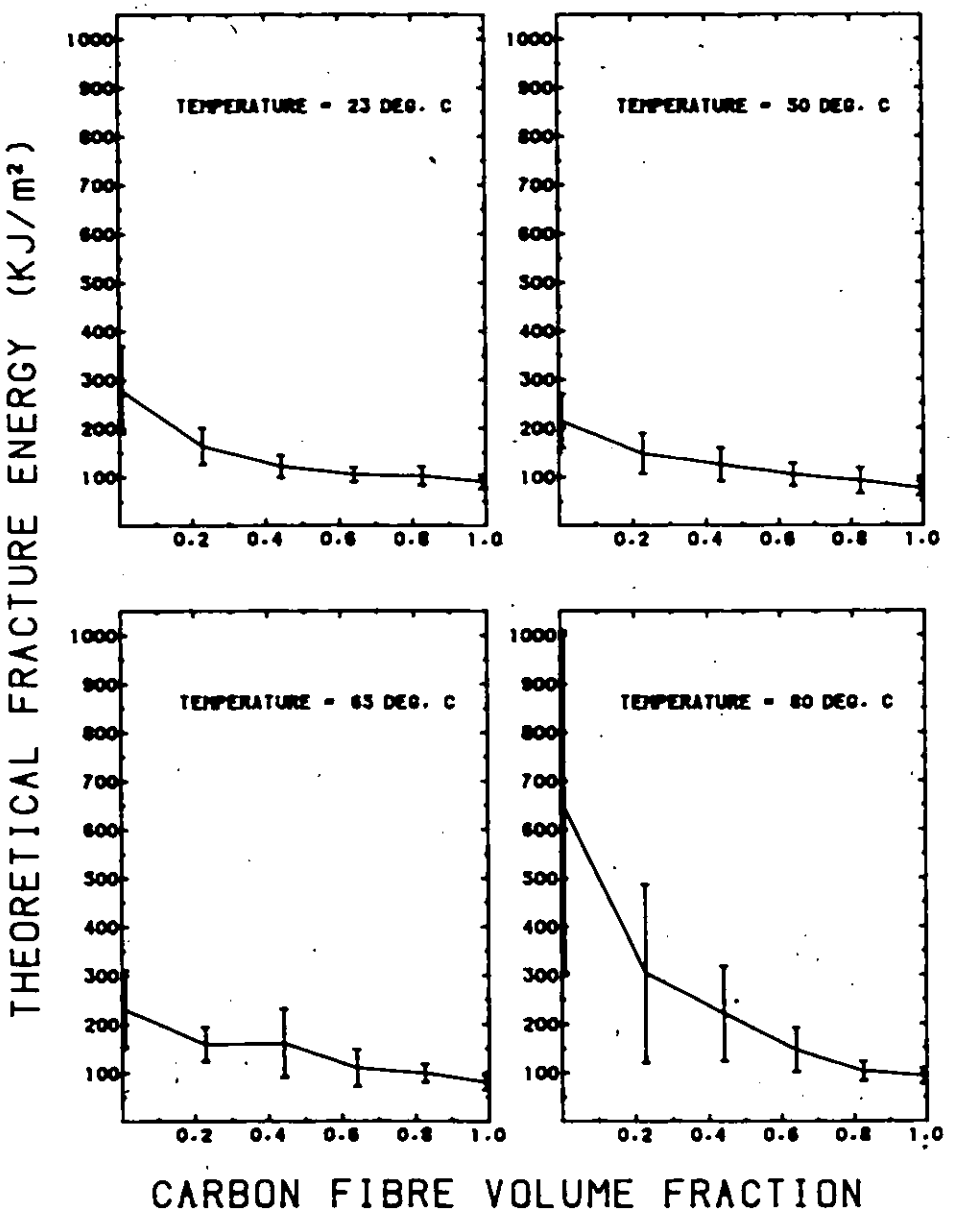

Figure F1: Theoretical fracture energy versus carbon fibre volume fraction (mean ±1 standard deviation)

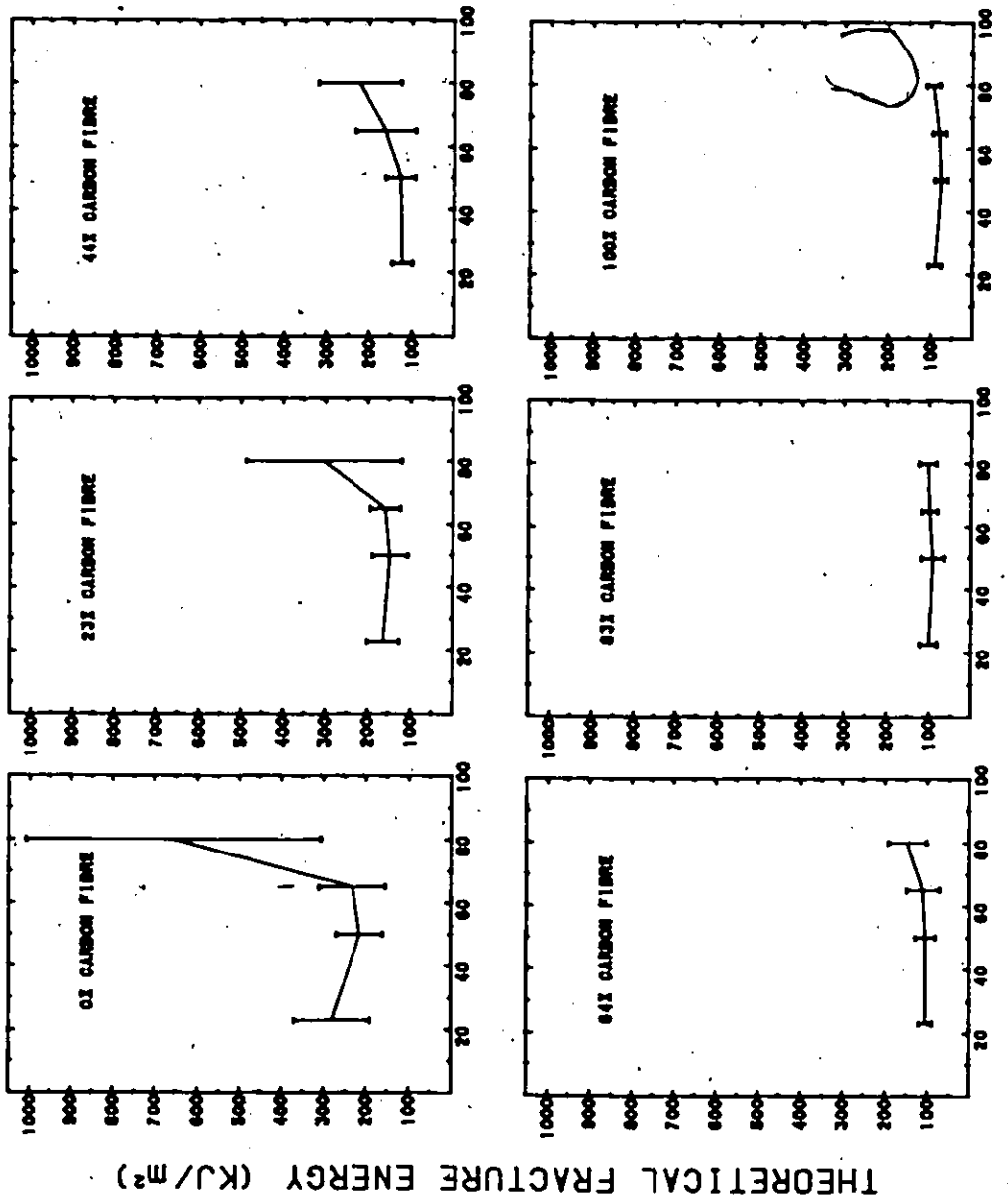

Figure F2: Theoretical fracture energy as a function of temperature (mean ±1 standard deviation)